Photoluminescence and Intermolecular Interaction of Diaroylmethanatoboron Difluorides in Solution and the Solid State

Photoluminescence and Intermolecular Interaction of Diaroylmethanatoboron Difluorides in Solution and the Solid State

（溶液および固体状態におけるジアロイルメタナートボロンジフロリドのフォトルミネッセンスと分子間相互作用）

Atsushi SAKAI

酒井 敦史

February 2016

Doctoral Thesis at Osaka Prefecture University

CONTENTS

GENERAL INTRODUCTION

Photoluminescence (PL) is the spontaneous emission of light from a material under optical excitation. The study of PL is important for the developments of new emitting materials.[1,2] Important transitions involved in PL have already been reported,[3–7] which can be illustrated using a "Jabłoński diagram" (Figure 0-1). The connection between the fluorescence (FL) and phosphorescence (PH) was reported by Lewis and Kasha.[5] They reported that FL describes an emission from an excited singlet state to the ground singlet state (radiative transition between the electronic states of the same multiplicity), and that PH originates from a singlet–triplet transition, or intersystem crossing (ISC), in the excited state. The PH is an emission that arises owing to a transition from an excited triplet state to the ground singlet state (radiative transition between the electronic states of the different multiplicities).

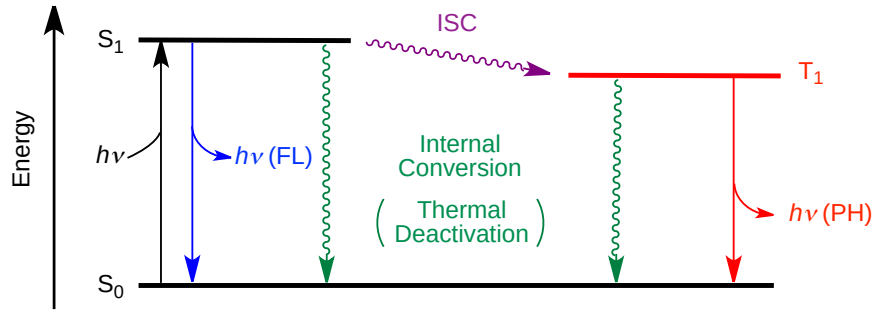

Figure 0-1. Jabłoński diagram.[1–4]

The PL properties of many organic compounds have been studied. In general, PL occurring in dilute solutions with less intermolecular interactions is attributed to "excited monomer".[2] It is also known that some compounds in highly concentrated solutions, emit excimer PL.[6,7] The excimer is an electronically excited dimer, which is "non-bonding" in the ground state.

Recently, studies on the PL of organic compounds in the solid state have attracted much attention owing to their applications in organic light-emitting diodes (OLEDs), dyes for illumination, imaging, and sensors, and other such applications. Unfortunately, however, the PL properties (e.g., the wavelengths, lifetimes, and quantum yields) of some compounds in the solid state are known to be quite different from those exhibited in the solution.[3,5] The PL properties are influenced by the arrangements of molecules with complicated intermolecular interactions. In the case of some organic molecules, the difference can be explained by intermolecular interactions between transition dipole moments,[3,5] exciton interactions, but the relationship between the PL and intermolecular interactions of many organic compounds in the solid states remains unclear.[6]

Organoboron complexes such as dibenzoylmethanatoboron difluoride (**P1BF$_2$**, Chart 0-1) exhibit intense FL emissions in solution and in the solid state.[8–13] The parent compound **P1BF$_2$** was synthesized for the first time by Morgan and Tunstall in 1924.[10] A report on the FL properties of **P1BF$_2$** in $CHCl_3$, published by Karasev and Korotkikh[11a] in 1986 opened up a field of wide ranging emission abilities, including FL in the crystalline states and films.[12] In 1991, Chow reported that at low concentration of **P1BF$_2$**, the acetonitrile solution showed blue FL of the excited monomer with two bands at 398 and 416 nm, and at high concentration, the solution showed yellow FL of the excimer with a band at 522 nm.[11b] As of 2016, the number of the published articles containing the substructure of **P1BF$_2$** is more than 200 (Figure 0-1).

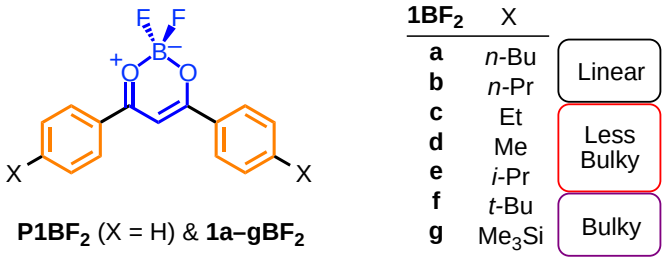

Chart. 0-1. Structures of **P1BF$_2$** and **1a–gBF$_2$**.

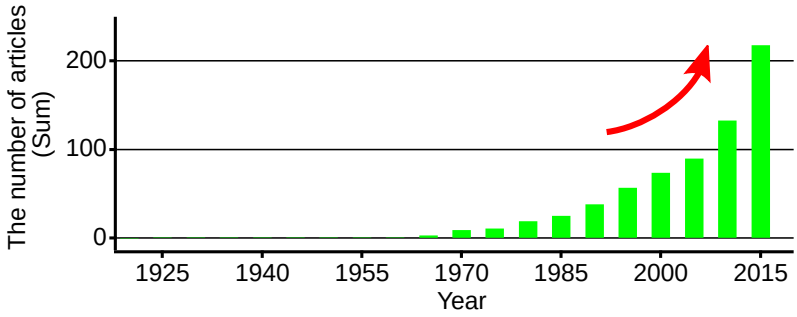

Figure 0-1. The number of the published articles containing the "substructure of **P1BF$_2$**", surveyed by SciFinder.

In 2009, Yoshimoto from the Ikeda–Mizuno research group also started investigation of the PL properties of **P1BF$_2$** and diaroylmethanatoboron difluorides (**1BF$_2$**, Chart 0-1) possessing several substituents (e.g., MeO group) at *p*-position of phenyl groups.[13a] However, the relationships between the PL properties and the intermolecular interactions of **1BF$_2$** in the solid state were not fully explained.[13]

The present doctoral thesis comprises one introduction section, four chapters, a conclusion section, and an acknowledgement section to appreciate the support received for this work.

In chapter 1, the author describes that the crystal-packing structures of seven alkyl- and silyl-substituted **1a–gBF$_2$** compounds (X = **a**: *n*-Bu, **b**: *n*-Pr, **c**: Et, **d**: Me, **e**: *i*-Pr, **f**: *t*-Bu, and **g**: Me_3Si, Chart 0-1) can be categorized into three different groups. Compounds belonging to the type I category (**1a,bBF$_2$**) exhibit *no* overlap of the π-conjugated main units of two adjacent molecules, whereas in type II crystals (**1c–eBF$_2$**), the benzene ring π-orbitals of two adjacent molecules overlap. Type III compounds (**1f,gBF$_2$**) are characterized by the overlap of π-orbitals of benzene and those of the dihydrodioxaborinine rings of adjacent molecules. The crystal-packing structure governs the FL properties in the crystalline state. The FL domain that is present in type I crystals, in which intermolecular orbital interactions are absent, leads to excited monomer-like FL properties. In type II crystals, the intermolecular overlap of the benzene rings π-orbitals generates new FL domains, referred to as "excited multimers" (Figure 0-2). These multimers possess allowed $S_1 \rightarrow S_0$ electronic transitions; as a result, they show similar FL lifetimes at longer wavelengths than the wavelengths required for the FL of the type I crystals. Finally, intermolecular overlap of the benzene and dihydrodioxaborinine ring π-orbitals in the type III crystals leads to "excited multimer" domains with forbidden $S_1 \rightarrow S_0$ electronic transitions and longer FL lifetimes at similar wavelengths to those exhibited by type I crystals.

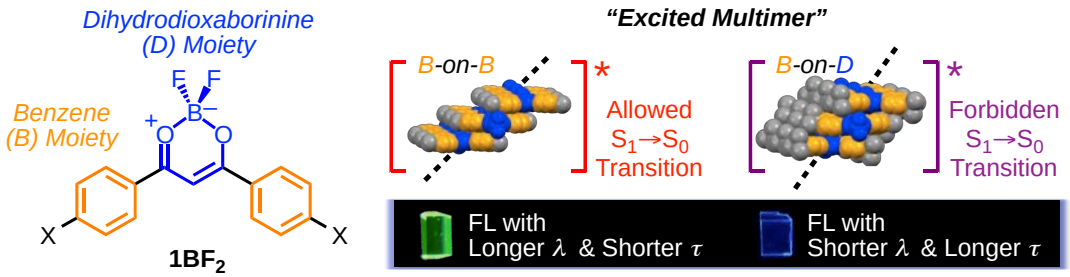

Figure 0-2. Graphical abstract in chapter 1: New FL domain "excited multimer" of **1BF$_2$**.

In chapter 2, the author investigates the effect of concentration on the FL emission of **P1BF$_2$** and its diisopropyl derivative (**1eBF$_2$**) in KBr and CH_2Cl_2 (Figure 0-3). Powder samples of **P1BF$_2$** and **1eBF$_2$** in KBr exhibit yellow and white FL emissions, respectively, whose intensities and wavelengths are not significantly affected by concentration. In contrast, remarkable concentration effects on the FL properties of these compounds in CH_2Cl_2 solutions are observed. An increase in the concentrations of the **P1BF$_2$** and **1eBF$_2$** solutions from 1×10^{-7} to *ca.* 2×10^{-1} M dramatically changes in the FL colors from blue (398 and 411 nm, respectively) to yellow (548 and 558 nm, respectively) via white. Careful analysis of the FL spectra, involving lifetime determinations and wave deconvolutions, reveals that emissions from **1BF$_2$** involve two FL domains, corresponding to an excited monomer and an excimer, respectively. This investigation also shows that increasing the

concentration promotes a continuous change from the former to the latter major FL domain. Thus, white FL of **P1BF$_2$** and **1eBF$_2$** is achieved by modulating the dual FL of the excited monomer (blue) and excimer (yellow). These findings indicate that **1BF$_2$** represents a new white light-emitting material with advantageous features, such as simple preparation and low molecular weight and the fact that it is a single-component system without any heavy metal atom.

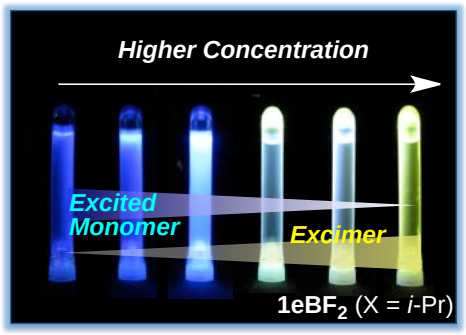

Figure 0-3. Graphical abstract in chapter 2: White light emission from **1eBF$_2$** in CH_2Cl_2.

In chapter 3, the author describes that the mechanofluorochromism (MFC)[8d,14] of **1BF$_2$** depends on the steric bulk of the substituents (Figure 0-4). MFC is a phenomenon in which changes in luminescence color of solid materials are induced by mechanical perturbations such as pulverization, shearing, and application of tension. The **1e,f,gBF$_2$** show MFC comprised of reversible color change of FL between blue and yellow. However, other derivatives do not show MFC. Observations in this study strongly suggest that the bulkiness of secondary and tertiary substituents such as *i*-Pr, *t*-Bu, and Me_3Si in **1eBF$_2$**, **1fBF$_2$**, and **1gBF$_2$**, respectively, is required for manifestation of MFC.

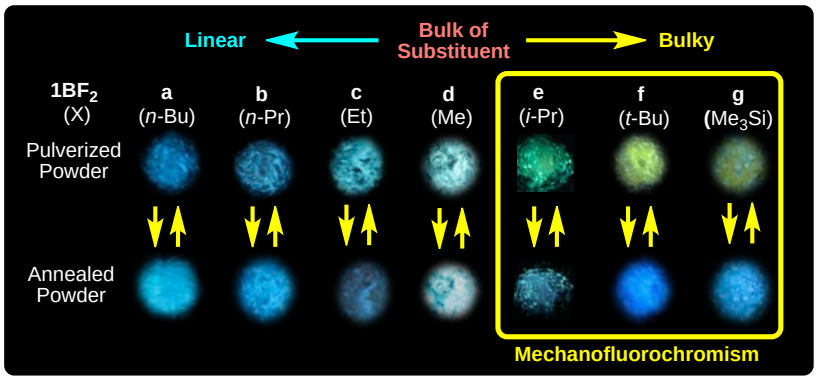

Figure 0-4. Graphical abstract in Chapter 3: Mechanofluorochromism (MFC) of **1BF$_2$** dependent on the steric bulk of substituents at *p*-position of phenyl group.

In chapter 4, the author elucidates the PL properties of metal-free bis(4-iodobenzoyl)-methanatoboron difluoride (**1hBF$_2$**) (Figure 0-5). At room temperature, an *n*-BuCl solution of **1hBF$_2$** emits blue FL ($\lambda_{FL,S}$ = 421 nm) upon photoexcitation. In contrast, crystals of **1hBF$_2$** emit green PL comprising both FL ($\lambda_{FL,C}$ = 460 nm) and PH ($\lambda_{PH,C}$ = 527 nm). The room-temperature phosphorescence (RTP) of crystalline **1hBF$_2$** is a consequence of two factors: a suppression of the thermal deactivation of the S_1 and T_1 excited states of **1hBF$_2$** and an enhancement of ISC from the S_1 state to form the T_1 state. Evidence that the former phenomenon is a result of intermolecular interactions caused by π-stacking in the rigid crystal structure of **1hBF$_2$** is obtained by using X-ray crystallographic analysis and density functional theory calculations. The enhanced ISC is a consequence of both the well-known heavy atom effect induced by iodine, and the continuous π-stacking arrangement of **1hBF$_2$** molecules in crystals, which leads to a forbidden $S_1 \rightarrow S_0$ electronic transition and a small energy gap between S_1 and T_2/T_1 states.

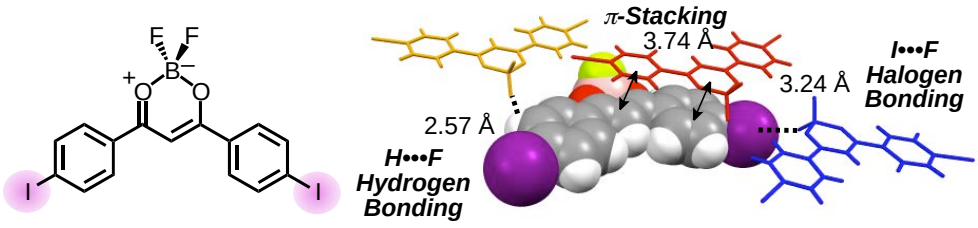

Figure 0-5. Graphical abstract in chapter 4: Intermolecular interactions required for room-temperature phosphorescence (RTP) of **1hBF$_2$**.

References

1. Braslavsky, S. E. *Glossary of terms used in photochemistry, 3rd edition (IUPAC Recommendations 2006). Pure Appl. Chem.* **2007**, *79*, 293–465.
2. Turro, N. J.; Ramamurthy, V.; Scaiano, J. C. *Principles of Molecular Photochemistry: An Introduction* **2009**, University Science Books: Herndon, VA.
3. Demchenko, A. P.; Heldt, J.; Waluk, J.; Chou, P.-T.; Sengupta, P. K.; Brizhik, L.; del Valle, J. C. *Angew. Chem. Int. Ed.* **2014**, *53*, 14316–14324.
4. Jabłon´ski, A. *Nature* **1933**, *131*, 839–840.
5. (a) Lewis, G. N.; Kasha, M. *J. Am. Chem. Soc.* **1945**, *67*, 994–1003. (b) Kasha, M.; Rawls, H. R.; Ashraf El-Bayoumi, M. *Pure Appl. Chem.* **1965**, *11*, 371–392.
6. (a) Verhoeven. J. W. *Glossary of terms used in photochemistry, 3rd edition (IUPAC Recommendations 2006). Pure Appl. Chem.* **2007**, *79*, 293–465. (b) Birks, J. B. *Nature* **1967**, *214*, 1187–1190.
7. (a) Gregoly, D. S.; Garry, R. *Nature Mater.* **2006**, *64*, 361–386. (b) Allendorf, M. D.; Bauer, C. A.; Bhakta R. K.; Houka, R. J. T. *Chem. Soc. Rev.*, **2009**, *38*, 1330–1352.
8. (a) Chow, Y. L.; Cheng, X.; Johansson, C. I. *J. Photochem. Photobiol. A: Chem.* **1991**, *57*, 247–255. (b) Mirochnik, A. G.; Fedorenko, E. V.; Karpenko, A. A.; Gizzatulina, D. A.; Karasev, V. E. *Luminescence* **2007**, *22*, 195–198. (c) Zhang, G.; Chen, J.; Payne, S. J.; Kooi, S. E.; Demas, J. N.; Fraser, C. L. *J. Am. Chem. Soc.* **2007**, *129*, 8942–8943. (d) X. Sun, X. Zhang, X. Li, S. Liu, G. Zhang, *J. Mater. Chem.* **2012**, *22*, 17332–17339.
9. (a) Loudet, A.; Burgess, K. *Chem. Rev.* **2007**, *107*, 4891−4932. (b) Gómez-Durán, C. F. A.; García-Moreno, I.; Costela, A.; Martin, V.; Sastre, R.; Bañuelos, J.; Arbeloa, F. L.; Arbeload I. L.; Peña-Cabrera, E. *Chem. Commun.* **2010**, *46*, 5103–5105.
10 Morgan, G. T.; Tunstall, R. B. J. *Chem. Soc., Trans.* **1924**, *125*, 1963–1967.
11 (a) Karasev, V. E.; Korotkikh, O. A. *Russ. J. Inorg. Chem.* **1986**, *31*, 493–496. (b) Chow, Y. L.; Chaeng, X.; Johansson, C. I. *J. Photochem. Photobiol. A: Chem.* **1991**, *57*, 247–255.
12 (a) Mirochnik, A. G.; Gukhman, E. V.; Karasev, V. E.; Zhikhareva, P. A. *Russ. Chem. Bull.* **2000**, *49*, 1024–1027. (b) Cogné-Laage, E.; Allemand, J. F.; Ruel, O.; Baudin, J. B.; Croquette, V.; Blanchard-Desce, M.; Jullien, L. *Chem. Eur. J.* **2004**, *10*, 1445–1455.
13. (a) Yoshimoto, Y. Master Thesis, Osaka Prefecture University (**2010**). (b) Tanaka, M. Master Thesis, Osaka Prefecture University (**2014**). (c) Nishida, S. Graduation Thesis, Osaka Prefecture University (**2015**).
14. (a) Chi, Z.; Zhang, X.; Xu, B.; Zhou, X.; Ma, C.; Zhang, Y.; Liu, S.; Xu, J. *Chem. Soc. Rev.* **2012**, *41*, 3878–3896. (b) Xue, P.; Sun, J.; Chen, P.; Gong, P.; Yao, B.; Zhang, Z.; Qiana, C.; Lu, R. *J. Mater. Chem. C* **2015**, *3*, 4086–4092.

CHAPTER 1

Novel Fluorescence Domain "Excited Multimer" Formed upon Photoexcitation of Continuously-stacked Diaroylmethanatoboron Difluoride Molecules with Fused π-Orbital in Crystals

1.1. Introduction.

In spite of many efforts,[1–7] relationships that exist between the modes of molecular aggregation and fluorescence (FL) properties of organic compounds have remained unclear. Because crystals are a fundamental mode of molecular aggregation that can be unambiguously delineated by using X-ray crystallographic analysis, one of the best ways to investigate this relationship is through systematic and thorough studies of the FL properties and packing structures of crystalline substances.[8–10] However, implementation of this approach is difficult because the preparation of single crystals of different crystalline forms of single organic substances or closely related derivatives is nontrivial.

Organoboron complexes[11–22] have attracted growing attention as organic fluorescent materials owing to several advantages that include ease of preparation, large molar extinction coefficients and high FL quantum yields (Φ_{FL}). Among substances in this family, dibenzoylmethanatoboron difluoride (**P1BF$_2$**, Scheme 1-1) is an especially interesting compound from the viewpoint of probing relationships between aggregation mode and FL properties.[23–35] From the time of the report by Mirochnik and coworkers showing that **P1BF$_2$** FL involves emission from arrays of molecules in crystals in which intermolecular orbital interactions occur,[30–35] many others observed that **P1BF$_2$** derivatives exhibit interesting molecular aggregation-based emission phenomena such as mechanochromic luminescence,[36–39] aggregation-induced emission,[40] and room-temperature phosphorescence.[41,42]

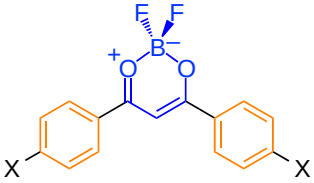

P1BF$_2$ (X = H) & **1a–gBF$_2$**

1BF$_2$	X
a	*n*-Bu
b	*n*-Pr
c	Et
d	Me
e	*i*-Pr
f	*t*-Bu
g	Me_3Si

Scheme 1-1. Structures of **P1BF$_2$** and **1a–gBF$_2$**.

Guided by the earlier efforts, the author carried out an investigation aimed at elucidating the FL properties and crystal-packing structures of **1BF$_2$** derivatives. The results of this effort showed that the crystals of parent compound **P1BF$_2$** exhibit FL with a longer lifetime (τ_{FL}) than that in CH_2Cl_2 solution but that its *i*-Pr derivative **1eBF$_2$** (Scheme 1-1) exhibits FL with almost identical τ_{FL} in CH_2Cl_2 as it does in the crystalline state.[43,44] In a continuation of this investigation, we explored the FL properties of the alkyl- and trimethylsilyl-substituted dibenzoylmethanatoboron difluorides **1a–gBF$_2$** (Scheme 1-1) in CH_2Cl_2 solutions and in the crystalline states. As described below, the results of this comprehensive study show that **1a–gBF$_2$** each have one of three types of crystal-packing structures that differ in manner in which intermolecular π-orbital overlap takes place. Interestingly, the FL properties, especially the FL wavelength maxima (λ_{FL}) and τ_{FL}, are affected by the nature of the crystal-packing structures. The observation demonstrates that the differences in FL properties originate from differences in intermolecular orbital interactions taking place in the crystals.

1.2. Results.

1.2.1. Crystal-packing structures. Crystals of **1a–gBF$_2$** all have packing structures in which molecules are stacked in face-to-face manner (Figure 1-1). In contrast to **1cBF$_2$**, whose crystalline state contains molecules existing in a zigzag array to the molecular long-axis direction, crystals of all other substances have continuously-stacked molecular arrays with oblique angles to the long-axis molecular direction (Figure 1-1, Front View). Importantly, the crystals of **1aBF$_2$**, **1bBF$_2$**, **1dBF$_2$**, **1eBF$_2$**, **1fBF$_2$**, and **1gBF$_2$** have the same space group of *C*2/*c* while **1cBF$_2$** is in the space group of *Pnma*. Therefore, the major differences in crystal-packing structure among **1a–gBF$_2$** excepting **1cBF$_2$** could be simply considered to be differences in distances between neighboring molecules. Distances between centroids of adjacent molecules (D_C) in crystals of **1a–gBF$_2$** are listed in Table 1-1. Adjacent molecules in crystals of **1aBF$_2$** and **1bBF$_2$**, which possess linear alkyl groups, are aligned at longer distances from each other (D_C = 12.69 Å for **1aBF$_2$** and 11.34 Å for **1bBF$_2$**).[34] As a result, molecules in these crystals are stacked in a manner which does not allow intermolecular overlap of the parent units that correspond to **P1BF$_2$**, but enables stacking of the *n*-Bu or *n*-Pr alkyl chain and benzene moiety (Figure 1-1, *No* overlap). The D_C values for **1cBF$_2$**, **1dBF$_2$**, and **1eBF$_2$** that contain less bulky substituents are smaller than those for **1aBF$_2$** and **1bBF$_2$** (Table 1-1, D_C = 9.67 Å for **1cBF$_2$**, 6.80 Å for **1dBF$_2$**, and 8.63 Å for **1eBF$_2$**). As a result, adjacent molecules in crystals of **1c–eBF$_2$** are stacked in a manner that allows overlap of benzene ring π-orbitals (Figure 1-1, *B-on-B* overlap).[43b] Molecules of **1fBF$_2$** and **1gBF$_2$** with bulky substituents are stacked in a more close way (Table 1-1, D_C = 5.41 Å for **1fBF$_2$** and 5.62 Å for **1gBF$_2$**) in order to avoid

intermolecular overlap of the parent unit and bulky substituents of adjacent molecules. Thus, molecules in the crystalline states of **1fBF$_2$** and **1gBF$_2$** are stacked in a manner that enables overlap of benzene groups with the 1,2-dihydro-2,6-dioxaborinine moieties in the neighboring molecules (Figure 1-1, *B-on-D* overlap). The face-to-face distances (D_F) of molecules of **1a–gBF$_2$** are all less than 4 Å (Table 1-1), indicating that π-orbital interactions exist when the parent units overlap with each other.

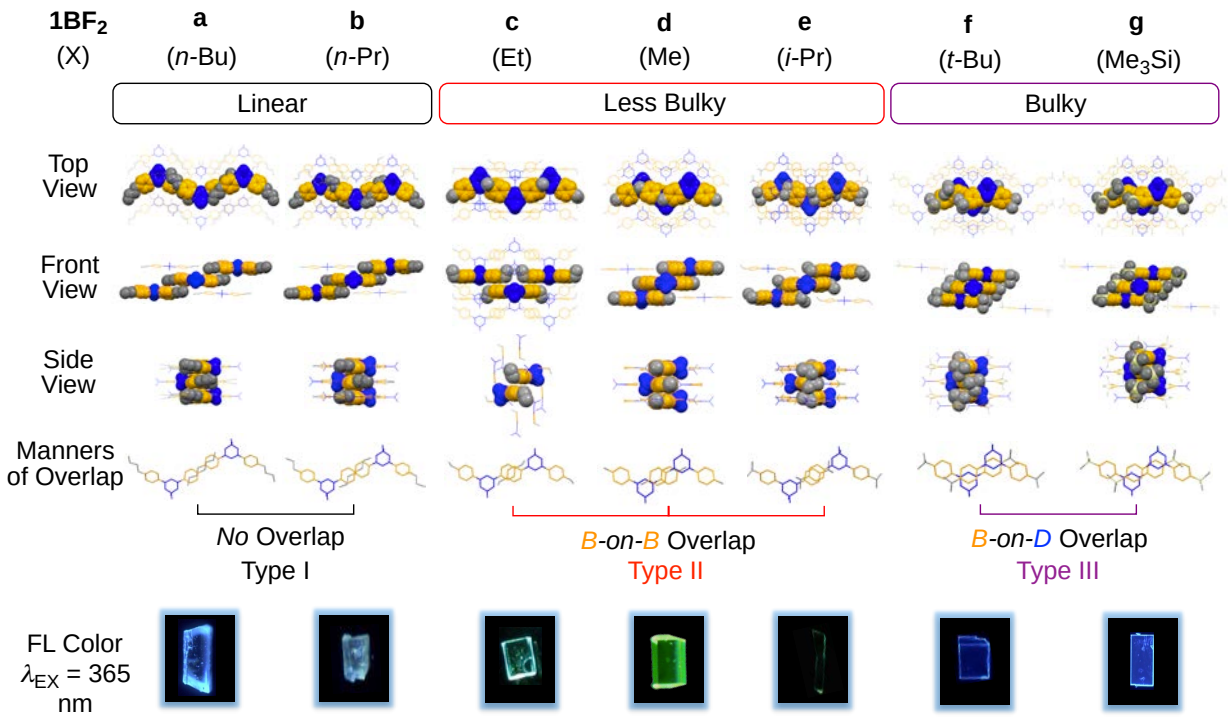

Figure 1-1. Crystal-packing structures of **1a–gBF$_2$** determined by using X-ray crystallographic analysis. The manners of overlap of adjacent molecules in continuously-stacked molecular arrays are classified into three types.

Table 1-1. Manner of Overlap and D_C and D_F between Adjacent Molecules in Crystals of **1a–gBF$_2$**

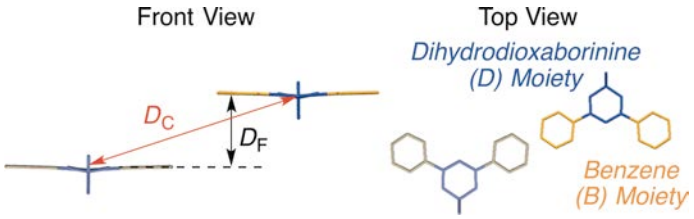

1BF$_2$	Manner of Overlap	D_C[a] / Å	D_F[a] / Å
a	*No*	12.69	3.94
b	*No*	11.34	3.81
c	*B-on-B*	9.67	3.74
d	*B-on-B*	6.80	3.42
e	*B-on-B*	8.63	3.82
f	*B-on-D*	5.41	3.71
g	*B-on-D*	5.62	3.73

[a] Determined by using X-ray crystallographic analyses.

1.2.2. UV–vis absorption and FL properties in CH_2Cl_2. Substances **1a–gBF$_2$** in low concentration CH_2Cl_2 solutions have almost identical absorption wavelength maxima ($\lambda_{AB,S}$) of 381–392 nm (Figure 1-2a and Table 1-2). Upon photoexcitation using 365-nm light, **1a–gBF$_2$** emit blue FL with almost the same $\lambda_{FL,S}$ of 409–414 nm (Figure 1-2b and Table 1-2) and $\tau_{FL,S}$ of 1.3–1.6 ns. The $\Phi_{FL,S}$ of **1a–fBF$_2$** were found to be high (0.81–0.91) while that of **1gBF$_2$** is lower (0.66). Notably, $\lambda_{AB,S}$ and $\lambda_{FL,S}$ of **1a–fBF$_2$** do not display remarkable change when the solvent polarity is altered.[45]

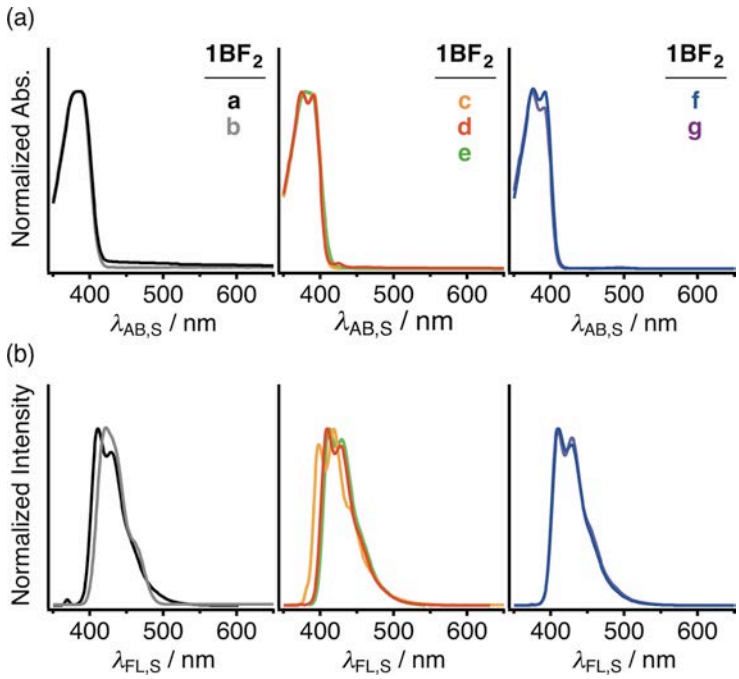

Figure 1-2. (a) UV–vis absorption spectra and (b) FL spectra of **1a–gBF$_2$** in CH_2Cl_2 (*ca.* 0.5×10^{-5} M, λ_{EX} = 365 nm).

Table 1-2. UV–vis Absorption and FL Properties of **1a–gBF$_2$** in CH_2Cl_2 and in Crystals at 298 K

	In CH_2Cl_2[a]				In Crystal			
1BF$_2$	$\lambda_{AB,S}$ / nm	$\lambda_{FL,S}$[b] / nm	$\tau_{FL,S}$[c,d] / ns	$\Phi_{FL,S}$[b]	$\lambda_{EX,C}$ (band)[e] / nm	$\lambda_{FL,C}$[b] / nm	$\tau_{FL,C}$[c,f] / ns	$\Phi_{FL,C}$[g]
a	387	411	1.5	0.91	404 (386–448)	450	1.8	~0.71
b	381	412	1.6	0.90	404 (386–453)	456	1.8	~0.58
c	391	411	1.6	0.83	428 (386–481)	476	3.5	~0.37
d	391	414	1.5	0.81	469 (388–517)	518	3.2	~0.41
e	388	411	1.6	0.83	405 (386–498)	500	1.5	~0.17
f	392	411	1.5	0.81	406 (386–443)	467	6.8	~0.46
g	391	409	1.3	0.66	405 (385–441)	469	5.6	~0.29

[a] The maximal absorbance of the solution was controlled to be 0.3 (ca. 0.5×10^{-5} M). [b] λ_{EX} = 365 nm. [c] λ_{EX} = 371 nm. [d] The detected wavelength λ_{DET} of FL is controlled to be $\lambda_{FL,S}$. χ^2 values are in the range of 1.0 ± 0.2. [e] Analysis range: $Int/Int_{max} > 0.3$, λ_{DET} = 560 nm. [f] Average of values detected at $\lambda_{FL,C}$ = 460, 480, 500, 520, 540, and 560 nm. χ^2 values are in the range of 1.0 ± 0.2. [g] Excitation was done at the peak top wavelength (±5 nm) in the excitation spectrum ($\lambda_{EX,C}$).

1.2.3. FL properties in the crystalline states. Crystals of **1aBF$_2$** and **1bBF$_2$** have $\lambda_{FL,C}$ at 450 and 456 nm, respectively (Figure 1-3a and Table 1-2), which are *ca.* 40 nm higher than $\lambda_{FL,S}$ for CH_2Cl_2 solutions of these substances. The crystals of **1cBF$_2$**, **1dBF$_2$**, and **1eBF$_2$** have $\lambda_{FL,C}$ at longer wavelengths (476, 518, and 500 nm, respectively) than those of **1aBF$_2$** and **1bBF$_2$**. The $\lambda_{FL,C}$ values for crystalline **1fBF$_2$** and **1gBF$_2$** are 467 and 469 nm, respectively, which are higher than those of crystals of **1aBF$_2$** and **1bBF$_2$** and similar to those of **1cBF$_2$**, **1dBF$_2$**, and **1eBF$_2$**. However, the differences in the $\lambda_{FL,C}$ values between **1f–gBF$_2$** and **1a–bBF$_2$** are smaller than those between **1c–eBF$_2$** and **1a–bBF$_2$**.

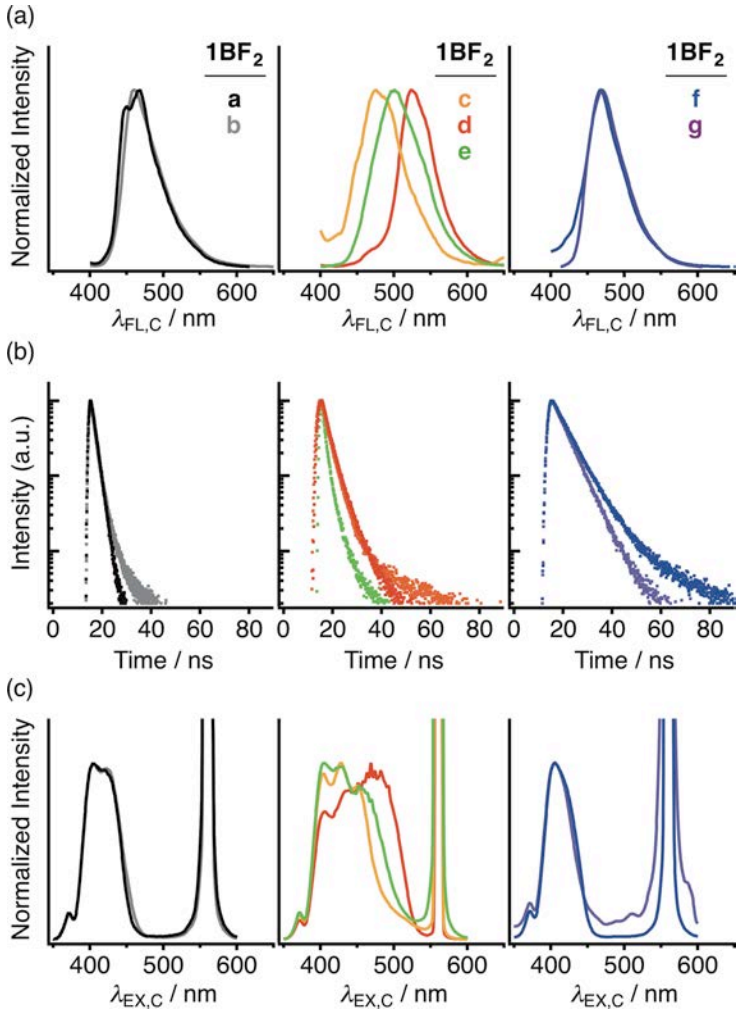

Figure 1-3. (a) FL spectra (λ_{EX} = 365 nm), (b) time-dependent changes of FL intensity (λ_{DET} = 500 nm, λ_{EX} = 371 nm), and (c) excitation spectra (λ_{DET} = 560 nm) of **1a–gBF$_2$** crystals.

One FL transient arising from both crystalline **1aBF$_2$** and **1bBF$_2$** has $\tau_{FL,C}$ of 1.8 ns (Figure 1-3b and Table 1-2),[46] which is similar to $\tau_{FL,S}$ (*ca.* 1.5 ns) observed in CH_2Cl_2 solutions of these substances. In addition, the $\tau_{FL,C}$ values of crystalline **1cBF$_2$** and **1dBF$_2$** are 3.5 and 3.2 ns, respectively, while those of crystalline **1fBF$_2$** and **1gBF$_2$** are 6.8 and 5.6 ns, respectively. Finally, only **1eBF$_2$** exhibits a short $\tau_{FL,C}$ of 1.5 ns in its crystalline state.

1.2.4. Excitation wavelength associated with FL from crystals. Inspection of excitation spectra determined for FL emission of crystalline **1aBF$_2$** and **1bBF$_2$** show that the FL is associated with absorption between *ca.* 385–450 nm (Figure 1-3c and Table 1-2). Moreover, while the FL bands of crystalline **1cBF$_2$**, **1dBF$_2$**, and **1eBF$_2$** are associated with excitation between *ca.* 385–520 nm, those of crystalline **1fBF$_2$** and **1gBF$_2$** are promoted by excitation in a shorter wavelength region of *ca.* 385–445 nm, which is almost identical to peak top wavelength in the excitation spectrum ($\lambda_{EX,C}$) of **1aBF$_2$** and **1bBF$_2$** crystals.

1.2.5. Theoretical calculations. Calculations using the density functional theory (DFT) method gave optimum geometries for **1a–gBF$_2$** in which the parent **P1BF$_2$** unit in each adopts a nearly planar conformation. The calculated HOMO (E_H) and LUMO (E_L) energies of **1a–fBF$_2$** (*ca.* –6.8 and –2.9 eV, respectively) are not significantly different, while the respective E_H and E_L for **1gBF$_2$** are –6.96 and –3.04 eV (Table 1-3). By using time-dependent (TD)-DFT calculations, the wavelengths associated with the $S_0 \rightarrow S_1$ electronic transitions ($\lambda_{ET,S0\rightarrow S1}$) of **1a–gBF$_2$** are *ca.* 350 nm. The results also show that the oscillator strengths of the S_0–S_1 electronic transition ($f_{S0\rightarrow S1}$) of **1a–gBF$_2$** are *ca.* 1.

The results of single-point calculations for stacked molecules of **1a–gBF$_2$**, having X-ray-determined packing structures, were performed for the sake of elucidation of the intermolecular π-orbital interactions operating in crystal-packing structure. The results reveal that the E_L values for three stacked molecules are lower than those for the corresponding single molecule. On the other hand, the stacking-dependent trends of E_H values are not uniform. For example, the E_H values for three stacked molecules of **1aBF$_2$**, **1cBF$_2$**, and **1eBF$_2$** are lower than those for the respective single molecules, while the E_H values for three stacked molecules of **1dBF$_2$** and **1fBF$_2$** are higher than those for the corresponding single molecule. Furthermore, E_H of **1bBF$_2$** and **1gBF$_2$** are not dependent on the stacking manner.

The $\lambda_{ET,S0\rightarrow S1}$ values for three stacked molecules of **1a–gBF$_2$** calculated by using TD-DFT are longer than those for the respective single molecules (Figure 1-4 and Table 1-3). Especially,

$\lambda_{ET,S0\rightarrow S1}$ for **1dBF$_2$**, **1fBF$_2$**, and **1gBF$_2$** are remarkably shifted to longer wavelength by more than 30 nm when the number of molecules in the stack is increased from one to three, while $\lambda_{ET,S0\rightarrow S1}$ for three stacked molecules of **1bBF$_2$**, **1cBF$_2$**, and **1eBF$_2$** are longer than those for the respective single molecules by less than 20 nm. In addition, $\lambda_{ET,S0\rightarrow S1}$ for a single molecule and the three stacked molecules of **1aBF$_2$** are nearly the same. The respective $f_{S0\rightarrow S1}$ values calculated for the three stacked molecules of **1aBF$_2$**, **1bBF$_2$**, and **1cBF$_2$** are 3.15, 2.36, and 2.26, which are larger than those for the corresponding single molecules. On the other hand, the respective $f_{S0\rightarrow S1}$ values for the three stacked molecules of **1fBF$_2$** and **1gBF$_2$** are reduced to 0.24 and 0.00 when the number of molecules is increased from one to three. Finally, the $f_{S0\rightarrow S1}$ values for three stacked molecules of **1dBF$_2$** and **1eBF$_2$** are 1.03 and 1.29, respectively, which are almost identical to those for the respective single molecules.

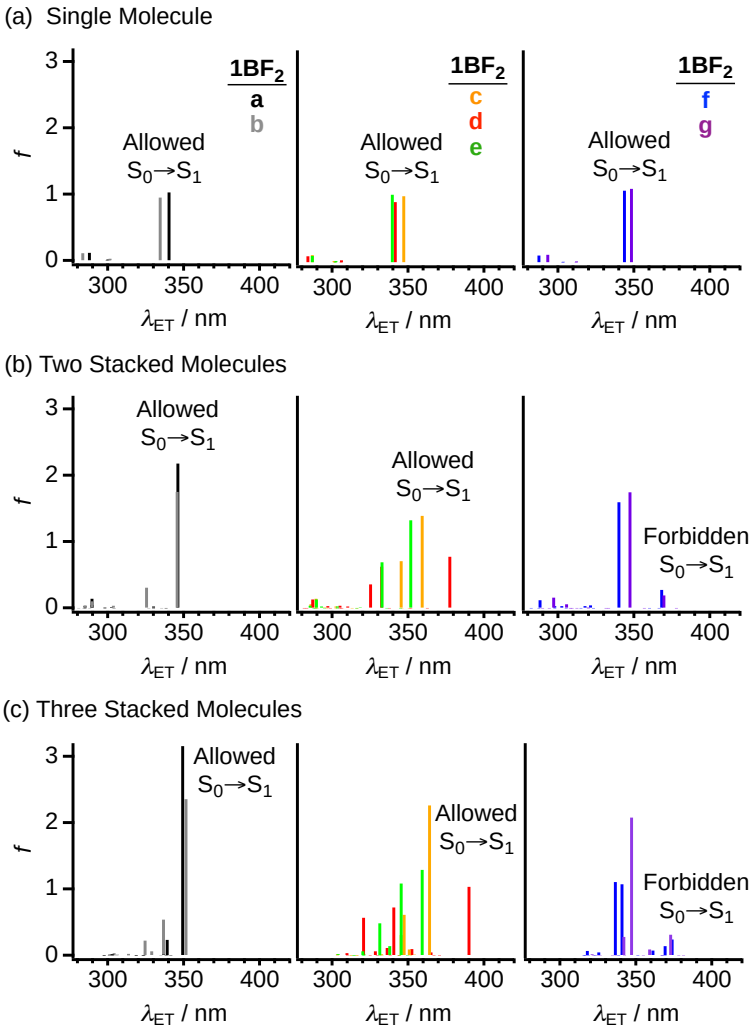

Figure 1-4. Electronic transitions estimated for (a) a single molecule and (b) two and (c) three stacked molecules of **1a–gBF$_2$** with geometries in crystals. Molecular geometries for TD-DFT calculations with B3LYP method and 6-311G(d) basis set were derived from X-ray-determined crystal-packing structures.

Table 1-3. Calculated E_H, E_L, $\lambda_{ET,S0\rightarrow S1}$, and $f_{S0\rightarrow S1}$ for a Single Molecule with Optimized Geometry and Two and Three Stacked Molecules of **1a–gBF$_2$** with Geometries in Crystals

	Single Molecule with Optimized Geometry[a]				Single Molecule with Geometry in Crystals[b,c]			
1BF$_2$	E_H / eV	E_L / eV	$\lambda_{ET,S0\rightarrow S1}$ / nm	$f_{S0\rightarrow S1}$	E_H / eV	E_L / eV	$\lambda_{ET,S0\rightarrow S1}$ / nm	$f_{S0\rightarrow S1}$
a	–6.77	–2.88	352	1.01	–6.76	–2.75	340	1.03
b	–6.79	–2.89	352	1.03	–6.80	–2.70	334	0.95
c	–6.81	–2.90	351	0.98	–6.74	–2.82	347	1.00
d	–6.85	–2.94	349	0.94	–6.80	–2.82	342	0.91
e	–6.83	–2.93	352	1.03	–6.77	–2.74	340	1.02
f	–6.80	–2.90	353	1.07	–6.72	–2.74	344	1.08
g	–6.96	–3.04	354	1.09	–6.88	–2.94	348	1.11

	Two Stacked Molecules with Geometry in Crystals[b,c]				Three Stacked Molecules with Geometry in Crystals[b,c]			
1BF$_2$	E_H / eV	E_L / eV	$\lambda_{ET,S0\rightarrow S1}$ / nm	$f_{S0\rightarrow S1}$	E_H / eV	E_L / eV	$\lambda_{ET,S0\rightarrow S1}$ / nm	$f_{S0\rightarrow S1}$
a	–6.86	–2.87	346	2.18	–6.88	–2.98	349	3.15
b	–6.87	–2.81	346	1.75	–6.83	–2.89	351	2.36
c	–6.77	–2.93	359	1.39	–6.82	–3.01	364	2.26
d	–6.66	–2.96	378	0.77	–6.63	–3.03	391	1.03
e	–6.84	–2.91	352	1.32	–6.89	–3.03	359	1.29
f	–6.62	–2.78	368	0.27	–6.59	–2.80	374	0.24
g	–6.85	–3.05	378	0.00	–6.86	–3.01	381	0.00

[a] Calculated using B3LYP method and a 6-311+G(d) basis set. [b] Calculated using B3LYP method and a 6-311G(d) basis set. [c] Molecular geometries were derived from X-ray-determined crystal-packing structures.

The transition dipole moments related to the $S_0\rightarrow S_1$ electronic transition ($\mu_{S0–S1}$) calculated for three stacked molecules of **1aBF$_2$**, **1bBF$_2$**, and **1cBF$_2$** are 15.3, 13.3, and 13.2 D, respectively (Figure 1-5). These values are larger than those determined for the respective single molecules. The $\mu_{S0\rightarrow S1}$ for three stacked molecules of **1dBF$_2$** and **1eBF$_2$** are observed to be 9.27 and 9.92 D, respectively, which are larger than those for the respective single molecules but much smaller than those for three stacked molecules of **1aBF$_2$**, **1bBF$_2$**, and **1cBF$_2$**. Moreover, the $\mu_{S0\rightarrow S1}$ values for three stacked molecules of **1fBF$_2$** and **1gBF$_2$** are calculated to be 4.35 and 0.16 D, respectively.

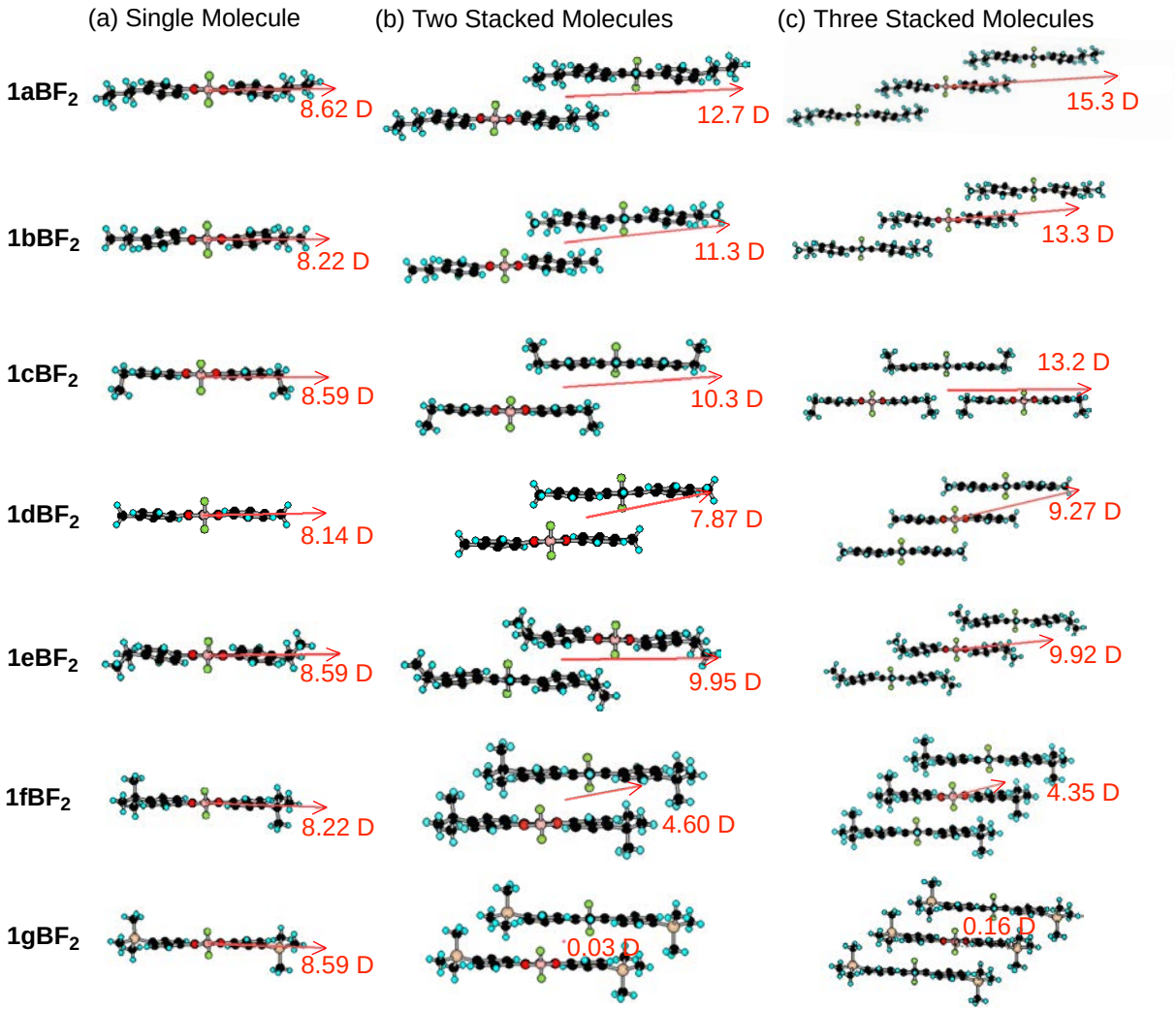

Figure 1-5. Transition dipole moments related to $S_0 \rightarrow S_1$ electronic transitions estimated for (a) a single molecule and (b) two and (c) three stacked molecules of **1a–gBF$_2$** with geometries in crystals. Molecular geometries for TD-DFT calculations with B3LYP method and 6-311G(d) basis set were derived from X-ray-determined crystal-packing structures.

The results of single-point calculations for a single molecule and two or three stacked molecules of **1a–gBF$_2$** show that molecules in some members of this group participate in intermolecular interactions involving LUMO (Figure 1-6). The LUMO of two and three stacked molecules of **1cBF$_2$**, **1dBF$_2$**, **1fBF$_2$**, and **1gBF$_2$** are comprised of a fusion of the LUMOs of the corresponding single molecules, while this fusion phenomenon is not displayed by the LUMO of two and three stacked molecules of **1aBF$_2$** and **1eBF$_2$**. Two stacked molecules of **1bBF$_2$** to a lesser degree display similar fusion of the LUMO at edge of the parent unit, while the three stacked molecules of this substance do not.

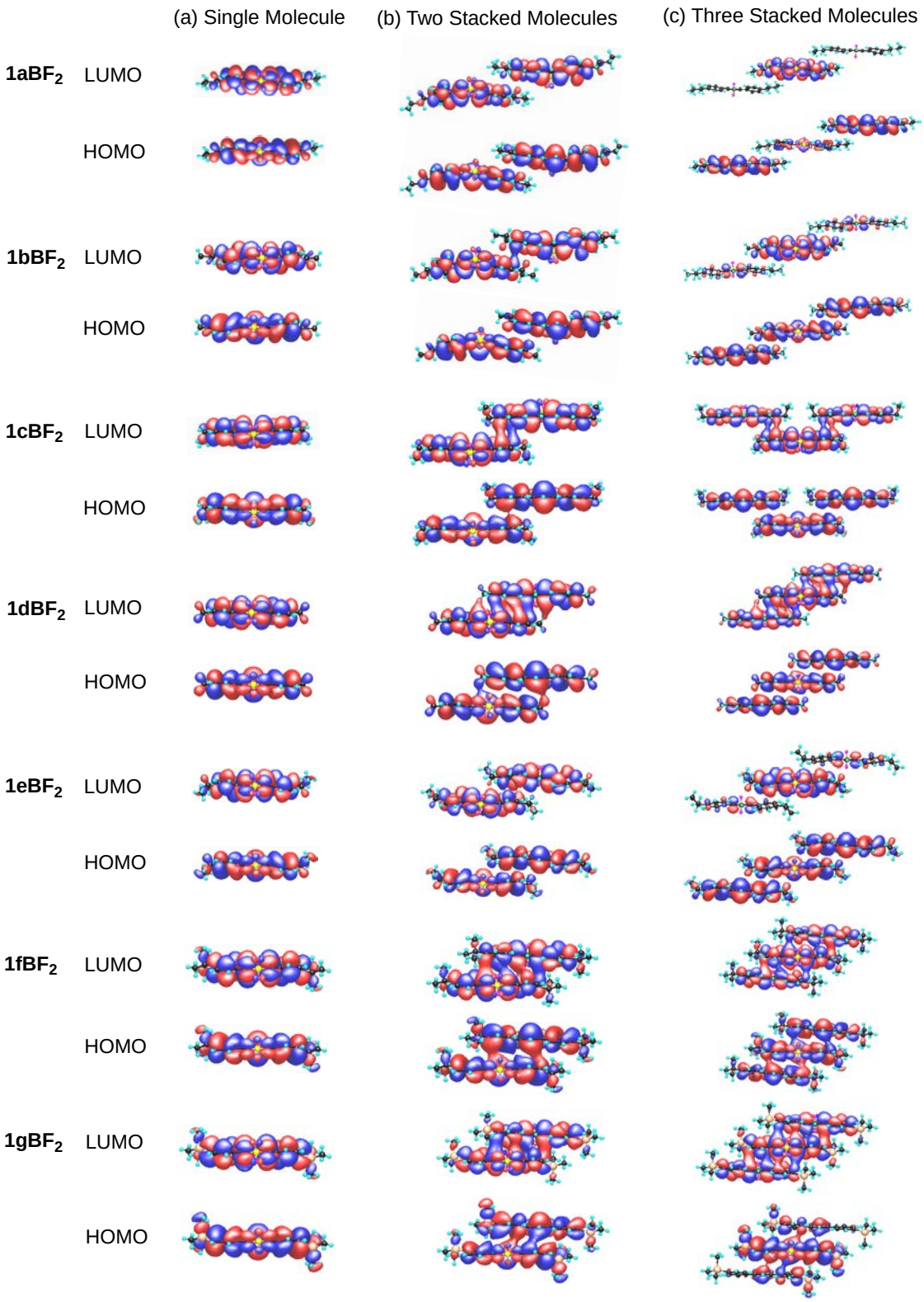

Figure 1-6. Distributions of the HOMOs and LUMOs estimated for (a) a single molecule and (b) two and (c) three stacked molecules of **1a–gBF$_2$** with geometries in crystals. Molecular geometries for single-point calculations with B3LYP method and 6-311G(d) basis set were derived from X-ray-determined crystal-packing structures. Isovalue = 0.01.

1.3 Discussion.

1.3.1. Electronic effects of substituents on absorption and FL properties. Substances **1a–gBF$_2$** have nearly identical $\lambda_{AB,S}$, $\lambda_{FL,S}$ and $\tau_{FL,S}$ values in CH_2Cl_2 solutions (Figure 1-2 and Table 1-2). Moreover, optimized structures of **1a–gBF$_2$** have almost the same $\lambda_{ET,S0–S1}$ values. These findings clearly show that the electronic effects of substituents on absorption and FL properties of **1a–gBF$_2$** in CH_2Cl_2 are negligible. It is reasonable to assume that electronic effects of substituents do not operate significantly in determining the FL properties of crystals of **1a–gBF$_2$**. Thus, differences observed in the FL properties of **1a–gBF$_2$** in their crystalline states likely originate from differences in the degree and/or manner of intermolecular stacking that alter intermolecular orbital interactions.

1.3.2. Crystal-packing structures governed by substituents. Molecules in crystals of **1a–gBF$_2$** are aligned to form continuous stacks in a diagonal direction, except for those of **1cBF$_2$** that stack in a lateral direction (Figure 1-1). Adjacent molecules in crystals of **1a–gBF$_2$** are stacked in three types of molecular arrays, classified as type I for **1a–bBF$_2$**, II for **1c–eBF$_2$** and III for **1f–gBF$_2$**. Because **1a–bBF$_2$** possess long alkyl substituents, individual molecules in crystals of these substances must be separated by relatively large distances. Consequently, molecules of **1a–bBF$_2$** representing type I crystals are stacked in a way that does not allow intermolecular π-orbital overlap of the parent units but does allow overlap of the alkyl chains and benzene moieties of adjacent molecules. In type II packing structures that crystals of small alkyl substituent containing **1c–eBF$_2$** adopt, π-stacking exists between benzene moieties of adjacent molecules (*B-on-B* overlap). Although, similar packing structures with *B-on-B* overlap is possible for molecules in crystals of **1f–gBF$_2$**, in fact severe steric repulsion would exist between bulky substituents and dihydrodioxaborinine moieties of adjacent molecules in this type of structure. Therefore, molecules in crystals of **1f–gBF$_2$** align in a type III fashion, in which the parent units do not overlap with the bulky substituents of the adjacent molecules and continuous π-overlap of benzene and dihydrodioxaborinine rings (*B-on-D* overlap) occurs.

1.3.3. Packing structure-dependent FL properties of crystals. The observation that crystals of **1a–gBF$_2$** have longer $\lambda_{FL,C}$ than $\lambda_{FL,S}$ observed for CH_2Cl_2 solutions of these substances probably is a consequence of *J*-aggregation.[1,2,34] The $\lambda_{FL,C}$ of **1c–eBF$_2$** are longer than those of **1a–bBF$_2$** by *ca.* 20–70 nm (Figure 1-3a and Table 1-2). While the $\lambda_{FL,C}$ of **1f–gBF$_2$** are also longer than those of **1a–bBF$_2$**, the differences between them are only less than 20 nm, suggesting that the crystals of

1f–gBF$_2$ resemble those of **1a–bBF$_2$** in λ_{FL}. However, the $\tau_{FL,C}$ of **1f–gBF$_2$** are more than three times as long as those of **1a–bBF$_2$**.

Importantly, the results show that the grouped FL properties of **1a–gBF$_2$** are well correlated with their grouped crystal-packing structures. Namely, crystals of **1c–eBF$_2$** that have the type II packing structure emit at long $\lambda_{FL,C}$ and **1f–gBF$_2$**, which have type III crystalline structures, have larger $\tau_{FL,C}$ values than do **1a–bBF$_2$** whose crystalline structures fall in the type I family. Judging from the fact that λ_{EX} associated with FL emission of **1c–gBF$_2$** are longer than those of **1a–bBF$_2$**, the differences in $\lambda_{FL,C}$ observed between **1a–gBF$_2$** are likely a consequence of the degree of *J*-aggregation, which takes place more effectively in crystals of **1c–gBF$_2$** than in those of **1a–bBF$_2$**. However, further consideration needs to be given to the differences in $\tau_{FL,C}$ of **1a–gBF$_2$**.

1.3.4. Orbital interactions operating in crystals and the corresponding excited species. The $\mu_{S0–S1}$, estimated for three stacked molecules of **1aBF$_2$** and **1bBF$_2$**, which are in the type I crystal packing group, have directions that are nearly parallel to the long axis of the molecules, and magnitudes (10 D) that are larger than those for the respective single molecules (Figure 1-5). The results suggest that $\mu_{S0–S1}$ for continuously stacked molecular arrays of **1aBF$_2$** and **1bBF$_2$** are simply the sum of $\mu_{S0–S1}$ for the individual molecules contained in the arrays.[2] Moreover, the HOMOs and LUMOs for two and three stacked molecules in the array of **1aBF$_2$** and **1bBF$_2$** are not fusions of the LUMOs of the corresponding single molecules. This finding indicates that π-orbital interactions between the parent units of molecules in each array is poor because of the packing features of type I crystals. Therefore, based on the results of calculations, we conclude that the emitting species formed in the type I crystals of **1aBF$_2$** and **1bBF$_2$** are excited monomer like. This proposal is consistent with the fact that crystals of **1aBF$_2$** and **1bBF$_2$** exhibit FL with $\tau_{FL,C}$ values that are similar to those for FL in CH_2Cl_2 solutions.

In contrast, different FL domains exist in the type II and III crystals as a result of the presence of molecular alignments that enable intermolecular π-orbital overlap of the parent units. The differences are reflected the distinct FL properties of **1c–gBF$_2$**, especially $\lambda_{FL,C}$ and $\tau_{FL,C}$, which differ significantly from those of **1aBF$_2$** and **1bBF$_2$**. Moreover, FL from **1cBF$_2$**, **1dBF$_2$**, and **1eBF$_2$**, which are in the type II crystal group, occurs at long $\lambda_{FL,C}$ which is reflective of excimer emission. However, $\tau_{FL,C}$ of crystals of **1cBF$_2$**, **1dBF$_2$**, and **1eBF$_2$** (3.5, 3.2, and 1.5 ns, respectively) are much shorter than $\tau_{FL,S}$ (*ca*. 50 ns) from the corresponding excimers formed in CH_2Cl_2 at high concentrations.[43,45] Moreover, $\tau_{FL,C}$ of type III crystals of **1fBF$_2$** and **1gBF$_2$** are longer (6.8 and 5.6 ns, respectively) than those of crystalline **1aBF$_2$** and **1bBF$_2$** (both 1.8 ns), while $\lambda_{FL,C}$ of these

crystals are nearly identical. Thus, it appears that the excited state species responsible for FL in type II and III crystals are neither excited monomer nor excimer like, but rather unique species created by unique intermolecular orbital interactions[47] arising from respective *B-on-B* and *B-on-D* overlap. We have termed the novel FL domains in these crystals "excited multimers" (Figure 1-7),[43] where "multimers" refer to ground-state species with "bonding" orbital interactions. A similar terminology "excited oligomer" has recently been proposed by Tohnai and coworkers,[9] but the phenomenon to which it refers is completely different because "excited multimers" is utilized to designate excited species with "bonding" orbital interactions, while the "excited oligomers" relates to excited species with "nonbonding" π-orbital interactions.

The magnitudes of $\mu_{S0\rightarrow S1}$ estimated for the three stacked molecules of **1dBF$_2$** and **1eBF$_2$** (type II) are nearly equal to those for the respective single molecules (Figure 1-5). Moreover, the directions of $\mu_{S0\rightarrow S1}$ for three stacked molecules of **1dBF$_2$** and **1eBF$_2$** are at oblique angles with respect to the long-axis direction of the molecule. These findings strongly suggest that $\mu_{S0\rightarrow S1}$ for the continuously stacked molecular arrays of **1dBF$_2$** and **1eBF$_2$** are reflective of intermolecular orbital interactions that enable formation of "excited multimers". Owing to the unique way in which molecules of **1cBF$_2$** pack in the crystalline state (type II), the $\mu_{S0\rightarrow S1}$ estimated for this substance cannot be categorized employing the terminology presented above. However, the existence of intermolecular orbital interactions in the crystalline molecular array of **1cBF$_2$** is strongly suggested by the LUMO fusion (Figure 1-6) seen for three stacked molecules in the array. The lack of LUMO fusion in two and three stacked molecules of **1eBF$_2$** is likely a consequence of the uniquely large D_F of this substance. However, the existence of intermolecular orbital interactions in crystals of **1eBF$_2$** is strongly suggested by the experimentally determined $\lambda_{FL,C}$ that is larger than those of **1aBF$_2$** and **1bBF$_2$**, which do not exhibit intermolecular orbital interactions in their crystalline state. In the cases of **1fBF$_2$** and **1gBF$_2$** (type III), the magnitudes of $\mu_{S0\rightarrow S1}$ estimated for three stacked molecules in the arrays are much smaller than those for the respective single molecules (Figure 1-5). Furthermore, significant fusion takes place in the HOMOs and LUMOs for the two and three stacked molecules of **1fBF$_2$** and **1gBF$_2$**. Consequently, continuously-stacked molecular arrays in the type III crystals of **1fBF$_2$** and **1gBF$_2$** enable intermolecular orbital interactions that are responsible for formation of "excited multimers".

The results of TD-DFT calculations reveal that $\lambda_{ET,S0\rightarrow S1}$ for single **1a–gBF$_2$** molecules are nearly identical (Figures 1-4 and 1-5 and Table 1-3). Although $\lambda_{ET,S0\rightarrow S1}$ values for **1aBF$_2$** and **1bBF$_2$** (type I) do not show marked changes when the number of molecules in the arrays increase, the values for **1cBF$_2$**, **1dBF$_2$**, and **1eBF$_2$** (type II) become larger upon increasing in the number of

molecules in the arrays. On the other hand, $f_{S0\rightarrow S1}$ values for these crystals become smaller with increasing the number of molecules, while $\lambda_{ET,S0\rightarrow S1}$ for **1fBF$_2$** and **1gBF$_2$** (type III) get longer.

The results indicate that $S_1\rightarrow S_0$ electronic transitions, arising from intermolecular π-orbital interactions caused by *B-on-B* overlap in type II crystals, are "allowed" while those resulting from *B-on-D* overlap in type III crystals are "forbidden" (Figure 1-7) probably due to symmetrical reason. This explanation is consistent with the fact that the type II crystals exhibit FL at longer $\lambda_{FL,C}$ as compared to those of type I crystals, and that type III crystals do not exhibit FL at long $\lambda_{FL,C}$. Since $S_1\rightarrow S_0$ electronic transitions are forbidden in the type III crystals, S_n–S_0 ($n \geq 2$) transitions should be dominant and may lead to FL emission with long $\tau_{FL,C}$ as compared with that observed in types I and II crystals.

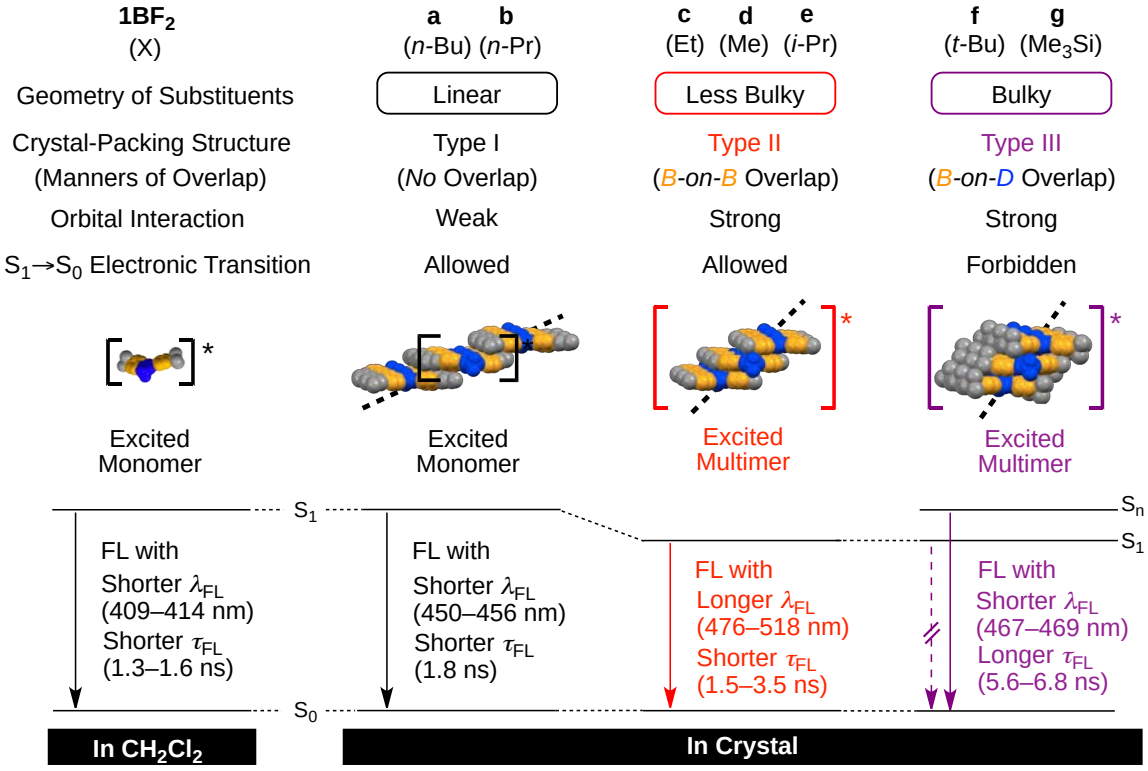

Figure 1-7. Summarized illustration for emissive species of **1a–gBF$_2$** in CH_2Cl_2 and in crystals, in which the strengths of orbital interactions and the $S_1\rightarrow S_0$ electronic transitions were governed by geometry of substituents.

Further evidence supporting the proposal that intermolecular π-orbital interactions govern FL properties in the crystalline state comes from the observation of a linear relationship between melting points and energies associated with $S_0\rightarrow S_1$ electronic transitions ($E_{ET,S0\rightarrow S1}$), which

converted from $\lambda_{ET,S0\rightarrow S1}$, estimated for three stacked **1a–gBF$_2$** molecules having X-ray determined geometries (Figure 1-8a). This relationship is in accord with the general tendency that melting points of organic compounds become higher when intermolecular attractive forces such as those arising from bonding orbital interactions become larger in crystals.[51–54] Thus the relationship suggests that intermolecular orbital interactions elongate $\lambda_{FL,C}$ of **1a–gBF$_2$**. Note that the S_0–S_1 electronic transitions in the molecular arrays of **1fBF$_2$** and **1gBF$_2$** do not contribute to the FL emission because they are forbidden. Thus, other allowed $S_n\rightarrow S_0$ transitions are involved in FL emission of **1fBF$_2$** and **1gBF$_2$**. In fact, melting points and experimentally determined energies for FL emission (E_{FL}), which converted from λ_{FL}, of **1a–gBF$_2$** also show linear relationships, except in the cases of **1fBF$_2$** and **1gBF$_2$** (Figure 1-8b).

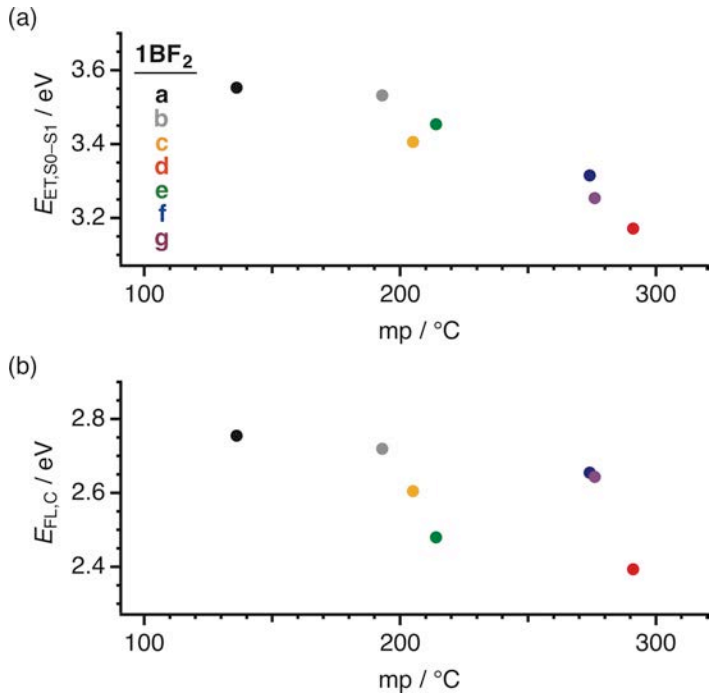

Figure 1-8. (a) The relationship between melting point (mp) and $E_{ET,S0\rightarrow S1}$ estimated for three stacked molecules of **1a–gBF$_2$** with geometries in crystals. (b) The relationship between melting point (mp) and $E_{FL,C}$ of **1a–gBF$_2$** in crystals. **1aBF$_2$** (black), **1bBF$_2$** (gray), **1cBF$_2$** (orange), **1dBF$_2$** (red), **1eBF$_2$** (green), **1fBF$_2$** (blue), and **1gBF$_2$** (purple).

1.4 Conclusion.

In the investigation described above, a relationship was observed between crystal-packing structures and FL properties of crystals of various alkyl- and silyl-substituted dibenzoylmethanatoboron difluoride derivatives **1a–gBF$_2$**. The results of this comprehensive study reveal that the crystal-packing structures of these substances can be classified into three groups referred to as type I, II, and III and that the structures are governed by the geometry of substituents. No intermolecular orbital overlap of the parent unit exists in type I crystals. In contrast, type II and type III crystals are comprised of continuously-stacked molecular arrays, with the former having "*B-on-B* overlap" and the latter "*B-on-D* overlap". FL properties of **1a–gBF$_2$** crystals are affected by the nature of their packing structures. The FL domain of type I crystals (**1a–bBF$_2$**) is excited monomer like, owing to the absence of intermolecular orbital interactions. As a result, type I crystals emit FL with $\lambda_{FL,C}$ of 450–456 nm and $\tau_{FL,C}$ of *ca*. 1.8 ns. The $\tau_{FL,C}$ values are similar to those at low concentrations in CH_2Cl_2 solutions. In the case of type II crystals (**1c–eBF$_2$**), *B-on-B* overlap results in formation of novel electronically excited molecular arrays that we term "excited multimers", which have allowed $S_1 \rightarrow S_0$ electronic transitions as a result of intermolecular orbital interactions in the ground state. As a result, type II crystals show FL with $\lambda_{FL,C}$ of 476–518 nm and $\tau_{FL,C}$ of 1.5–3.5 ns, which are larger values than those for the type I crystals. Finally, excited species of type III crystals (**1f–gBF$_2$**) having *B-on-D* overlap are longer lived "excited multimers", which are associated with $S_n \rightarrow S_0$ ($n \geq 2$) electronic transitions since $S_1 \rightarrow S_0$ transition is forbidden. Since $S_1 \rightarrow S_0$ electronic transition does not be involved in the FL emission, the $\lambda_{FL,C}$ of type III crystals are 467–469 nm, which are smaller values than those for type II crystals. Moreover, the participation of $S_n \rightarrow S_0$ transitions may lead to the FL with long τ_{FL} of 5.6–6.8 ns. The insight gained in this effort concerning the novel "excited multimer" FL domain could shed light on ways to manipulate of FL properties through changes in the nature of molecular aggregation.

1.5. Experimental Section.

1.5.1. General Methods. The melting points were measured using a Rigaku Thermo plus EVO II/DSC8230 differential scanning calorimeter. X-Ray diffraction data of crystals were collected using a Rigaku RAXIS-RAPID diffractometer and were refined using SHELX[48] and Yadokari-XG 2009[49] programs. UV–vis absorption spectra were recorded using a JASCO V-570 spectrophotometer. FL spectra were recorded using a JASCO FP-8500 spectrophotometer. The τ_{FL} values were determined using a HORIBA Jobin Yvon FluoroCube lifetime spectrofluorometer and analyzed by a DAS6 FL decay analysis software. The absolute Φ_{FL} values were determined by utilizing the integrating sphere method using a Hamamatsu Photonics C9920-02 absolute photoluminescence quantum yields measurement system.

NMR spectra in $CDCl_3$ were recorded on a Varian Mercury 300 spectrometer, operating at 300 and 75 MHz for ^{1}H NMR and ^{13}C NMR, respectively, where chemical shifts were determined with respect to tetramethylsilane (TMS) as an internal standard. Melting points were measured using a Yanaco MP-500 apparatus and are reported uncorrected. FAB-mass spectra were recorded on a JEOL JMS-700 spectrometer. Elemental analyses were performed at Kanazawa University, Advanced Science Research Center, Research Institute for Instrumental Analysis.

1.5.2. Materials. Diaroylmethanes **1a–gH** possessing two alkyl or trimethylsilyl groups were prepared using Claisen condensation reactions between the corresponding 4-substituted methyl benzoate and 4'-substituted acetophenone. Treatment of **1a–gH** with BF_3•OEt_2 gave the corresponding BF_2 complexes **1a–gBF$_2$**.[4345]

1.5.3. X-ray crystallographic analysis. [4345] X-Ray crystallographic analyses were performed on single crystals of **1a–gBF$_2$**, obtained by recrystallization from benzene or toluene. CCDC-1412042–1412048 contain the supplementary crystallographic data for this chapter. These data can be obtained free of charge from The Cambridge Crystallographic Data Centre via www.ccdc.cam.ac.uk/ data_request/cif.

Crystal data for $C_{23}H_{27}O_2BF_2$ (**1aBF$_2$**): Pale yellow needle, 1.0 × 0.5 × 0.2 mm^3, monoclinic, *C*2/*c*, a = 17.257(4), b = 6.9753(14), c = 17.605(4) Å, β= 93.218(5)°, V = 2115.8(8) Å^3, Z = 4, ρ_{calcd} = 1.206 g cm^{-3}, μ = 0.086 mm^{-1}, MoKα radiation, λ = 0.71070 Å, T = 298 K, 2θ_{max} = 55.0°, 9801 reflections measured, 2408 unique reflections, R_{int} = 0.103, 129 parameters, R_1 = 0.081 (I > 2σI), wR_2 = 0.234 (all data), CCDC-1412048.

Crystal data for $C_{21}H_{23}O_2BF_2$ (**1bBF$_2$**): Pale yellow needle, 0.8 × 0.3 × 0.2 mm^3, monoclinic, *C*2/*c*, a = 16.8514(15), b = 6.8712(5), c = 15.9835(17) Å, β = 93.412(4)°, V = 2115.8(8) Å^3, Z = 4, ρ_{calcd} = 1.281 g cm^{-3}, μ = 0.093 mm^{-1}, MoKα radiation, λ = 0.71070 Å, T = 298 K, 2θ_{max} = 55.0°, 8690 reflections measured, 2103 unique reflections, R_{int} = 0.068, 120 parameters, R_1 = 0.054 (I > 2σI), wR_2 = 0.186 (all data), CCDC-1412045.

Crystal data for $C_{19}H_{19}O_2BF_2$ (**1cBF$_2$**): Pale yellow platelet, 0.8 × 0.5 × 0.3 mm^3, orthorhombic, *Pnma*, a = 12.5719(12), b = 17.2908(19), c = 7.9430(7) Å, V = 1726.6(3) Å^3, Z = 4, ρ_{calcd} = 1.262 g cm^{-3}, μ = 0.094 mm^{-1}, MoKα radiation, λ = 0.71070 Å, T = 298 K, 2θ_{max} = 55.0°, 15820 reflections measured, 2014 unique reflections, R_{int} = 0.083, 118 parameters, R_1 = 0.086 (I > 2σI), wR_2 = 0.297 (all data), CCDC-1412047.

Crystal data for $C_{17}H_{15}O_2BF_2$ (**1dBF$_2$**): Yellow block, 0.8 × 0.6 × 0.2 mm^3, monoclinic, *C*2/*c*, a = 15.3182(13), b = 7.0036(5), c = 13.5957(10) Å, β = 95.440(2)°, V = 1452.01(19) Å^3, Z = 4, ρ_{calcd} = 1.386 g cm^{-3}, μ = 0.105 mm^{-1}, MoKα radiation, λ = 0.71070 Å, T = 93.1 K, 2θ_{max} = 55.0°, 6790 reflections measured, 1645 unique reflections, R_{int} = 0.026, 102 parameters, R_1 = 0.047 (I > 2σI), wR_2 = 0.149 (all data), CCDC-1412043.

Crystal data for $C_{21}H_{23}O_2BF_2$ (**1eBF$_2$**): Yellow needle, 1.0 × 0.5 × 0.1 mm^3, monoclinic, *C*2/*c*, a = 21.794(3), b = 7.0013(13), c = 16.034(3) Å, β = 129.094(6)°, V = 1898.9(5) Å^3, Z = 4, ρ_{calcd} = 1.246 g cm^{-3}, μ = 0.091 mm^{-1}, MoKα radiation, λ = 0.71070 Å, T = 298 K, 2θmax = 55.0°, 8709 reflections measured, 2150 unique reflections, R_{int} = 0.092, 121 parameters, R_1 = 0.070 (I > 2σI), wR_2 = 0.234 (all data), CCDC-412046.

Crystal data for $C_{23}H_{27}O_2BF_2$ (**1fBF$_2$**): Pale yellow platelet, 1.0 × 0.5 × 0.4 mm^3, monoclinic, *C*2/*c*, a = 29.455(3), b = 7.0775(6), c = 10.4286(8) Å, β = 104.082(3)°, V = 2108.7(3) Å^3, Z = 4, ρ_{calcd} = 1.210 g cm^{-3}, μ = 0.086 mm^{-1}, MoKα radiation, λ = 0.71070 Å, T = 298 K, 2θ_{max} = 55.0°,

9679 reflections measured, 2387 unique reflections, R_{int} = 0.074, 131 parameters, R_1 = 0.061 ($I > 2\sigma I$), wR_2 = 0.194 (all data), CCDC-1412042.

Crystal data for $C_{21}H_{27}O_2BF_2Si_2$ (**1gBF$_2$**): Pale yellow platelet, 0.6 × 0.3 × 0.1 mm^3, monoclinic, *C*2/*c*, a = 29.625(5), b = 7.2557(15), c = 10.8706(18) Å, β = 103.918(4)°, V = 2268.0(7) Å^3, Z = 4, ρ_{calcd} = 1.220 g cm^{-3}, μ = 0.186 mm^{-1}, MoKα radiation, λ = 0.71070 Å, T = 298 K, $2\theta_{max}$ = 55.0°, 10636 reflections measured, 2546 unique reflections, R_{int} = 0.194, 131 parameters, R_1 = 0.085 ($I > 2\sigma I$), wR_2 = 0.248 (all data), CCDC-1412044.

1.5.4. Measurement of UV–vis absorption and FL spectra. UV–vis absorption spectra were recorded on *ca.* 0.5 × 10^{-5} M CH_2Cl_2 solutions of **1a–gBF$_2$**. FL spectra were recorded using the same solutions and crystals of these substances with a λ_{EX} of 365 nm. Analyses of time-dependent changes of FL intensities in CH_2Cl_2 solutions and in crystals were carried out by using first- and multi-order fittings to give $\tau_{FL,S}$ and $\tau_{FL,C}$, respectively.

1.5.5. Computational Methods. Theoretical studies were carried out using a Gaussian 09 program.[47] Geometry optimizations for **1a–gBF$_2$** were carried out by DFT calculations with B3LYP method and a 6-311+G(d) basis set. Single-point calculations for a single molecule or two or three stacked molecules in geometries derived from X-ray-determined packing structures were performed using a 6-311G(d) basis set to determine E_H and E_L. Electronic transitions associated with a single molecule or two or three stacked molecules were estimated by using TD-DFT calculations with a 6-311G(d) basis set.

1.6. References and Notes.

1. Yan, D.; Evans, D. G. *Mater. Horiz.* **2014**, *1*, 46–57.
2. Kasha, M.; Rawls, H. R.; Ashraf El-Bayoumi, M. *Pure Appl. Chem.* **1965**, *11*, 371–392.
3. Birks, J. B. *Nature* **1967**, *214*, 1187–1190.
4. Jenekhe, S. A.; Osaheni, J. A. *Science* **1994**, *265*, 765–768.
5. Scholes, G. D.; Rumbles, G. *Nat. Mater.* **2006**, *5*, 683–696.
6. Jagtap, S. P.; Mukhopadhyay, S.; Coropceanu, V.; Brizius, G. L.; Brédas, J.-L.; Collard, D. M. *J. Am. Chem. Soc.* **2012**, *134*, 7176–7185.
7. Sekiguchi, R.; Takahashi, K.; Kawakami, J.; Sakai, A.; Ikeda, H.; Ishikawa, A.; Ohta, K.; Ito, S. *J. Org. Chem.* **2015**, *80*, 5092–5110.
8. Hong, Y.; Lam, J. W. Y.; Tang, B. Z. *Chem. Soc. Rev.* **2011**, *40*, 5361–5388.
9. Hinoue, T.; Shigenoi, Y.; Sugino, M.; Mizobe, Y.; Hisaki, I.; Miyata, M.; Tohnai, N. *Chem. Eur. J.* **2012**, *18*, 4634–4643.
10. Kitamura, C.; Abe, Y.; Ohara, T.; Yoneda, A.; Kawase, T.; Kobayashi, T.; Naito, H.; Komatsu, T. *Chem. Eur. J.* **2010**, *16*, 890–898.
11. Loudet, A.; Burgess, K. *Chem. Rev.* **2007**, *107*, 4891–4932.
12. Yamaguchi, S.; Wakamiya, A. *Pure Appl. Chem.* **2006**, *78*, 1413–1424.
13. Maeda, H.; Haketa, Y.; Nakanishi, T. *J. Am. Chem. Soc.* **2007**, *129*, 13661–13674.
14. Gorman, A.; Killoran, J.; O'Shea, C.; Kenna, T.; Gallagher, W. M.; O'Shea, D. F. *J. Am. Chem. Soc.* **2004**, *126*, 10619–10631.
15. Pérez-Ojeda, M. E.; Thivierge, C.; Martín, V.; Costela, Á.; Burgess, K.; García-Moreno, I. *Opt. Mater. Express* **2011**, *1*, 243–251.
16. Wang, L.; Zhang, Z.; Cheng, X.; Ye, K.; Li, F.; Wang, Y.; Zhang, H. *J. Mater. Chem. C* **2015**, *3*, 499–505.
17. Cheng, X.; Li, D.; Zhang, Z.; Zhang, H.; Wang, Y. *Org. Lett.* **2014**, *16*, 880–883.
18. Yoshii, R.; Hirose, A.; Tanaka, K.; Chujo, Y. *J. Am. Chem. Soc.* **2014**, *136*, 18131–18139.
19. Fedorenko, E. V.; Mirochnik, A. G.; Lvov, I. B.; Vovna, V. I. *Spectrochim. Acta Part A* **2014**, *120*, 119–125.
20. Nagai, A.; Kokado, K.; Nagata, Y.; Arita, M.; Chujo, Y. *J. Org. Chem.* **2008**, *73*, 8605–8607.
21. Nagai, A.; Kokado, K.; Nagata, Y.; Chujo, Y. *Macromolecules* **2008**, *41*, 8295–8298.
22. Zojer, E.; Wenseleers, W.; Halik, M.; Grasso, C.; Barlow, S.; Perry, J. W.; Marder, S. R.; Brédas, J.-L. *ChemPhysChem* **2004**, *5*, 982–988.
23. Ono, K.; Yoshikawa, K.; Tsuji, Y.; Yamaguchi, H.; Uozumi, R.; Tomura, M.; Taga, K.; Saito, K. *Tetrahedron* **2007**, *63*, 9354–9358.
24. Cogné-Laage, E.; Allemand, J.-F.; Ruel, O.; Baudin, J.-B.; Croquette, V.; Blanchard-Desce,

M.; Jullien, L. *Chem. Eur. J.* **2004**, *10*, 1445–1455.

25. Nagai, A.; Chujo, Y. *Chem. Lett.* **2010**, *39*, 430–435.
26. Sun, Y.; Rohde, D.; Liu, Y.; Wan, L.; Wang, Y.; Wu, W.; Di, C.; Yu, G.; Zhu, D. *J. Mater. Chem*. **2006**, *16*, 4499–4503.
27. Chow, Y. L.; Cheng, X.; Johansson, C. I. *J. Photochem. Photobiol. A: Chem.* **1991**, *57*, 247–255.
28. Mizuno, Y.; Yisilamu, Y.; Yamaguchi, T.; Tomura, M.; Funaki, T.; Sugihara, H.; Ono, K. *Chem. Eur. J.* **2014**, *20*, 13286–13295.
29. Morris, W. A.; Liu, T.; Fraser, C. L. *J. Mater. Chem. C* **2015**, *3*, 352–363.
30. Mirochnik, A. G.; Gukhman, E. V.; Karasev, V. E.; Zhikhareva, P. A. *Russ. Chem. Bull.* **2000**, *49*, 1024–1027.
31. Mirochnik, A. G.; Fedorenko, E. V.; Bukvetskii, B. V.; Karasev, V. E. *Russ. Chem. Bull.* **2005**, *54*, 1060–1062.
32. Mirochnik, A. G.; Fedorenko, E. V.; Karpenko, A. A.; Gizzatulina, D. A.; Karasev, V. E. *Luminescence* **2007**, *22*, 195–198.
33. Mirochnik, A. G.; Fedorenko, E. V.; Karasev, V. E. *Russ. Chem. Bull.* **2008**, *57*, 1190–1193.
34. Bukvetskii, B. V.; Fedorenko, E. V.; Mirochnik, A. G.; Beloliptsev, A. Y. *J. Struct. Chem.* **2012**, *53*, 73–81.
35. Safonov, A.; Bagaturyants, A. A.; Sazhnikov, V. *J. Phys. Chem. A* **2015**, *84*, 36–53.
36. Zhang, G.; Lu, J.; Sabat, M.; Fraser, C. L. *J. Am. Chem. Soc.* **2010**, *132*, 2160–2162.
37. Krishna, G. R.; Kiran, M. S. R. N.; Fraser, C. L.; Ramamurty, U.; Reddy, C. M. *Adv. Funct. Mater.* **2013**, *23*, 1422–1430.
38. Ito, F.; Sagawa, T. *RSC Advances* **2013**, *3*, 19785–19788.
39. Galer, P.; Korošec, R. C.; Vidmar, M.; Šket, B. *J. Am. Chem. Soc.* **2014**, *136*, 7383–7394.
40. Hu, J.; He, Z.; Wang, Z.; Li, X.; You, J.; Gao, G. *Tetrahedron Lett.* **2013**, *54*, 4167–4170.
41. Zhang, G.; Chen, J.; Payne, S. J.; Kooi, S. E.; Demas, J. N.; Fraser, C. L. *J. Am. Chem. Soc.* **2007**, *129*, 8942–8943.
42. Zhang, G.; Palmer, G. M.; Dewhirst, M. W.; Fraser, C. L. *Nat. Mater.* **2009**, *8*, 747–751.
43. The details have been described in (a) Chapter 2 and (b) Tanaka, M. Master thesis, Osaka Pref. Univ. (**2014**). [Tanaka, M. Ohta, E.; Sakai, A.; Yoshimoto, Y.; Mizuno, K. Ikeda, H. *Tetrahedron Lett.* **2013**, *54*, 4380–4384.].
44. Yoshimoto, Y. Master thesis, Osaka Pref. Univ. (**2010**).
45. Appendix Section for further details.
46. The $\tau_{FL,C}$ value (20–30 ns) of **1fBF$_2$** and **1gBF$_2$** in crystals were determined to arise from minor (<20%) transients. The contribution of the longer $\tau_{FL,C}$ transient increases when the

crystals are pulverized.

47. Brédas, J.-L.; Beljonne, D.; Coropceanu, V.; Cornil, J. *Chem. Rev.* **2004**, *104*, 4971–5004.
48. (a) Sheldrick, G. M.; SHELXS-97, Program for Crystal Structure Determination; University of Gçttingen (Germany), **1997**. (b) Sheldrick, G. M.; SHELXL-97, Program for the Refinement of Crystal Structure; University of Gçttingen (Germany), **1997**.
49. (a) Wakita, K.; Yadokari-XG, Software for Crystal Structure Analyses, **2001**. (b) C. Kabuto, S. Akine, T. Nemoto, E. Kwon, Release of Software (Yado- kari-XG 2009) for Crystal Structure Analyses, *J. Cryst. Soc. Jpn.* **2009**, *51*, 218–224.
50. Frisch, M. J.; Trucks, G. W.; Schlegel, H. B.; Scuseria, G. E.; Robb, M. A.; Cheeseman, J. R.; Scalmani, G.; Barone, V.; Mennucci, B.; Petersson, G. A.; Nakatsuji, H.; Caricato, M.; Li, X.; Hratchian, H. P.; Izmaylov, A. F.; Bloino, J.; Zheng, G.; Sonnenberg, J. L.; Hada, M.; Ehara, M.; Toyota, K.; Fukuda, R.; Hasegawa, J.; Ishida, M.; Nakajima, T.; Honda, Y.; Kitao, O.; Nakai, H.; Vreven, T.; Montgomery, J. A., Jr.; Peralta, J. E.; Ogliaro, F.; Bearpark, M.; Heyd, J. J.; Brothers, E.; Kudin, K. N.; Staroverov, V. N.; Kobayashi, R.; Normand, J.; Raghavachari, K.; Rendell, A.; Burant, J. C.; Iyengar, S. S.; Tomasi, J.; Cossi, M.; Rega, N.; Millam, J. M.; Klene, M.; Knox, J. E.; Cross, J. B.; Bakken, V.; Adamo, C.; Jaramillo, J.; Gomperts, R.; Stratmann, R. E.; Yazyev, O.; Austin, A. J.; Cammi, R.; Pomelli, C.; Ochterski, J. W.; Martin, R. L.; Morokuma, K.; Zakrzewski, V. G.; Voth, G. A.; Salvador, P.; Dannenberg, J. J.; Dapprich, S.; Daniels, A. D.; Farkas, Ö.; Foresman, J. B.; Ortiz, J. V.; Cioslowski, J.; Fox, D. J. *Gaussian 09, Revision D.01*, Gaussian, Inc., Wallingford CT, **2009**.
51. An, B.-K.; Lee, D.-S.; Lee, J.-S.; Park, Y.-S.; Song, H.-S.; Park, S. Y. *J. Am. Chem. Soc.* **2004**, *126*, 10232–10233.
52. Li, Z.; Shi, Y.; Liu, H.; Chen, F.; Zhang, Q. Wang, K. Fu, Q. *RSC Adv.* **2014**, *4*, 45234–45243.
53. Guckian, K. M.; Schweitzer, B. A.; Ren, R. X.-F.; Sheils, C. J.; Paris, P. L.; Tahmassebi, D. C.; Kool, E. T. *J. Am. Chem. Soc.* **1996**, *118*, 8182–8183.
54. Li, W.; Wu, X.; Qi, C.; Rong, H.; Gong, L. *J. Mol. Struct. (THEOCHEM)* **2010**, *942*, 19–25.

1.7. Appendix Section.

1.7.1. General. NMR spectra in $CDCl_3$ were recorded on a Varian Mercury 300 spectrometer, operating at 300 and 75 MHz for ^1H NMR and ^{13}C NMR, respectively, where chemical shifts were determined with respect to tetramethylsilane (TMS) as an internal standard. Melting points were measured using a Yanaco MP-500 apparatus and are reported uncorrected. FAB-mass spectra were recorded on a JEOL JMS-700 spectrometer. Elemental analyses were performed at Kanazawa University, Advanced Science Research Center, Research Institute for Instrumental Analysis.

1.7.2. Synthesis. Syntheses of **1aBF$_2$**, **1bBF$_2$**, **1cBF$_2$**, **1dBF$_2$**, **1fBF$_2$**, and **1gBF$_2$** were carried out according to Scheme 1-A1.[43,44]

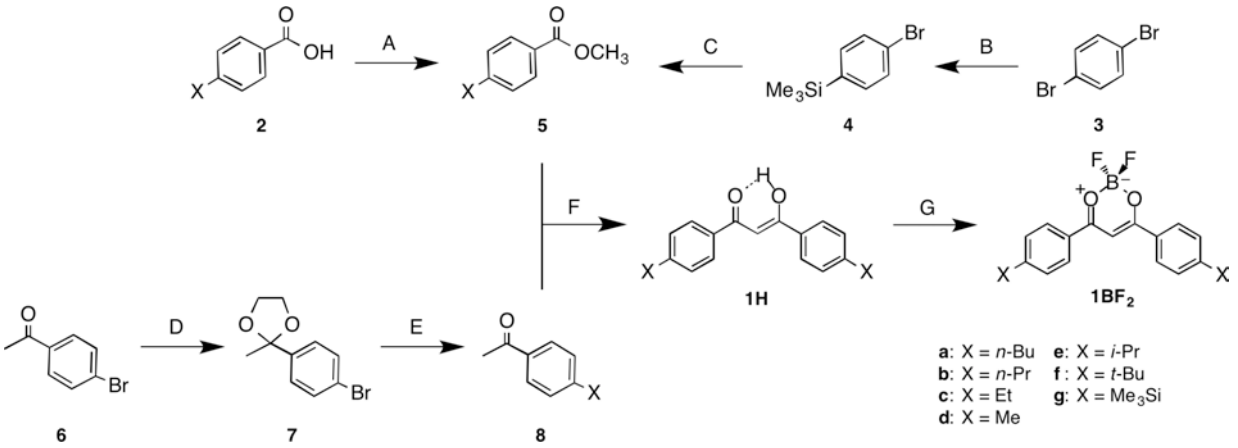

Scheme 1-A1. Syntheses of **1a–gBF$_2$**. **A**: MeOH, H_2SO_4 or 1) $SOCl_2$, 2) MeOH; **B**: 1) *n*-BuLi, 2) Me_3SiCl; **C**: 1) Mg, 2) $(MeO)_2CO$; **D**: ethylene glycol, TsOH; **E**: 1) Mg, 2) Me_3SiCl, 3) PPTS, H_2O; **F**: NaH; **G**: BF_3•OEt_2.

1.7.2.1. Synthesis of methyl 4-*n*-butylbenzoate (5a).[A1,A2] Conc. sulfuric acid (0.3 mL) was added into a solution of 4-*n*-butylbenzoic acid (**2a**, 2.67 g, 15 mmol) in methanol (9.0 mL, 0.23 mol) under argon atmosphere. After refluxing for 24 h, the reaction mixture was evaporated to dryness under a reduced pressure, and then the resultant residue was poured into iced water (10 mL). After extraction with diethyl ether, the combined organic extract was washed with brine, dried over Na_2SO_4, and filtered off from an insoluble fraction. The filtrate was evaporated to dryness under a reduced pressure, and the residue was distilled (89 °C/0.9 mmHg) to allow isolation of **5a** as colorless oil (2.32 g) in 81% yield. ^1H NMR (300 MHz, $CDCl_3$, 25°C, TMS): δ = 0.93 (t, J = 7.2 Hz, 3H), 1.35 (qt, J = 7.2, 7.8 Hz, 2H), 1.60 (tt, J = 7.8, 7.8 Hz, 2H), 2.96 (t, J = 7.8 Hz, 2H), 3.90 (s, 3H), 7.23 (AA'XX', J = 8.7, 2.1 Hz, 2H), 7.94 (AA'XX', J = 8.7, 2.1 Hz, 2H) ppm.

1.7.2.2. Synthesis of methyl 4-*n*-propylbenzoate (5b).[A1,A2] Colorless oil of **5b** (3.03 g) was obtained in 85% yield from 4-*n*-propylbenzoic acid (**2b**, 3.28 g, 20 mmol) by the similar procedure to preparation of **5a** and distillation under reduced pressure (76 °C/1.1 mmHg). ^{1}H NMR (300 MHz, $CDCl_3$, 25°C, TMS): δ = 0.94 (t, J = 7.5 Hz, 3H), 1.65 (qt, J = 7.5, 7.2 Hz, 2H), 2.64 (t, J = 7.2 Hz, 2H), 3.90 (s, 3H), 7.23 (AA'XX', J = 8.3, 1.7 Hz, 2H), 7.94 (AA'XX', J = 8.3, 1.7 Hz, 2H) ppm.

1.7.2.3. Synthesis of methyl 4-ethylbenzoate (5c).[A1,A3] Thionyl chloride (2.17 mL, 30 mmol) was added dropwise into 4-ethylbenzoic acid (**4c**, 0.90 g, 6.0 mmol) under argon atmosphere, then the resultant mixture was refluxed for 3 h. Remaining thionyl chloride was distilled away, then methanol (0.49 mL, 12 mmol) was added dropwise into the resultant mixture. After refluxing for 2 h, the resultant mixture was evaporated to dryness under reduced pressure. The residue was subjected to column chromatography (SiO_2, *n*-hexane) to afford **5c** as yellow oil (0.89 g) in 91% yield. ^{1}H NMR (300 MHz, $CDCl_3$, 25°C, TMS): δ = 1.25 (t, J = 7.7 Hz, 3H), 2.70 (q, J = 7.7 Hz, 3H), 3.90 (s, 3H), 7.25 (AA'XX', J = 8.3 Hz, 2H), 7.95 (AA'XX', J = 8.3 Hz, 2H) ppm.

1.7.2.4. Synthesis of 1-bromo-4-(trimethylsilyl)benzene (4).[A4] A solution of 1.6 M *n*-butyllithium in hexane (12.5 mL, 20 mmol) was added dropwise into a solution of 1,4-dibromobenzene (**3**, 4.72g, 20 mmol) in *tert*-butyl methyl ether (20 mL) under argon atmosphere at 0 °C. After stirring for 15 min at the same temperature and the successive addition of trimethylsilyl chloride (0.27 mL, 25 mmol), the resultant mixture was stirred continuously at 25 °C. After 1.5 h, the reaction was quenched by addition of a saturated aqueous solution of ammonium chloride (25 mL) and water (25 mL). After stirring for 15 min, the resultant mixture was extracted with diethyl ether. The combined organic extract was washed with brine, dried over Na_2SO_4, and filtered off from an insoluble fraction. The filtrate was evaporated to dryness under a reduced pressure, and the residue was distilled to allow isolation of **4** as colorless oil (3.20 g) in 70% yield. ^{1}H NMR (300 MHz, $CDCl_3$, 25°C, TMS): δ = 0.25 (s, 9H), 7.37 (AA'BB', J = 1.8 Hz, 2H), 7.48 (AA'BB', J = 1.8 Hz, 2H) ppm.

1.7.2.5. Synthesis of methyl 4-(trimethylsilyl)benzoate (5g).[A4] After heating a mixture of magnesium (607 mg, 25 mmol), iodine (3 mg, 0.02 mmol), 1,2-dibromoethane (35 μL), and THF (6 mL) for 5 min at 65 °C, a solution of **6** (4.72 g, 20 mmol) in THF (4 mL) was added dropwise into the mixture under argon atmosphere. After stirring for 30 min at the same temperature, a solution of dimethyl carbonate (5.65 mL, 60 mmol) in THF (2 mL) was added dropwise into the resultant mixture at –30 °C, and the mixture was continuously stirred for 1 h and for 16.5 h at 25 °C. After

addition of 10% aqueous HCl (10 mL) and the successive stirring for 10 min, the resultant mixture was extracted with *n*-heptane. The combined organic extract was washed with brine, dried over Na_2SO_4, and filtered off from an insoluble fraction. The filtrate was evaporated to dryness under a reduced pressure, and the residue was distilled at reduced pressure to allow isolation of **5g** as yellow oil (2.46 g) in 60% yield. ^{1}H NMR (300 MHz, $CDCl_3$, 25°C, TMS): δ = 0.28 (s, 9H), 3.92 (s, 3H), 7.59 (AA'XX', *J* = 8.3 Hz, 2H), 7.99 (AA'XX', *J* = 8.3 Hz, 2H) ppm.

1.7.2.6. Synthesis of 2-(4-bromophenyl)-2-methyl-1,3-dioxolane (7).[A5,A6] A solution of 4'-bromoacetophenone (**6**, 9.95 g, 50 mmol), ethylene glycol (6.00 mL, 0.11 mol), and *p*-toluenesulfonic acid monohydrate (595 mg, 3.1 mmol) in benzene (180 mL) was refluxed under argon atmosphere for 14 h with Dean–Stark apparatus. After addition of ethylene glycol (2.75 mL, 49 mmol), the resultant mixture was continuously refluxed for 36 h, and then extracted with diethyl ether. The combined organic extract was washed with aqueous sodium hydrogencarbonate aqueous solution and brine, dried over Na_2SO_4, and filtered off from an insoluble fraction. The filtrate was evaporated to dryness under a reduced pressure to give **7** as colorless needles (12.2 g) in 100% yield. ^{1}H NMR (300 MHz, $CDCl_3$, 25°C, TMS): δ = 1.63 (s, 3H), 3.75 (A_2X_2, *J* = 3.0, 7.0, 15.0 Hz, 2H), 4.03 (A_2X_2, *J* = 3.0, 7.0, 15.0 Hz, 2H), 7.35 (AA'XX', *J* = 7.0, 15.0 Hz, 2H), 7.45 (AA'XX', *J* = 7.0, 15.0 Hz, 2H) ppm.

1.7.2.7. Synthesis of 4'-(trimethylsilyl)acetophenone (8g).[A5,A6] Iodomethane (0.45 mL, 0.7 mmol) was added into a suspension of magnesium (1.25 g, 50 mmol) in THF (7.5 mL) under argon atmosphere. After stirring for 1.5 h at 90 °C, a solution of **7** (12.2 g, 50 mmol) in THF (100 mL) was slowly added dropwise into the resultant mixture. After a stirring for 1 h, trimethylsilyl chloride (6.5 mL, 51 mmol) was added dropwise into the reaction mixture. After stirring for 4 h at the same temperature, additional trimethylsilyl chloride (1.75 mL, 14 mmol) was added dropwise. After stirring for 1.5 h at the same temperature, the reaction mixture was allowed to cool 25 °C and was stirred for 11 h. After extraction with diethyl ether, the combined organic extract was washed with 1 M aqueous hydrochloric acid and brine, dried over Na_2SO_4, and filtered off from an insoluble fraction. The filtrate was evaporated to dryness under a reduced pressure, and the residue was subjected to column chromatography [SiO_2, *n*-hexane/$CHCl_3$ = 50/3 (v/v)] to give a mixture of 2-[4-(trimethylsilyl)phenyl]-2-methyl-1,3-dioxolane and 4'-(trimethylsilyl)acetophenone (**8g**). The mixture was dissolved into acetone (30 mL) and water (5 mL). Pyridinium *p*-toluenesulfonate (197 mg, 0.78 mmol) was added into the resultant solution, and the solution was stirred at for 2.5 h at 80 °C. The resultant mixture was allowed to cool to 25 °C and was additionally stirred for 2 days.

The resultant mixture was evaporated to dryness under reduced pressure, and the resultant residue was extracted with diethyl ether. The combined organic extract was washed with 1 M aqueous sodium carbonate solution, 0.1 M aqueous copper(II) sulfate solution, and brine, then was dried over Na_2SO_4, and was filtered off from an insoluble fraction. The filtrate was evaporated to dryness under a reduced pressure to give **8g** as yellow oil (8.88 g) in 92%. ^{1}H NMR (300 MHz, $CDCl_3$, 25°C, TMS): δ = 0.30 (s, 9H), 2.61 (s, 3H), 7.62 (AA'XX', *J* = 8.4 Hz, 2H), 7.91 (AA'XX', *J* = 8.4 Hz, 2H) ppm.

1.7.2.8. Synthesis of 1,3-bis(4-*n*-butylphenyl)propane-1,3-dione (1aH).[43,A1] A solution of **5a** (1.15 g, 6.0 mmol) and 4'-*n*-butylacetophenone (**8a**, 1.06 mL, 6.0 mmol) in THF (10.0 mL) was added dropwise (1–2 drops/s) into a solution of NaH (65% dispersion in mineral oil, 0.38 g, 9.5 mmol) in THF (7.5 mL) over 30 min at 20 °C. Then the reaction mixture was refluxed at 70 °C. After 24 h, the resultant mixture was poured into 10% aqueous HCl (25 mL), stirred for 30 min, and extracted with diethyl ether. The combined organic extract was washed with brine, dried over Na_2SO_4, and filtered off from an insoluble fraction. The filtrate was evaporated to dryness under a reduced pressure, and the residue was subjected to column chromatography [SiO_2, *n*-hexane/$CHCl_3$ = 5/1 (v/v)] and recrystallization from ethanol to allow isolation of **1aH** as pale yellow blocks (0.580 g) in 30% yield. m.p. 44–45 °C; ^{1}H NMR (300 MHz, $CDCl_3$, 25°C, TMS): δ = 0.94 (t, *J* = 7.2 Hz, 6H), 1.40 (qt, *J* = 7.2, 7.8 Hz, 4H), 1.64 (tt, *J* = 7.5, 7.8 Hz, 4H), 2.68 (t, *J* = 7.5 Hz, 4H), 6.81 (s, 1H), 7.29 (AA'XX', *J* = 8.4 Hz, 4H), 7.90 (AA'XX', *J* = 8.4. Hz, 4H), 16.9 (s, 1H) ppm.

1.7.2.9. Synthesis of 1,3-bis(4-*n*-propylphenyl)propane-1,3-dione (1bH).[A1] Colorless powder of **1bH** (1.81 g) was obtained in 19% yield from **5b** (5.34 g, 30 mmol) and 4'-*n*-propylacetophenone (**8b**, 6.0 mL, 36 mmol) by the similar procedure to preparation of **1aH** and recrystallization from methanol. mp 49–50 °C; ^{1}H NMR (300 MHz, $CDCl_3$, 25°C, TMS): δ = 0.96 (t, *J* = 7.5 Hz, 6H), 1.68 (qt, *J* = 7.5, 7.2 Hz , 4H), 2.66 (t, *J* = 7.2 Hz, 4H), 6.81 (s, 1H), 7.28 (AA'XX', *J* = 8.7 Hz, 4H), 7.90 (AA'XX', *J* = 8.7 Hz, 4H) ppm; ^{13}C NMR (75 MHz, $CDCl_3$, 25°C, TMS): δ = 14.14 (2C), 24.61 (2C), 38.33 (2C), 92.68 (1C), 127.14 (4C), 128.80 (4C), 133.14 (2C), 147.68 (2C), 185.27 (2C) ppm; GC-mass (EI, 70 eV): *m/z* (%) 308 (52) [M^+], 307 (77), 265 (18), 189 (17), 147 (100), 91 (50), 69 (58); IR (KBr): ν = 2954, 1700, 1685, 1654, 1560, 1522, 1183, 1015, 784 cm^{-1}; elemental analysis calcd (%) for $C_{24}H_{24}BF_2O_2$: C, 81.78; H, 7.84; Found: C, 81.70; H, 7.91.

1.7.2.10. Synthesis of 1,3-bis(4-ethylphenyl)propane-1,3-dione (1cH).[A7] Pale yellow plates of **1cH** (2.25 mg) was obtained in 94% yield from **5c** (1.97 g, 12 mmol) and 4'-ethylacetophenone (**8c**, 1.80 g, 12 mmol) by the similar reaction to preparation of **1aH** performed in THF and DMSO at 25 °C and a successive purification using column chromatography [SiO_2, *n*-hexane/$CHCl_3$ = 20/1 (v/v)] and recrystallization from methanol. mp 42–43 °C; ^{1}H NMR (300 MHz, $CDCl_3$, 25°C, TMS): δ = 1.28 (t, *J* = 7.8 Hz, 6H), 2.73 (q, *J* = 7.8 Hz, 4H), 6.82 (s, 1H), 7.31 (AA'XX', *J* = 8.1 Hz, 4H), 7.91 (AA'XX', *J* = 8.1 Hz, 4H) ppm.

1.7.2.11. Synthesis of 1,3-bis(4-methylphenyl)propane-1,3-dione (1dH).[43,A8] Beige needles of **1dH** (2.82 g) was obtained in 74% yield from methyl 4-methylbenzoate (**5d**, 2.48 g, 17 mmol) and acetophenone (**8d**, 2.01 g, 15 mmol) by the similar reaction to preparation of **1aH** performed in THF and DMSO at 25 °C and a successive recrystallization from ethanol. m.p. 120–122 °C; ^{1}H NMR (300 MHz, $CDCl_3$, 25°C, TMS): δ = 2.33 (weak s), 2.39 (s, 6H), 3.70 (weak q), 4.54 (weak s), 6.78 (s, 1H), 7.21–7.27 (m, 4H), 7.80–7.95 (m, 4H) ppm.

1.7.2.12. Synthesis of 1,3-bis(4-isopropylbenzoyl)propane-1,3-dione (1eH).[A9,A10] Yellow oil of **1eH** (2.82 g) was obtained in 49% yield from methyl 4-isopropylbenzoate (**5e**, 1.07 g, 6.0 mmol) and 4'-isopropylacetophenone (**8e**, 1.17 g, 7.2 mmol) by the similar reaction to preparation of **1aH** performed in THF at 25 °C and a successive purification using column chromatography [SiO_2, *n*-hexane/$CHCl_3$ = 50/3 (v/v)] and , followed by distillation under reduced pressure (250 ºC, 17 mmHg). ^{1}H NMR (300 MHz, $CDCl_3$) δ = 1.29 (d, *J* = 6.9 Hz, 12H), 2.98 (m, *J* = 6.9 Hz, 2H), 6.81 (s, 1H), 7.33 (AA'XX', *J* = 8.4 Hz, 4H), 7.91 (AA'XX', *J* = 8.4 Hz, 4H) ppm.

1.7.2.13. Synthesis of 1,3-bis[4-(1,1-dimethylethyl)phenyl]propane-1,3-dione (1fH).[A1,A8] Colorless plates of **1fH** (1.39 g) was obtained in 69% yield from methyl 4-*t*-butylbenzoate (**5f**, 1.14 mL, 6.0 mmol) and 4'-*t*-butylacetophenone (**8f**, 1.14 mL, 6.0 mmol) by the similar reaction to preparation of **1aH** performed in THF and DMSO at 25 °C and a successive purification using column chromatography [SiO_2, *n*-hexane/diethyl ether = 20/1 (v/v)] and recrystallization from ethanol. m.p. 105–106 °C; ^{1}H NMR (300 MHz, $CDCl_3$, 25°C, TMS): δ = 1.36 (s, 18H), 6.81 (s, 1H), 7.49 (AA'XX', *J* = 8.4 Hz, 4H), 7.92 (AA'XX', *J* = 8.4 Hz, 4H) ppm.

1.7.2.14. Synthesis of 1,3-bis[4-(trimethylsilyl)phenyl]propane-1,3-dione (1gH).[A1] Colorless needles of **1gH** (0.823 g) was obtained in 45% yield from **5g** (1.04 g, 5.0 mmol) and **8g** (0.96 g, 5.0 mmol) by the similar reaction to preparation of **1aH** performed in THF and DMSO at 25 °C and a successive purification using column chromatography [SiO_2, *n*-hexane/diethyl ether = 50/3 (v/v)] and recrystallization from *n*-hexane. m.p. 75–78 °C; ^{1}H NMR (300 MHz, $CDCl_3$, 25°C, TMS): δ = 0.33 (s, 18H), 6.86 (s, 1H), 7.64 (AA'XX', *J* = 8.1 Hz, 4H), 7.94 (AA'XX', *J* = 8.1 Hz, 4H) ppm; ^{13}C NMR (75 MHz, $CDCl_3$, 25°C, TMS): δ = 0.86 (2C), 93.35, 126.07 (4C), 133.52 (4C), 135.69 (2C), 146.25 (2C), 185.58 (2C) ppm; IR (KBr) ν = 2953, 1599, 1310, 1248, 1191, 1108, 1086, 828, 756, 661 cm^{-1}; GC-mass (EI, 70 eV): *m/z* 368 (54) [M^+], 367 (42) [M^+–H], 353 (100) [M^+–Me], 295 (83) [M^+–TMS], 177 (42) [$TMSC_6H_4CO^+$], 169 (62).

1.7.2.15. Synthesis of bis(4-*n*-butylbenzoyl)methanatoboron difluoride (1aBF$_2$).[23,43] A solution of **1aH** (320 mg, 1.0 mmol) and BF_3•OEt_2 (0.15 mL, 1.2 mmol) in benzene (3 mL) was stirred under argon atmosphere at room temperature for 15 h. The resultant mixture was concentrated under reduced pressure, and the residue was recrystallized from benzene to give **1aBF$_2$** as pale yellow needles (330 mg) in 90% yield. m.p. 135–136 °C; ^{1}H NMR (300 MHz, $CDCl_3$, 25°C, TMS): δ = 0.95 (t, *J* = 7.5 Hz, 6H), 1.38 (qt, *J* = 7.5, 7.2 Hz, 4H), 1.65 (tt, *J* = 7.5, 7.2 Hz, 4H), 2.72 (t, *J* = 7.5 Hz, 4H), 7.13 (s, 1H), 7.36 (AA'XX', *J* = 8.3 Hz, 4H), 8.07 (AA'XX', *J* = 8.3 Hz, 4H) ppm; ^{13}C NMR (75 MHz, $CDCl_3$, 25°C, TMS): δ = 14.06 (2C), 22.49 (2C), 33.26 (2C), 36.09 (2C), 92.83, 129.165 (4C), 129.42 (4C), 129.64 (2C), 151.77 (2C), 182.60 (2C) ppm; FAB-mass (NBA): *m/z* 384 [M^+]; IR (KBr): ν = 3149, 2925, 1701, 1654, 1534, 1375, 1312, 1014, 820, 745, 599, 566 cm^{-1}; elemental analysis calcd (%) for $C_{23}H_{27}BF_2O_2$: C, 71.89; H, 7.08; Found: C, 71.92; H, 7.21.

1.7.2.16. Synthesis of bis(4-*n*-propylbenzoyl)methanatoboron difluoride (1bBF$_2$).[23,43] Pale yellow needles of **1bBF$_2$** (820 mg) was obtained in 77% yield from **1bH** (924 mg, 3.0 mmol) by the similar reaction to preparation of **1aBF$_2$** and a successive recrystallization from toluene. m.p. 192–193 °C; ^{1}H NMR (300 MHz, $CDCl_3$, 25°C, TMS): δ = 0.97 (t, *J* = 7.4 Hz, 6H), 1.70 (qt, *J* = 7.4, 7.7 Hz, 4H), 2.70 (t, *J* = 7.7 Hz, 4H), 7.13 (s, 1H), 7.35 (AA'XX', *J* = 8.7 Hz, 4H), 8.06 (AA'XX', *J* = 8.7 Hz, 4H) ppm; ^{13}C NMR (75 MHz, $CDCl_3$, 25°C, TMS): δ = 13.91 (2C), 24.30 (2C), 38.36 (2C), 92.83 (1C), 129.142 (4C), 129.46 (4C), 129.67 (2C), 151.50 (2C), 182.59 (2C) ppm; FAB-mass (NBA): *m/z* 356 [M^+]; IR (KBr): ν = 2957, 1700, 1684, 1653, 1559, 1499, 1375, 1045, 1014 cm^{-1}; elemental analysis calcd (%) for $C_{21}H_{24}BF_2O_2$: C, 70.81; H, 6.51; Found: C, 70.79; H, 6.65.

1.7.2.17. Synthesis of bis(4-ethylbenzoyl)methanatoboron difluoride (1cBF$_2$).[24,43] Pale yellow plates of **1cBF$_2$** (856 mg) was obtained in 90% yield from **1cH** (841 mg, 3.0 mmol) by the similar reaction to preparation of **1aBF$_2$** and a successive recrystallization from toluene. mp 204–205 °C; ^{1}H NMR (300 MHz, $CDCl_3$, 25°C, TMS): δ = 1.30 (t, J = 7.7 Hz, 6H), 2.77 (q, J = 7.7 Hz, 4H), 7.14 (s, 1H), 7.38 (AA'XX', J = 8.3 Hz, 4H), 8.08 (AA'XX', J = 8.3 Hz, 4H) ppm; ^{13}C NMR (75 MHz, $CDCl_3$, 25°C, TMS): δ = 15.8 (2C), 29.7 (2C), 93.0, 128.9 (4C), 129.3 (4C), 129.8 (2C), 152.8 (2C), 182.5 (2C) ppm; IR (KBr): ν = 1539, 1500, 1373, 1191, 1132, 1039 cm^{-1}; FAB-mass (NBA): *m/z* 328 (M^+); elemental analysis calcd (%) for $C_{19}H_{19}BF_2O_2$: C, 69.54; H, 5.84; Found: C, 69.39; H, 5.90.

1.7.2.18. Synthesis of bis(4-methylbenzoyl)methanatoboron difluoride (1dBF$_2$).[S2,A11] Yellow blocks of **1dBF$_2$** (632 mg) was obtained in 84% yield from **1dH** (630 mg, 2.50 mmol) by the similar reaction to preparation of **1aBF$_2$** and a successive recrystallization from toluene. mp 291–293 °C; ^{1}H NMR (300 MHz, $CDCl_3$) δ = 2.47 (s, 6H), 7.12 (s, 1H), 7.34 (AA'XX', J = 7.5 Hz, 4H), 8.03 (AA'XX', J = 7.5 Hz, 4H) ppm.

1.7.2.19. Synthesis of bis(4-isopropylbenzoyl)methanatoboron difluoride (1eBF$_2$).[23,24] Pale yellow needles of **1eBF$_2$** (375 mg) was obtained in 94% yield from **1eH** (460 mg, 1.5 mmol) by the similar reaction to preparation of **1aBF$_2$** and a successive recrystallization from benzene. mp = 214–215 ºC; ^{1}H NMR (300 MHz, $CDCl_3$) δ = 1.30 (d, J = 6.9 Hz, 12H), 3.01 (sep, J = 6.9 Hz , 2H), 7.13 (s, 1H), 7.39 (AA'XX', J = 8.4 Hz, 4H), 8.07 (AA'XX', J = 8.4 Hz, 4H); ^{13}C NMR (75 MHz, $CDCl_3$) δ = 23.90 (4C), 34.81 (2C), 92.83, 127.31 (4C), 129.11 (4C), 129.66 (2C), 157.18 (2C), 182.27 (2C); IR (KBr): ν = 2966, 1701, 1685, 1654, 1560, 1380, 1041, 822, 701, 557 cm^{-1}; FAB-mass (NBA): *m/z* 356 (M^+); elemental analysis calcd (%) for $C_{21}H_{24}BF_2O_2$: C, 70.81; H, 6.51. Found: C, 70.54; H, 6.63.

1.7.2.20. Synthesis of bis[4-(1,1-dimethylethyl)benzoyl]methanatoboron difluoride (1fBF$_2$).[24,A11] Pale yellow plates of **1fBF$_2$** (740 mg) was obtained in 96% yield from **1fH** (670 mg, 2.0 mmol) by the similar reaction to preparation of **1aBF$_2$** and a successive recrystallization from toluene. m.p. 272–274 °C; ^{1}H NMR (300 MHz, $CDCl_3$, 25°C, TMS): δ = 1.37 (s, 18H), 7.19 (s, 1H), 7.56 (AA'XX', J = 8.7 Hz, 4H), 8.08 (AA'XX', J = 8.7 Hz, 4H) ppm.

1.7.2.21. Synthesis of bis[4-(trimethylsilyl)benzoyl]methanatoboron difluoride (1gBF$_2$).[38] Pale yellow plates of **1gBF$_2$** (86 mg) was obtained in 94% yield from **1gH** (74 mg, 0.22 mmol) by the similar reaction to preparation of **1aBF$_2$** and a successive recrystallization from benzene. m.p. 275–277 °C; ^{1}H NMR (300 MHz, $CDCl_3$, 25°C, TMS): δ = 0.32 (s, 18H), 7.20 (s, 1H), 7.70 (AA'XX', J = 7.7 Hz, 4H), 8.09 (AA'XX', J = 7.7 Hz, 4H) ppm; ^{13}C NMR (75 MHz, $CDCl_3$, 25°C, TMS): δ = –0.97 (2C), 93.55, 127.61 (4C), 132.04 (2C), 133.93 (4C), 150.48 (2C), 183.13 (2C) ppm; IR (KBr): ν = 1557, 1402, 1373, 1248, 1084, 1043, 839, 804, 756, 661 cm^{-1}; FAB-mass (NBA): *m/z* 416 [M^+]; HR-mass Calcd. for $C_{21}H_{27}BF_2O_2Si_2$: 416.1611; Found: 416.1614.

1.7.3. NMR Spectra.

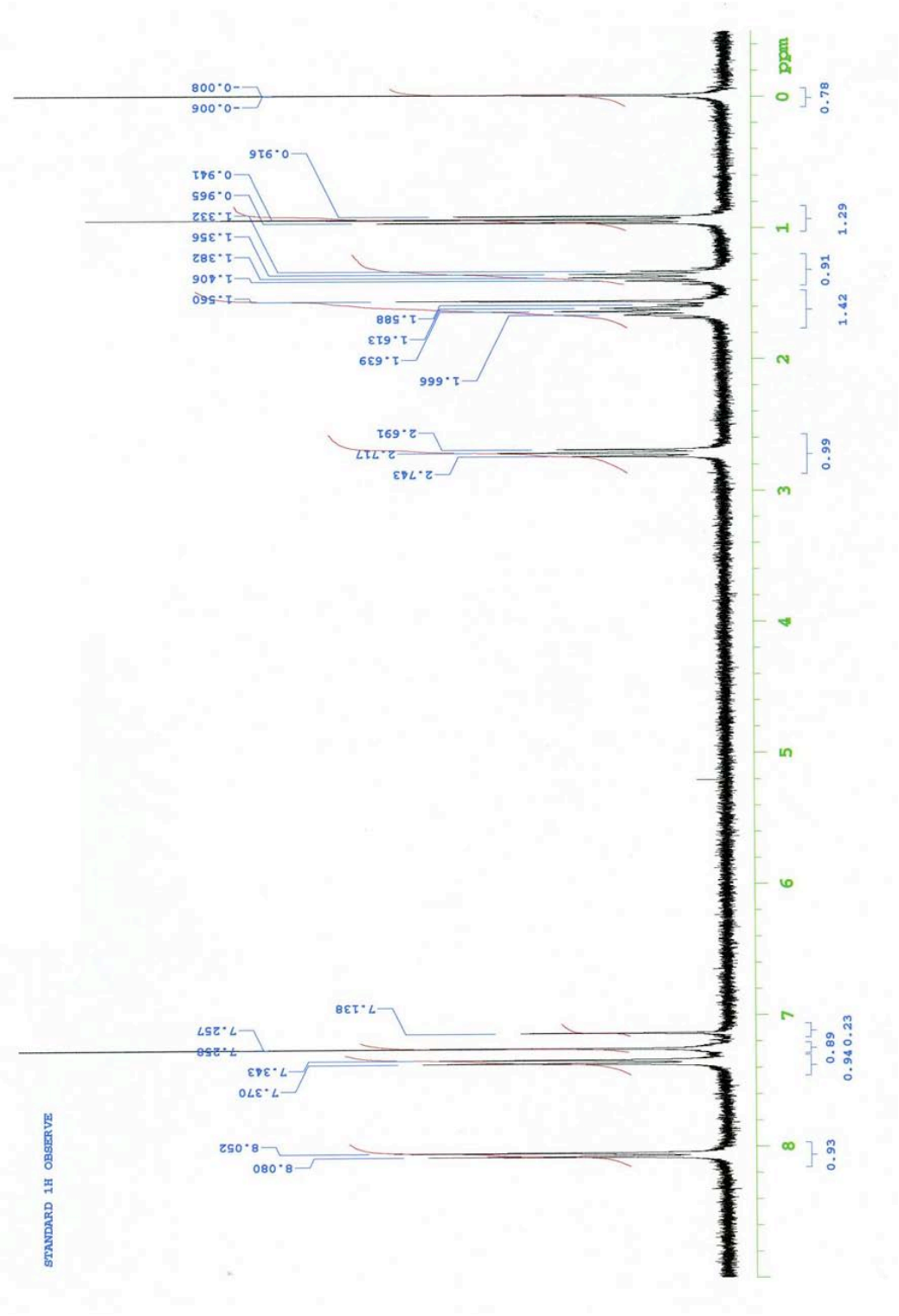

Figure 1-A1. ^{1}H NMR spectrum of **1aBF$_2$** in $CDCl_3$.

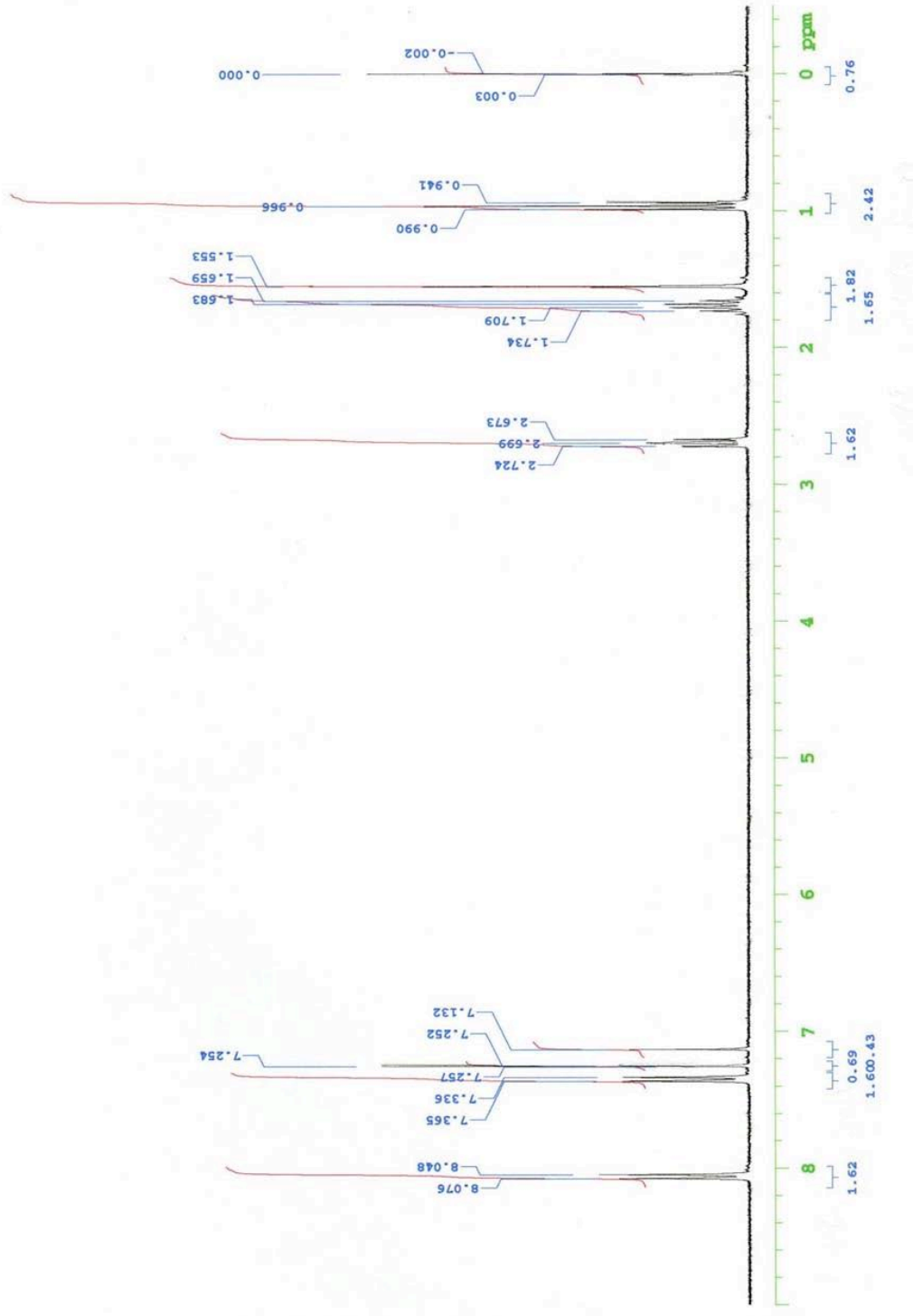

Figure 1-A2. ^{1}H NMR spectrum of **1bBF$_2$** in $CDCl_3$.

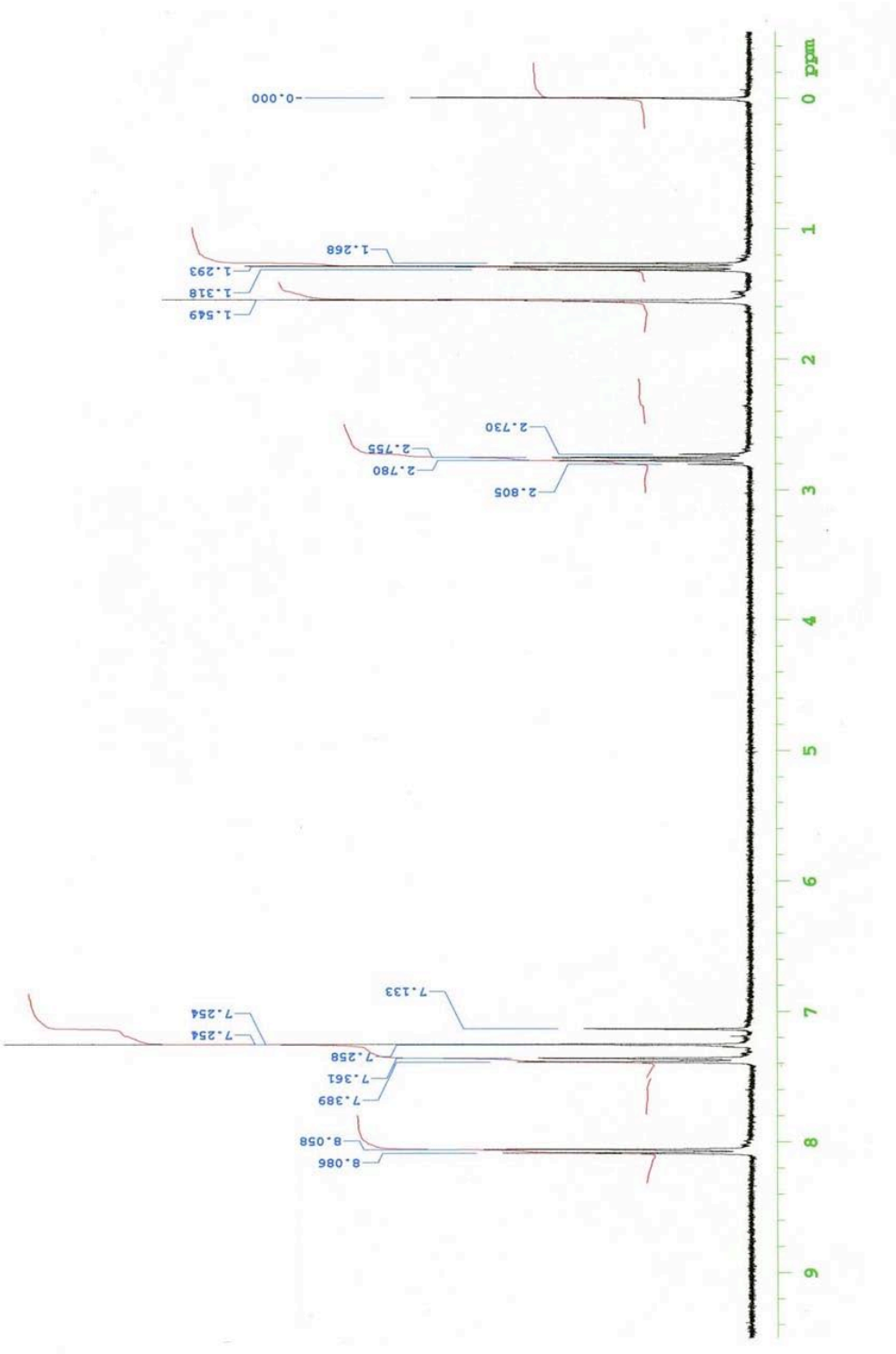

Figure 1-A3. ^{1}H NMR spectrum of **1cBF$_2$** in $CDCl_3$.

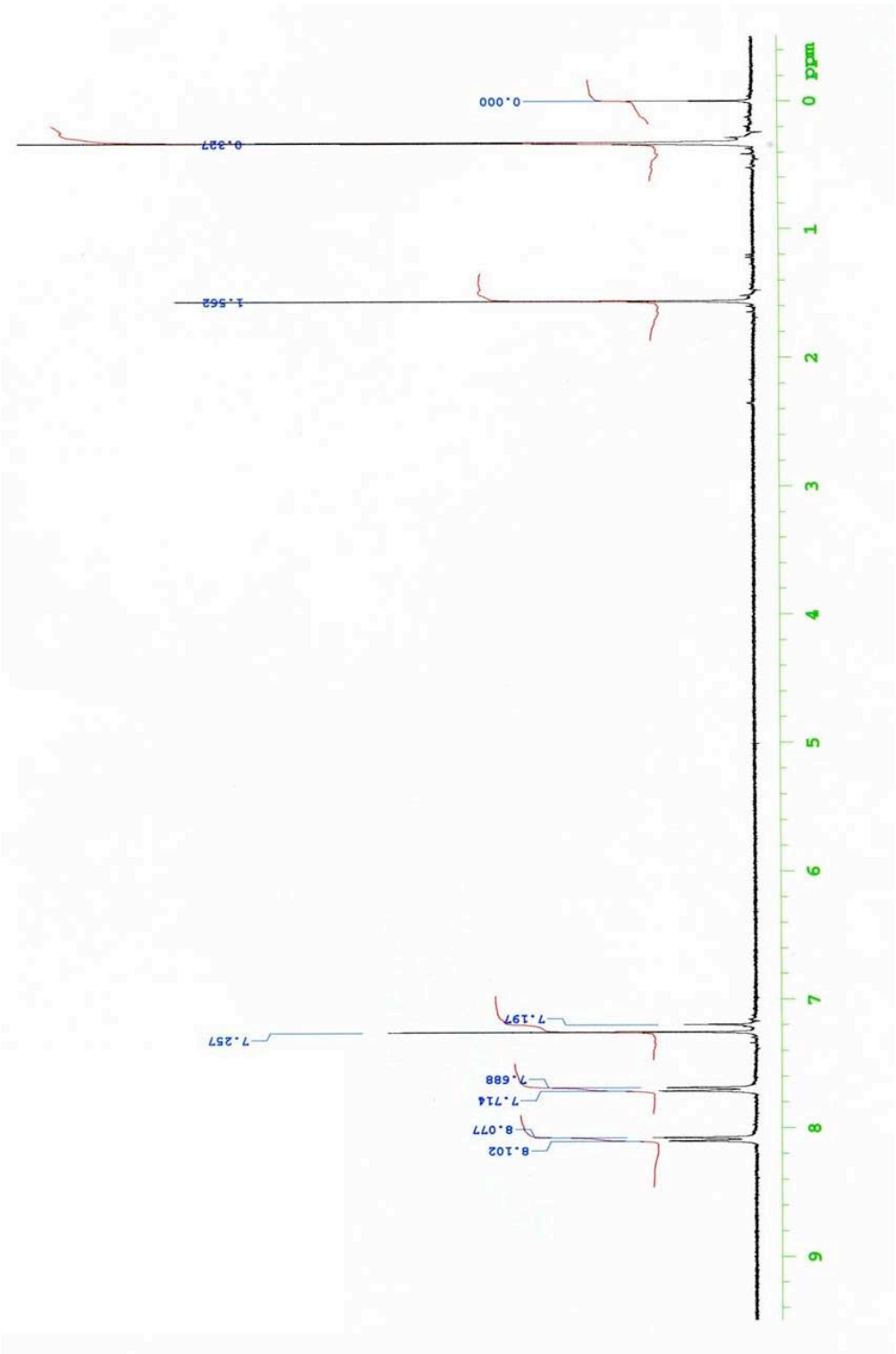

Figure 1-A4. ^{1}H NMR spectrum of **1gBF$_2$** in $CDCl_3$.

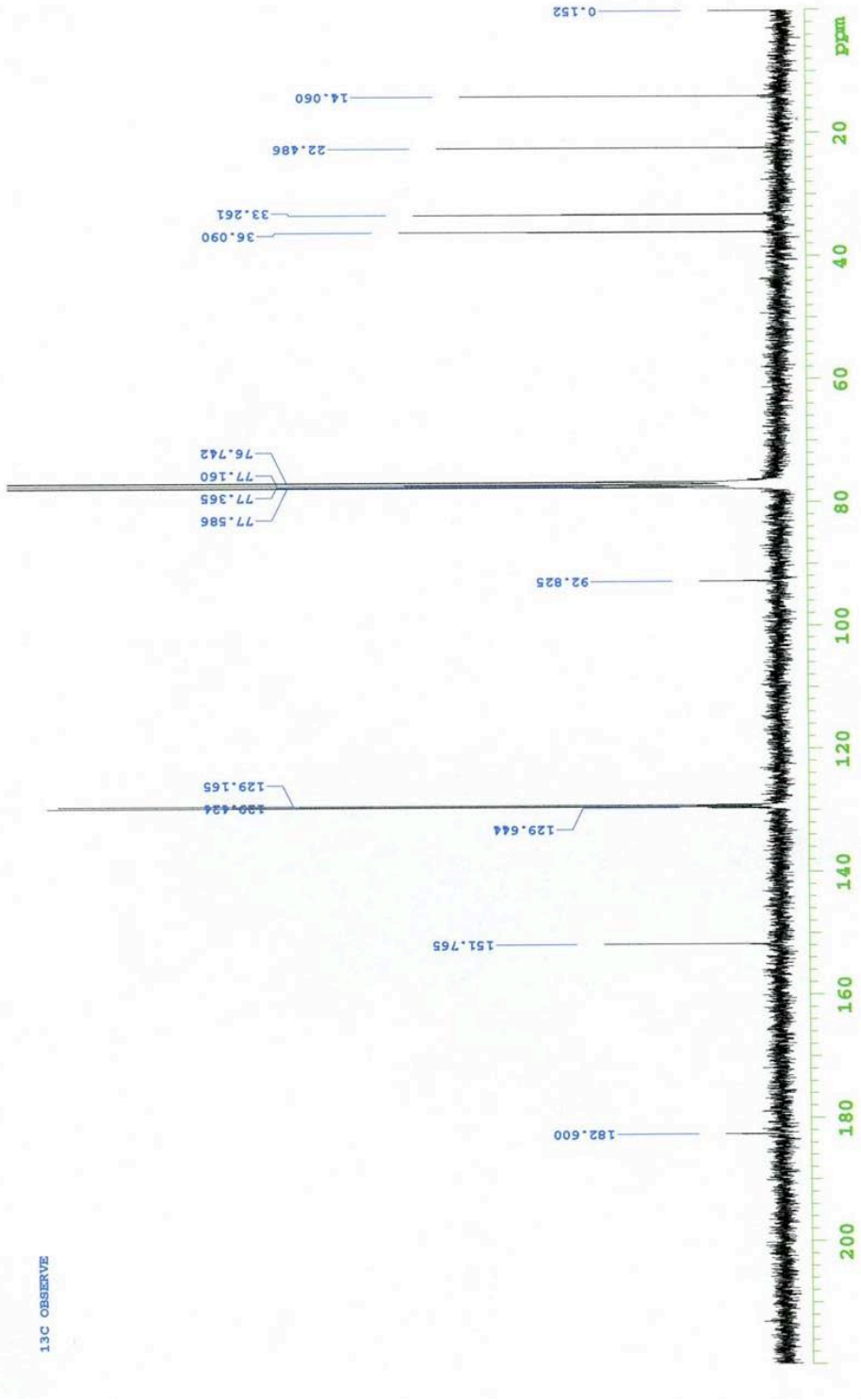

Figure 1-A5. ^{13}C NMR spectrum of **1aBF$_2$** in $CDCl_3$.

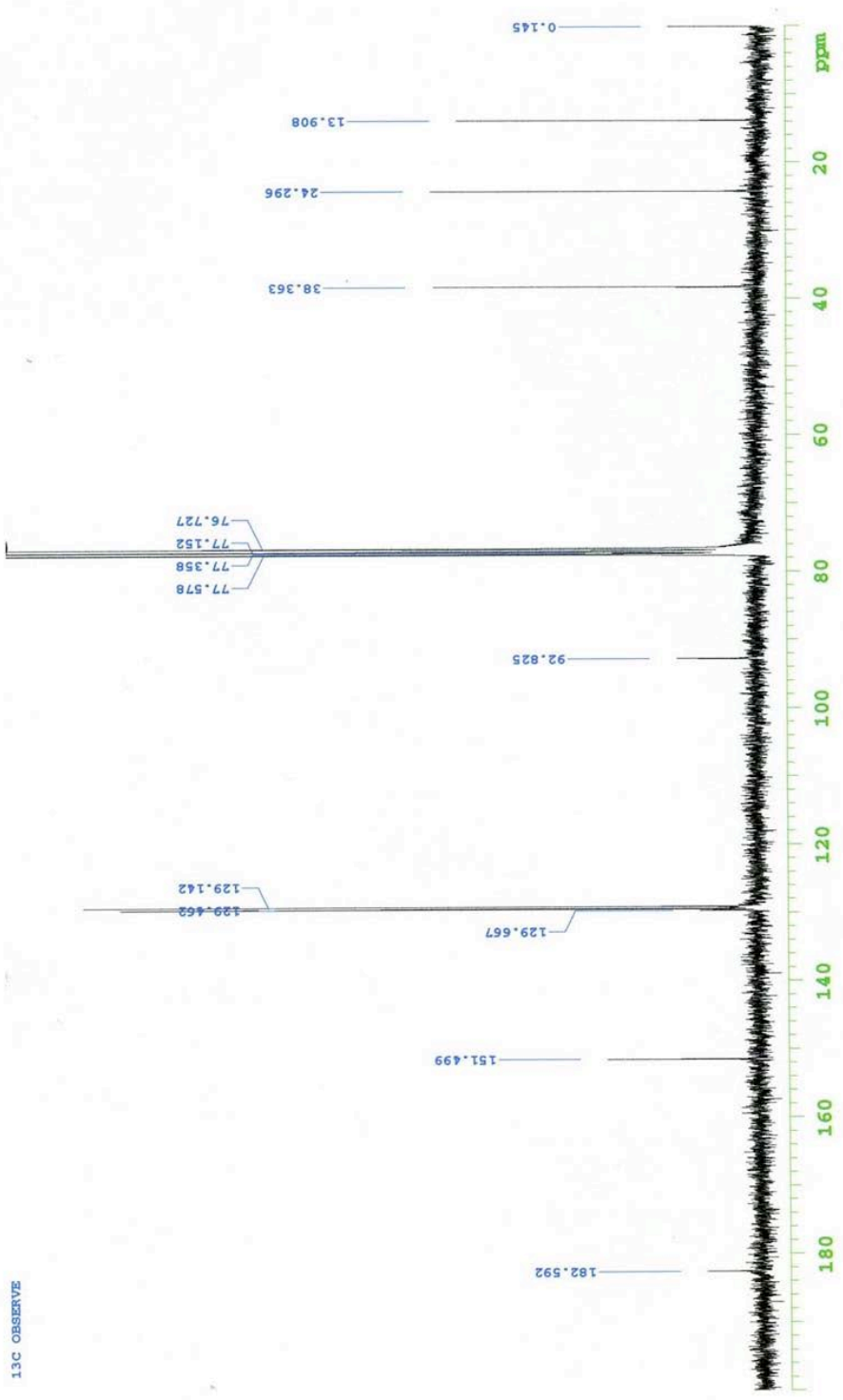

Figure 1-A6. ^{13}C NMR spectrum of **1bBF$_2$** in $CDCl_3$.

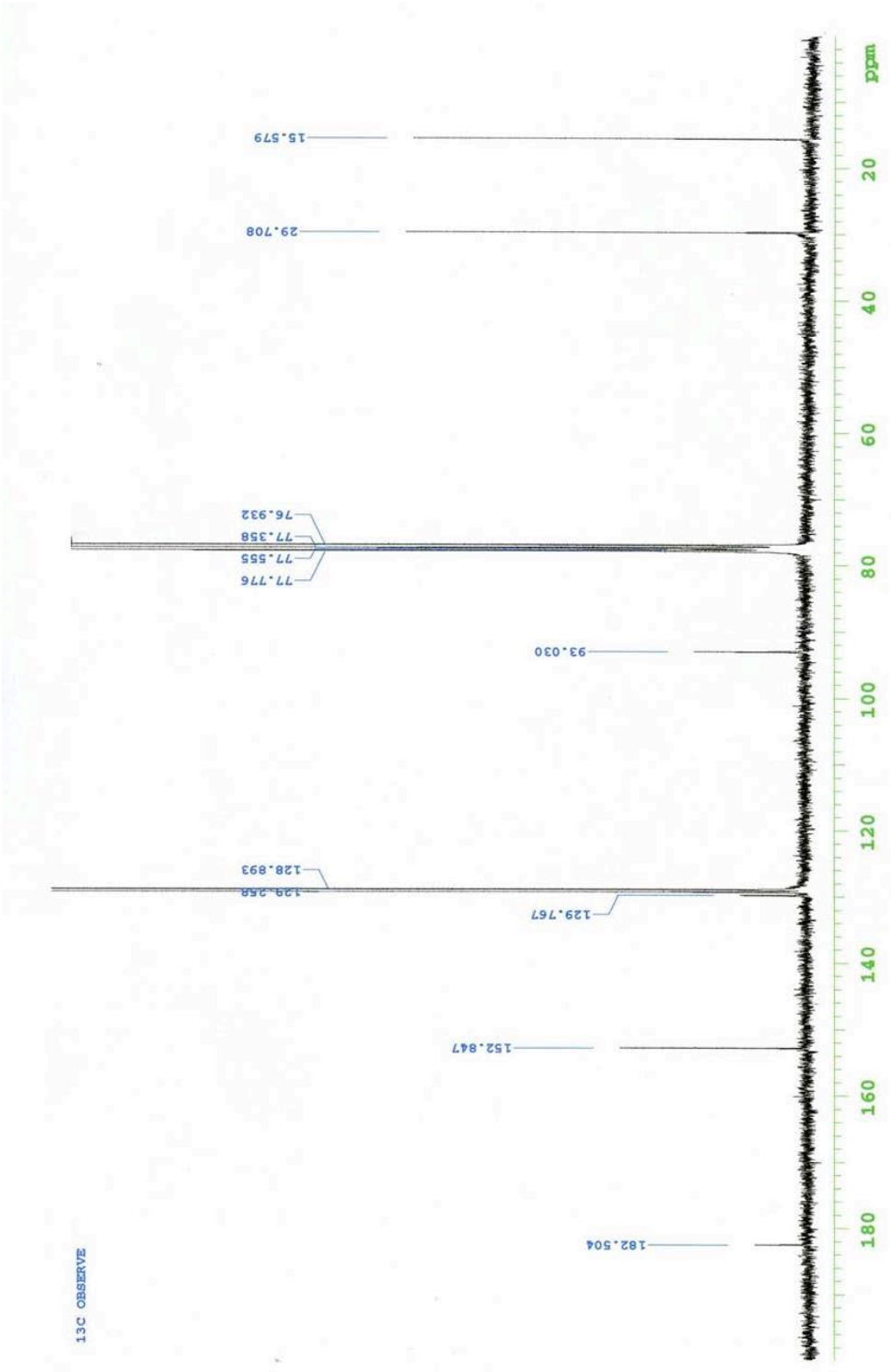

Figurw 1-A7. ^{13}C NMR spectrum of **1cBF$_2$** in $CDCl_3$.

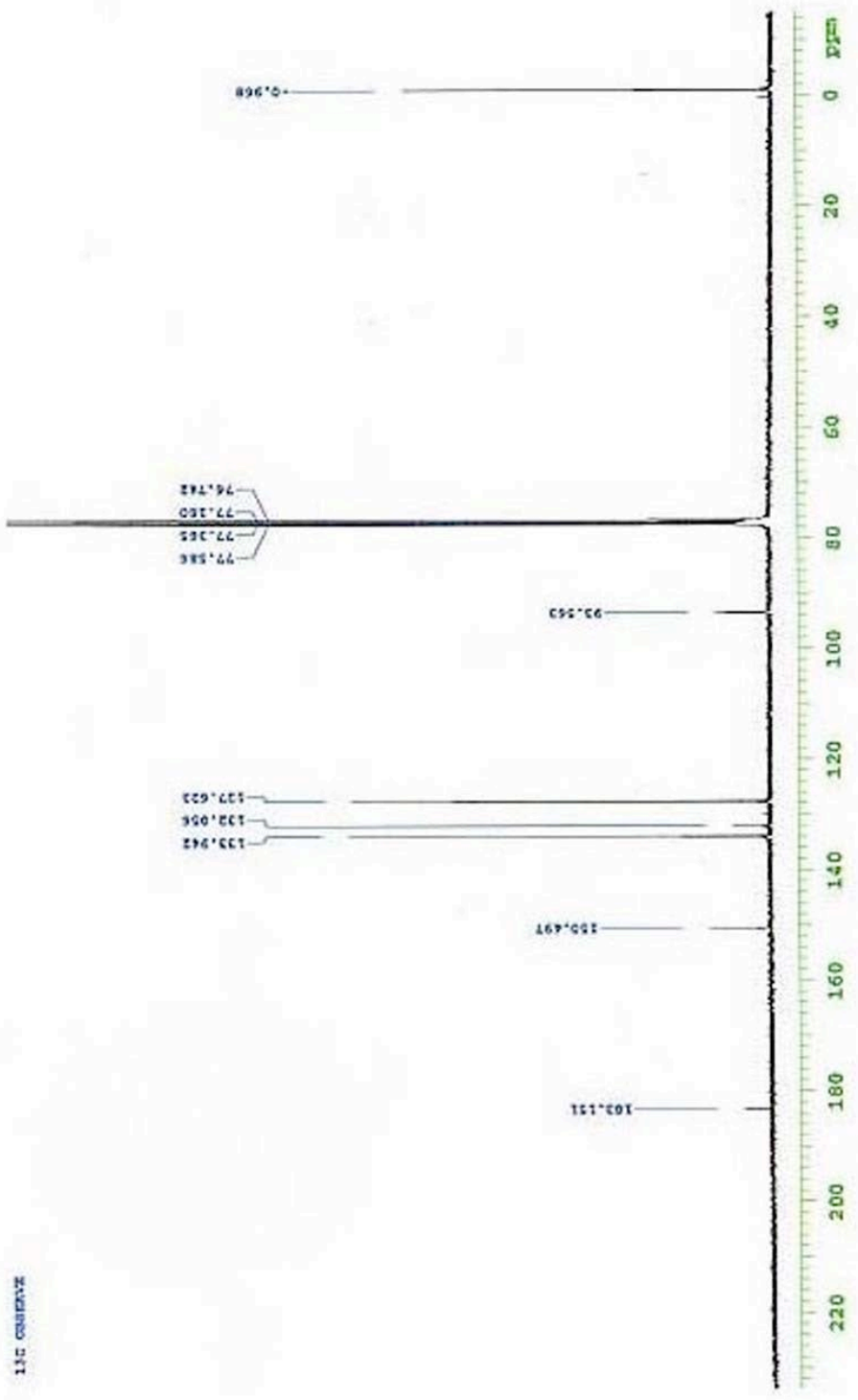

Figure 1-A8. ^{13}C NMR spectrum of **1gBF$_2$** in $CDCl_3$.

1.7.4. Optical Properties. Optical properties of **1a–gBF$_2$** were investigated in CH_2Cl_2, cyclohexane, and acetonitrile and in the crystalline state.

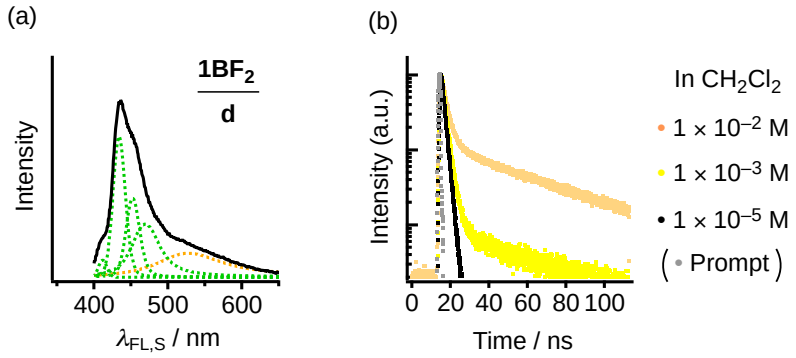

Figure 1-A9. (a) FL spectrum of **1dBF$_2$** in CH_2Cl_2 (1×10^{-2} M, black solid curve) with deconvoluted spectra (dashed curves, green: excited monomer-like FL, orange: excimer FL). (b) Time-dependent changes in FL intensity of **1dBF$_2$** in CH_2Cl_2 at various concentrations.

Table 1-A1. UV–Vis Absorption and FL Properties of **1dBF$_2$** in Cyclohexane and Acetonitrile at 298 K

	In Cyclohexane[a]				In Acetonitrile[a]			
	$\lambda_{AB,S}$ / nm	$\lambda_{FL,S}$[b] / nm	$\tau_{FL,S}$[c,d] / nm	$\Phi_{FL,S}$[b]	$\lambda_{AB,S}$ / nm	$\lambda_{FL,S}$[b] / nm	$\tau_{FL,S}$[c,d] / nm	$\Phi_{FL,S}$[b]
1dBF$_2$	383	396	0.9	0.39	390	409	1.5	0.80

[a] The maximal absorbance of the solution was controlled to be 0.3 (ca. 0.5×10^{-5} M). [b] λ_{EX} = 365 nm. [c] λ_{EX} = 371 nm. [d] Detection was done at $\lambda_{FL,S}$. χ^2 values are in the range of 1.0 ± 0.2.

Table 1-A2. The $\tau_{FL,C}$ of **1a–gBF$_2$** in Crystals at $\lambda_{FL,C}$ in the Range of 460–540 nm

$\lambda_{FL,C}$ / nm	$\tau_{FL,C}$ / ns (proportion / %)													
	1aBF$_2$		**1bBF$_2$**		**1cBF$_2$**		**1dBF$_2$**		**1eBF$_2$**		**1fBF$_2$**		**1gBF$_2$**	
560	N/A		2.0	7.6	3.6	9.0	4.1	11.2	1.9	6.4	N/A		N/A	
			(71)	(29)	(82)	(18)	(69)	(31)	(63)	(37)				
540	2.1	12.5	1.9	6.9	3.5	8.4	3.8	9.5	1.7	5.8	7.2	27.6	5.9	23.8
	(63)	(37)	(73)	(27)	(86)	(14)	(68)	(32)	(63)	(37)	(83)	(17)	(89)	(11)
520	2.0	9.7	1.9	5.3	3.3	7.6	3.4	8.7	1.5	4.8	6.7	21.7	5.8	11.8
	(72)	(28)	(76)	(24)	(80)	(20)	(70)	(30)	(61)	(39)	(83)	(17)	(92)	(8)
500	1.8	7.5	1.6	4.2	3.1	4.7	2.6	4.6	1.3	4.1	6.2	15.9	5.6	8.6
	(74)	(25)	(73)	(27)	(64)	(36)	(56)	(44)	(60)	(40)	(82)	(19)	(89)	(11)
480	1.6	6.1	1.4	2.8	3.9	2.0	2.3	4.6	1.6	4.8	6.5	12.6	5.1	7.3
	(76)	(24)	(55)	(45)	(83)	(17)	(58)	(41)	(60)	(40)	(83)	(17)	(70)	(30)
460	1.3	3.6	2.2	1.0	3.6	1.6	4.0	1.8	N/A		7.6	4.0	5.5	1.9
	(62)	(38)	(64)	(36)	(89)	(11)	(57)	(43)			(81)	(19)	(91)	(9)

λ_{EX} = 371 nm. χ^2 values for the all data are in the range of 0.80–1.20.

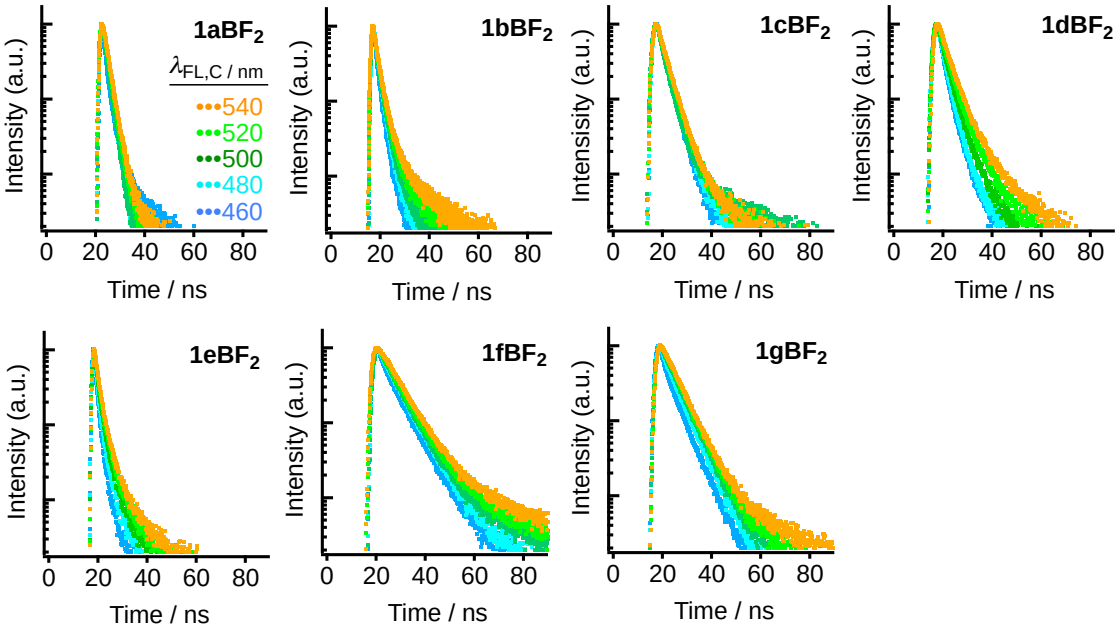

Figure 1-A10. Time-dependent changes in FL intensities of crystals of **1a–gBF$_2$** at various $\lambda_{FL,C}$ at 298 K. λ_{EX} = 371 nm.

1.7.5. Optical Properties. Geometry optimizations of **1a–gBF$_2$** were performed using B3LYP method with a 6-311+G(d) basis set. Electronic transitions for optimized structures of **1a–gBF$_2$** were also estimated by using TD-DFT method.

Table 1-A3. Cartesian Coordinates for Optimized Structure of **1aBF$_2$**, Using B3LYP Method with a 6-311+G(d) Basis Set

Atom	Coordinates		
	X / Å	Y / Å	Z / Å
B	0.000263	–3.640159	–0.034547
O	1.225451	–2.777097	–0.216893
O	–1.225545	–2.777572	–0.215099
C	–1.207353	–1.494628	–0.032399
C	1.207090	–1.494207	–0.033650
C	–0.000157	–0.807549	0.121732
C	–2.525272	–0.837847	–0.020194
C	2.524971	–0.837369	–0.020919
H	–0.000230	0.249537	0.327182
C	3.684852	–1.626856	0.063114
C	2.673940	0.553683	–0.093234
C	3.936020	1.138271	–0.074714
C	4.937312	–1.035450	0.085383
C	5.093405	0.357757	0.017802
H	1.806539	1.196919	–0.185286
H	4.010340	2.217403	–0.138178
H	3.585447	–2.703640	0.116315
H	5.819268	–1.665879	0.157650
C	6.491535	0.943997	0.042994
C	–3.685208	–1.627133	0.065156
C	–2.674197	0.553134	–0.094141
C	–3.936221	1.137850	–0.075872
C	–4.937600	–1.035530	0.087209
C	–5.093651	0.357587	0.018094
H	–1.806786	1.196190	–0.187317
H	–4.010441	2.216916	–0.140562
H	–3.585898	–2.703868	0.119608
H	–5.819562	–1.665827	0.160559
C	–6.491707	0.944007	0.043423
F	0.001337	–4.127153	1.257278
F	–0.000342	–4.610999	–0.997324
H	6.998166	0.576156	0.944574
H	7.056251	0.513937	–0.794481
C	6.609662	2.469335	–0.007407
H	6.135994	2.850260	–0.920605
H	6.059927	2.913167	0.831807
C	8.064962	2.949605	0.038041
H	8.543218	2.571936	0.950203
H	8.619979	2.506335	–0.797964
C	8.197079	4.473440	–0.013272
H	–7.056875	0.513407	–0.793465
H	–6.997961	0.576914	0.945521
C	–6.609617	2.469328	–0.007993
H	–6.059379	2.913650	0.830636
H	–6.136344	2.849535	–0.921695
C	–8.064804	2.949904	0.037870
H	–8.620337	2.506179	–0.797550
H	–8.542669	2.572949	0.950532
C	–8.196651	4.473729	–0.014416
H	–7.683782	4.948263	0.828261
H	–7.763938	4.881166	–0.933671
H	–9.244156	4.785485	0.021294
H	7.763992	4.881590	–0.932035
H	7.684717	4.947499	0.829980
H	9.244660	4.784978	0.022132

Table 1-A4. Cartesian Coordinates for Optimized Structure of **1bBF$_2$**, Using B3LYP Method with a 6-311+G(d) Basis Set

Atom	Coordinates		
	X / Å	Y / Å	Z / Å
B	0.000073	3.241070	–0.032583
O	–1.225523	2.378179	–0.213202
O	1.225495	2.377991	–0.213541
C	1.207149	1.094895	–0.032138
C	–1.207226	1.095064	–0.031908
C	–0.000070	0.407833	0.121781
C	2.525282	0.438447	–0.019562
C	–2.525389	0.438667	–0.019420
H	–0.000172	–0.649488	0.326095
C	–3.684815	1.228606	0.066484
C	–2.675049	–0.952121	–0.094900
C	–3.937499	–1.536030	–0.077983
C	–4.937628	0.637922	0.087141
C	–5.094421	–0.755002	0.016022
H	–1.807982	–1.595594	–0.188433
H	–4.012243	–2.614985	–0.144085
H	–3.584786	2.305209	0.122051
H	–5.819235	1.268664	0.160725
C	–6.492690	–1.340714	0.039027
C	3.684670	1.228512	0.065829
C	2.674995	–0.952372	–0.094301
C	3.937467	–1.536212	–0.077107
C	4.937499	0.637877	0.086730

C	5.094357	–0.755065	0.016386
H	1.807946	–1.595921	–0.187371
H	4.012319	–2.615192	–0.142602
H	3.584549	2.305137	0.120733
H	5.819117	1.268656	0.159853
C	6.492650	–1.340687	0.039804
F	0.000299	3.729022	1.258809
F	0.000024	4.210969	–0.996222
H	–7.000536	–0.975735	0.941201
H	–7.057589	–0.909143	–0.797688
C	–6.612492	–2.866152	–0.015274
H	–6.137762	–3.244058	–0.927986
H	–6.065025	–3.311219	0.823490
C	–8.069547	–3.334654	0.026655
H	–8.568723	–3.006857	0.943878
H	–8.641700	–2.938644	–0.818194
H	–8.137452	–4.425045	–0.012836
H	7.058036	–0.908400	–0.796203
H	6.999883	–0.976402	0.942609
C	6.612586	–2.866076	–0.015634
H	6.065041	–3.311838	0.822707
H	6.138010	–3.243310	–0.928704
C	8.069671	–3.334487	0.026193
H	8.641921	–2.937837	–0.818289
H	8.568673	–3.007292	0.943725
H	8.137674	–4.424844	–0.014055

Table 1-A5. Cartesian Coordinates for Optimized Structure of **1cBF$_2$**, Using B3LYP Method with a 6-311+G(d) Basis Set

Atom	Coordinates		
	X / Å	Y / Å	Z / Å
B	0.009676	2.798451	–0.022083
O	1.239673	1.929620	–0.132533
O	–1.205652	1.944772	–0.294406
C	–1.207095	0.660735	–0.120664
C	1.201861	0.645731	0.038925
C	–0.016702	–0.035170	0.107607
C	–2.527189	0.012013	–0.197424
C	2.512414	–0.019219	0.137137
H	–0.036126	–1.093344	0.306719
F	0.078346	3.780055	–0.970795
F	–0.073147	3.269432	1.272902
C	–3.683070	0.808204	–0.172202
C	–2.676813	–1.379609	–0.302696
C	–3.939978	–1.951278	–0.370555
C	–4.941777	0.226449	–0.235935
C	–5.096798	–1.161829	–0.333449
H	–1.807957	–2.025031	–0.357827
H	–4.030816	–3.029657	–0.463674
H	–3.578990	1.883472	–0.100285
H	–5.821858	0.862609	–0.213742
C	–6.469157	–1.792027	–0.361815
C	3.662608	0.762147	0.330785
C	2.658508	–1.412021	0.046425
C	3.912061	–1.999409	0.151746
C	4.910572	0.164782	0.440501
C	5.061764	–1.224737	0.352407
H	1.796998	–2.046920	–0.124625
H	4.000873	–3.079333	0.076248
H	3.561053	1.837594	0.403625
H	5.784701	0.788813	0.602634
C	6.428060	–1.864330	0.427687
H	6.339971	–2.867609	0.856824
C	7.116652	–1.957109	–0.945736
H	7.061908	–1.290297	1.111180
H	–6.441902	–2.700822	–0.971861
C	–6.992663	–2.138915	1.043312
H	–7.172798	–1.111677	–0.851890
H	–6.329629	–2.845048	1.550372
H	–7.066078	–1.246448	1.670423
H	–7.986108	–2.592250	0.985732
H	6.526511	–2.554927	–1.645507
H	7.250875	–0.966954	–1.389123
H	8.102507	–2.421402	–0.854595

Table 1-A6. Cartesian Coordinates for Optimized Structure of **1dBF$_2$**, Using B3LYP Method with a 6-311+G(d) Basis Set

Atom	Coordinates		
	X / Å	Y / Å	Z / Å
C	1.207220	0.439342	–0.034774
O	1.225697	1.721774	–0.218628
C	0.000035	–0.247994	0.118842
B	–0.000187	2.585986	–0.043520
C	–1.207140	0.439148	–0.035302
O	–1.225756	1.721552	–0.219480
C	2.525573	–0.217227	–0.018429
H	–0.000024	–1.304668	0.326503
F	–0.000647	3.081279	1.244754
C	–2.525446	–0.217489	–0.017879
F	0.000198	3.549737	–1.012999
C	3.682329	0.572230	0.079777
C	2.673835	–1.610395	–0.096426
C	3.935015	–2.190258	–0.070533
C	4.938632	–0.016863	0.109973
C	5.091267	–1.406808	0.033650
H	1.806745	–2.252866	–0.195470
H	4.024492	–3.270529	–0.135696
H	3.580460	1.648359	0.140930
H	5.818252	0.614004	0.196854
C	6.459556	–2.038155	0.032939

C	–2.673913	–1.610471	–0.098908
C	–3.681920	0.571933	0.083287
C	–4.938318	–0.017004	0.113175
C	–3.935159	–2.190156	–0.073213
C	–5.091216	–1.406718	0.033748
H	–3.579806	1.647930	0.146458
H	–5.817780	0.613773	0.202175
H	–1.806977	–2.252725	–0.200537
H	–4.024951	–3.270254	–0.140894
C	–6.459541	–2.038002	0.032440
H	–6.435511	–3.055157	0.429688
H	–6.860218	–2.095796	–0.985779
H	–7.170168	–1.458635	0.626164
H	6.434650	–3.056841	0.426130
H	6.862577	–2.091867	–0.984578
H	7.168858	–1.461088	0.630515

Table 1-A7. Cartesian Coordinates for Optimized Structure of **1eBF$_2$**, Using B3LYP Method with a 6-311+G(d) Basis Set

Atom	Coordinates		
	X / Å	Y / Å	Z / Å
B	0.000291	3.087899	–0.015827
O	1.224727	2.225127	–0.202850
O	–1.224806	2.225509	–0.200921
C	–1.207349	0.942520	–0.019678
C	1.207159	0.942185	–0.020969
C	–0.000081	0.255260	0.134938
C	–2.526286	0.286607	–0.013716
C	2.526084	0.286255	–0.014329
H	–0.000076	–0.803075	0.333299
F	–0.000437	4.063168	–0.973899
F	0.001378	3.568331	1.278261
C	–3.682984	1.078220	0.035344
C	–2.676517	–1.109022	–0.059810
C	–3.937593	–1.687093	–0.051571
C	–4.941045	0.489253	0.045793
C	–5.097798	–0.900612	0.002745
H	–1.808698	–1.755254	–0.121441
H	–4.017130	–2.768621	–0.093424
H	–3.582372	2.155643	0.069263
H	–5.821436	1.123669	0.088343
C	–6.482774	–1.525582	0.013108
C	3.682686	1.077970	0.034838
C	2.676392	–1.109374	–0.060149
C	3.937501	–1.687351	–0.051576
C	4.940799	0.489138	0.045638
C	5.097626	–0.900732	0.002799
H	1.808608	–1.755649	–0.121898
H	4.017152	–2.768876	–0.093283
H	3.581971	2.155391	0.068492
H	5.821153	1.123597	0.088280
C	6.482642	–1.525570	0.013385
C	6.713808	–2.380722	1.272193
C	6.757707	–2.333689	–1.267368
H	7.203621	–0.700430	0.041277
C	–6.757514	–2.333830	–1.267602
C	–6.713920	–2.380724	1.271921
H	–7.203818	–0.700489	0.040844
H	–6.041040	–3.242885	1.302841
H	–6.552060	–1.800769	2.184093
H	–7.738761	–2.762832	1.292791
H	–6.620220	–1.722443	–2.163110
H	–6.092060	–3.198252	–1.349888
H	–7.784914	–2.709437	–1.270149
H	6.092366	–3.198180	–1.349828
H	6.620455	–1.722238	–2.162836
H	7.785161	–2.709144	–1.269790
H	6.551711	–1.800810	2.184351
H	6.041120	–3.243034	1.303052
H	7.738737	–2.762582	1.293169

Table 1-S8. Cartesian Coordinates for Optimized Structure of **1fBF$_2$**, Using B3LYP Method with a 6-311+G(d) Basis Set

Atom	Coordinates		
	X / Å	Y / Å	Z / Å
B	0.000237	3.149982	–0.020807
O	1.225244	2.287574	–0.206565
O	–1.225324	2.287975	–0.204792
C	–1.207376	1.003992	–0.030975
C	1.207193	1.003636	–0.032265
C	–0.000099	0.315567	0.117449
C	–2.525472	0.347298	–0.023816
C	2.525276	0.346912	–0.024712
H	–0.000149	–0.743948	0.309615
F	–0.000422	4.124369	–0.980043
F	0.001300	3.632108	1.272664
C	–3.683237	1.132693	0.040353
C	–2.677634	–1.047393	–0.081627
C	–3.938362	–1.622779	–0.069074
C	–4.943682	0.545065	0.055861
C	–5.106857	–0.844596	0.002280
H	–1.811981	–1.695286	–0.156025
H	–4.010526	–2.703476	–0.120721
H	–3.586200	2.210223	0.083386
H	–5.807638	1.194670	0.111620
C	–6.483551	–1.526178	0.015374
C	3.682974	1.132455	0.038605
C	2.677525	–1.047816	–0.081378
C	3.938309	–1.623081	–0.068664
C	4.943475	0.544986	0.054298

C	5.106740	–0.844710	0.001717
H	1.811912	–1.695856	–0.154991
H	4.010601	–2.703813	–0.119374
H	3.585852	2.210007	0.080787
H	5.807382	1.194711	0.109334
C	6.483492	–1.526169	0.015316
C	6.578389	–2.461444	1.243105
C	6.656279	–2.357317	–1.277317
C	7.639064	–0.512511	0.091612
C	–6.656153	–2.356011	–1.278146
C	–6.578373	–2.462760	1.242172
C	–7.639224	–0.512738	0.092758
H	–5.810460	–3.239551	1.225986
H	–6.465855	–1.903633	2.175124
H	–7.551936	–2.961620	1.264247
H	–6.587975	–1.721769	–2.166251
H	–5.899322	–3.138591	–1.370426
H	–7.635789	–2.843229	–1.287396
H	5.899486	–3.140005	–1.368961
H	6.588308	–1.723985	–2.166091
H	7.635909	–2.844548	–1.285855
H	6.465795	–1.901339	2.175460
H	5.810487	–3.238285	1.227694
H	7.551999	–2.960191	1.265715
H	–7.597268	0.091534	1.003080
H	–7.651279	0.164113	–0.765855
H	–8.594674	–1.043913	0.100340
H	7.650890	0.163591	–0.767599
H	7.597233	0.092555	1.001411
H	8.594573	–1.043580	0.099512

Table 1-A9. Cartesian Coordinates for Optimized Structure of **1gBF$_2$**, Using B3LYP Method with a 6-311+G(d) Basis Set

Atom	Coordinates		
	X / Å	Y / Å	Z / Å
C	1.206821	1.153165	–0.035465
O	1.225751	2.435873	–0.211775
C	–0.000006	0.464898	0.115674
B	–0.000270	3.300219	–0.031662
C	–1.206783	1.152996	–0.036099
O	–1.225995	2.435689	–0.212599
C	2.526193	0.494223	–0.026932
H	–0.000179	–0.593263	0.314982
F	–0.000719	3.786705	1.259280
C	–2.526029	0.493845	–0.026656
F	0.000100	4.268456	–0.995852
C	3.683836	1.283087	0.065737
C	2.670238	–0.897824	–0.112923
C	3.933244	–1.479405	–0.099456
C	4.938816	0.689083	0.082317
C	5.100555	–0.705248	0.000991
H	1.800855	–1.537628	–0.212025
H	4.004007	–2.560082	–0.173904
H	3.583296	2.359416	0.129043
H	5.810018	1.334013	0.160273
Si	6.838092	–1.482215	0.018852
C	–2.670340	–0.897741	–0.118972
C	–3.683293	1.282478	0.072244
C	–4.938337	0.688664	0.088598
C	–3.933463	–1.479128	–0.105739
C	–5.100429	–0.705256	0.000809
H	–3.582375	2.358502	0.140132
H	–5.809282	1.333301	0.171430
H	–1.801172	–1.536989	–0.223382
H	–4.004654	–2.559401	–0.185446
Si	–6.838018	–1.482119	0.018424
C	–7.698086	–1.012896	1.632117
C	–7.815833	–0.811326	–1.450354
C	–6.695902	–3.359465	–0.108451
H	–6.212100	–3.679022	–1.036504
H	–6.134583	–3.791336	0.725750
H	–7.691081	–3.815418	–0.093677
H	–7.149700	–1.384736	2.502782
H	–7.793399	0.071113	1.746745
H	–8.708242	–1.433152	1.675783
H	–7.914504	0.277852	–1.414252
H	–7.335536	–1.062382	–2.400785
H	–8.828289	–1.227613	–1.473373
C	7.813161	–0.817910	–1.454710
C	7.701245	–1.005784	1.628762
C	6.695536	–3.360076	–0.099601
H	6.135792	–3.788313	0.737529
H	6.209884	–3.683543	–1.025333
H	7.690683	–3.816097	–0.084829
H	7.796874	0.078730	1.738228
H	7.154565	–1.373604	2.502197
H	8.711461	–1.425915	1.672357
H	7.331087	–1.073121	–2.403131
H	7.911995	0.271406	–1.423595
H	8.825541	–1.234385	–1.477768

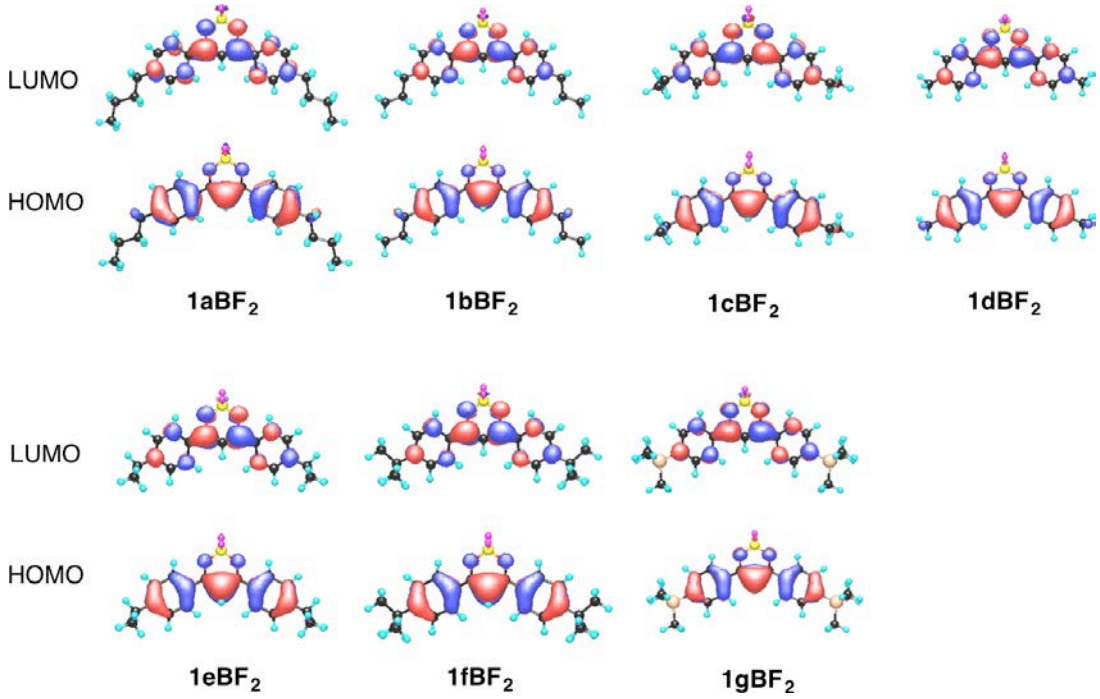

Figure 1-A11. The HOMO and LUMO distributions for optimized structures of **1a–gBF$_2$**. Isovalues = 0.03, using B3LYP method with a 6-311+G(d) basis set.

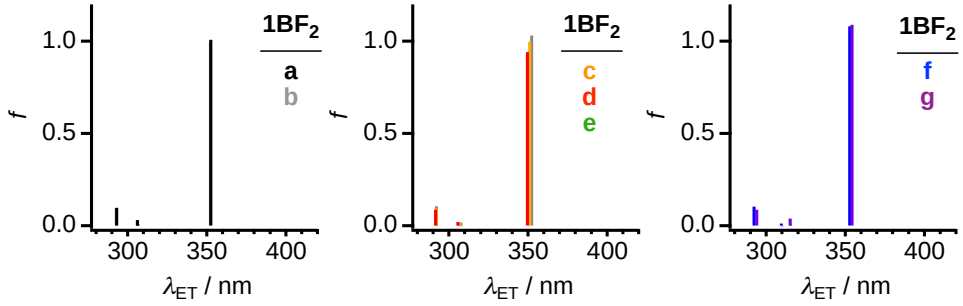

Figure 1–A12. Electronic transitions estimated for optimized structures of **1a–gBF$_2$**, using B3LYP method with a 6-311+G(d) basis set.

1.7.6. Intermolecular interactions of the optimized crystal-packing structures. In a single crystal of **1fBF$_2$**, an arbitrarily-chosen molecule of this substance, M_0, has a planar geometry and possesses 14 neighbors, *i.e.*, two sets of eight kinds of the pair, M_0/M_1, M_0/M_2, M_0/M_3, M_0/M_4, M_0/M_5, M_0/M_6, M_0/M_7, and M_0/M_8. Molecules in the M_0/M_1 pair form *B-on-D* overlap on the basis of the existence of a short face-to-face distance of 3.71 Å (Figure 1-A13). In addition, a short distance of 2.41 Å exists between an H atom in the *B* ring of M_0 and the F atom in M_3 (or an F atom in the *D* ring of M_0 and the H atom in M_2). The fact that this distance is shorter than the sum of van der Waals radii of H (1.20 Å) and F (1.47 Å)[A12] clearly shows the presence of H•••F hydrogen bonding[A13–16] in the M_0/M_3 (or M_0/M_2) pair. Furthermore, that the M_0/M_4 pair also contains an H•••F halogen bonding is strongly suggested by the 2.57 Å.

To estimate the energy of intermolecular interactions operating, DFT calculation[50] using the B97D method[A17] with basis set superposition error (BSSE) correction by the counterpoise method[A18], were performed. The 6-311G** basis set was used for the all elements. The geometries of molecules in the crystal packing structures of **1fBF$_2$** were optimized at PW91/DNP level[A19] under periodic boundary conditions with fixed cell parameters. Intermolecular interaction energies, $E_{0/1}$, $E_{0/2}$, $E_{0/3}$, $E_{0/4}$, $E_{0/5}$, $E_{0/6}$, $E_{0/7}$ and $E_{0/8}$, for two molecules with the geometry of respective M_0/M_1, M_0/M_2, M_0/M_3, M_0/M_4, M_0/M_5, M_0/M_6, M_0/M_7, and M_0/M_8 pairs were determined to be –21.6, –12.76, –12.76, –4.50, –4.10, –1.70, –1.63, and –1.63 kcal mol^{-1}, respectively. The M_0/M_2 and M_0/M_3 pairs are equivalent to each other although the F and H atoms of M_0 behave as interaction site in the M_0/M_2 and M_0/M_3 pair, respectively. In addition, the M_0/M_7 and M_0/M_8 pairs are equivalent to each other although the different H atoms of M_0 behave as interaction site in the M_0/M_6 and M_0/M_7 pair, respectively. The observation that the absolute value of $E_{0/1}$ is larger than the others, suggests that π-stacking interactions that occur in a continuous manner along the columns of stacked **1fBF$_2$** molecules (••••$M_1/M_0/M_1$••••) are dominant. The calculated absolute $E_{0/3}$ (and $E_{0/2}$) and $E_{0/4}$, which are substantially smaller than absolute $E_{0/1}$, show that the H•••F (and F•••H) bonding interactions add to stabilization of the crystal packing structure.

The HOMO and LUMO of the M_0/M_1 pair are delocalized across two stacked molecules of the pair (Figure 1-A13). The results suggest that the π-stacking strongly affects the electronic properties of **1fBF$_2$**. Wavelength associated with a $S_0 \rightarrow S_1$ electronic transition ($\lambda_{ET,S0\rightarrow S1}$) of **1fBF$_2$** single molecule was simulated at 386 nm (3.21 eV) with an oscillator strength ($f_{S0\rightarrow S1}$) of 0.9106 by time dependent (TD)-DFT calculation using B97D method with 6-311G** basis sets (Figure 1-A18a). On the other hand, $\lambda_{ET,S0\rightarrow S1}$ for M_0/M_1 pair was simulated at 483 nm (2.56 eV) with a quite small $f_{S0\rightarrow S1}$ of 0.0019, while $\lambda_{ET,S0\rightarrow S8}$ at 387 nm (3.20 eV) have a large $f_{S0\rightarrow S1}$ of 1.0695 (Figure 1-A18b).

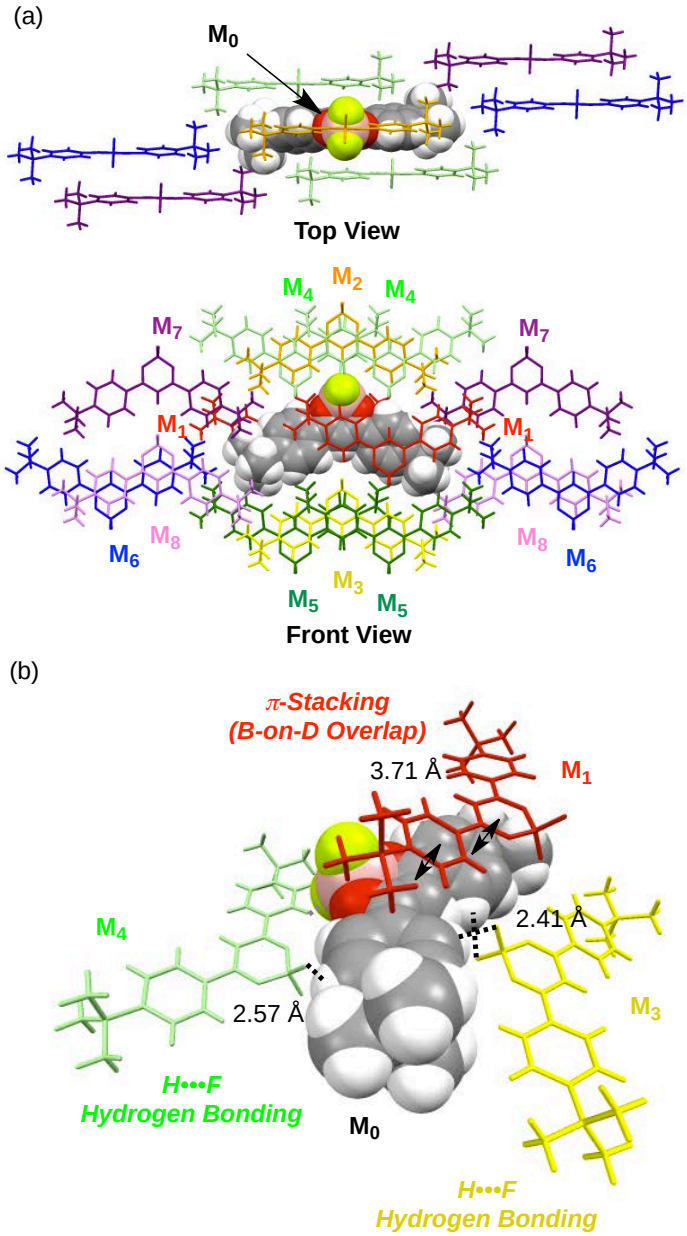

Figure 1–A13. (a) Crystal packing structure of **1fBF$_2$** in which a pair of molecules $M_{1–8}$ are adjacent to M_0. (b) The M_0/M_1, M_0/M_2 (M_0/M_3), and M_0/M_4 pairs in the crystal packing structure that form π-stacking (*B-on-D* overlap), and two kinds of H–F hydrogen bonding, respectively.

Table 1-A10. Cartesian Coordinates of Optimized Geometry of **1fBF$_2$** Simulated Using B97D Method with 6-311G** Basis Sets, Respectively

Atom	Coordinates		
	X / Å	Y / Å	Z / Å
B	–0.000036	3.251883	–0.176904
O	1.243856	2.377798	–0.389629
O	–1.243931	2.377789	–0.389563
C	–1.214758	1.097004	–0.150217
C	1.214704	1.097014	–0.150274
C	–0.000019	0.418661	0.040539
C	–2.523662	0.418273	–0.105407
C	2.523618	0.418297	–0.105511
H	–0.000009	–0.629044	0.306869
F	–0.000063	4.247774	–1.116183
F	-0.000002	3.676014	1.139211
C	–3.700090	1.177695	0.047782
C	–2.643726	–0.984173	–0.214300
C	–3.893284	–1.593664	–0.159805
C	–4.948609	0.554786	0.107430
C	–5.076640	–0.842643	0.007228
H	–1.759749	–1.598903	–0.368860
H	–3.956210	–2.675925	–0.254634
H	–3.621019	2.258644	0.128859
H	–5.832003	1.174275	0.236687
C	–6.428045	–1.567857	0.070712
C	3.700038	1.177735	0.047651
C	2.643698	–0.984145	–0.214416
C	3.893268	–1.593618	–0.159971
C	4.948568	0.554844	0.107256
C	5.076620	–0.842581	0.007023
H	1.759726	–1.598888	–0.368952
H	3.956205	–2.675879	–0.254803
H	3.620954	2.258682	0.128741
H	5.831957	1.174345	0.236492
C	6.428035	–1.567780	0.070480
C	6.417264	–2.556939	1.263903
C	6.645246	–2.359123	–1.244633
C	7.613041	–0.599029	0.255099
C	–6.645123	–2.359437	–1.244280
C	–6.417365	–2.556802	1.264314
C	–7.613082	–0.599092	0.255059
H	–5.617485	–3.301445	1.159684
H	–6.266303	–2.019276	2.210464
H	–7.378550	–3.088428	1.312924
H	–6.660116	–1.679089	–2.106713
H	–5.849298	–3.098872	–1.401963
H	–7.606098	–2.891781	–1.200745
H	5.849491	–3.098594	–1.402490
H	6.660240	–1.678628	–2.106951
H	7.606260	–2.891400	–1.201132
H	6.266154	–2.019581	2.210141
H	5.617372	–3.301542	1.159083
H	7.378434	–3.088596	1.312476
H	–7.519986	–0.028631	1.189403
H	–7.683352	0.110025	–0.581201
H	–8.547708	–1.173909	0.296326
H	7.683304	0.110304	–0.580977
H	7.519914	–0.028812	1.189589
H	8.547683	–1.173831	0.296237

Figure 1-A14. Optimized geometry of **1fBF$_2$** with the HOMO and LUMO simulated using B97D method with 6-311G** basis sets, respectively. Isovalue = 0.03.

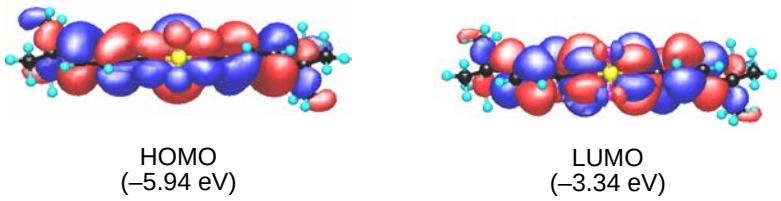

Figure 1-A15. Representation of the HOMO and LUMO of single molecule of **1fBF$_2$** with geometry in crystals (M_0) simulated by single-point calculations using B97D method with 6-311G** basis sets. The geometry was optimized at PW91/DNP based on results of X-ray crystallographic analyses of **1fBF$_2$**. Isovalue = 0.01.

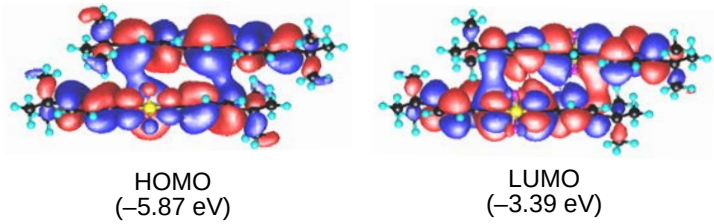

Figure 1-A16. The HOMO and LUMO of the M_0/M_1 pair of **1fBF$_2$** simulated by DFT calculation using B97D method with 6-311G** basis sets. Isovalue = 0.01.

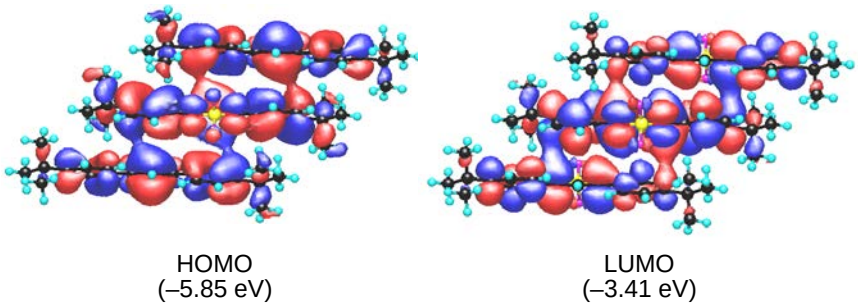

Figure 1-A17. Representation of the HOMO and LUMO of stacked three molecules of **1fBF$_2$** with geometries in crystals ($M_1/M_0/M_1$) simulated by single-point calculation using B97D method with 6-311G** basis sets. The geometry was optimized at PW91/DNP based on results of X-ray crystallographic analyses of **1fBF$_2$**. Isovalue = 0.01.

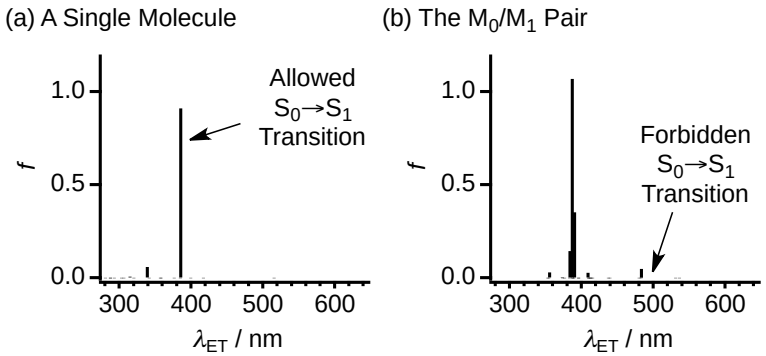

Figure 1-A18. Electronic transitions of a single molecule (a) and the M_0/M_1 pair (b) of **1fBF$_2$** estimated by TD-DFT calculation using B97D method with 6-311G**.

Table 1-A11. Electronic Transitions Estimated for **1fBF$_2$** with Optimized Geometry, Simulated Using B97D Method with 6-311G** Basis Sets

	λ_{ET} / nm (eV)	Transition (Coefficient)		f
$S_0 \rightarrow T_1$	515.82 (2.403)	H → L	(0.702)	0.0000
$S_0 \rightarrow T_2$	417.25 (2.971)	H–3 → L H–1 → L H → L+1	(0.110) (0.671) (–0.134)	0.0000
$S_0 \rightarrow T_3$	399.52 (3.103)	H–4 → L H–2 → L	(0.222) (0.657)	0.0000
$S_0 \rightarrow S_1$	385.67 (3.214)	H–4 → L H–2 → L H → L	(0.153) (0.106) (0.680)	0.9106
$S_0 \rightarrow T_4$	384.77 (3.222)	H–3 → L H–1 → L	(0.686) (–0.130)	0.0000
$S_0 \rightarrow T_5$	376.46 (3.293)	H–4 → L H–2 → L	(0.652) (–0.237)	0.0000
$S_0 \rightarrow S_2$	358.15 (3.462)	H–4 → L H–1 → L	(0.491) (–0.488)	0.0003
$S_0 \rightarrow S_3$	357.37 (3.470)	H–4 → L H–2 → L	(–0.214) (0.658)	0.0003
$S_0 \rightarrow T_6$	341.38 (3.632)	H–3 → L H–3 → L+3 H–2 → L+2 H–1 → L H → L+1	(0.103) (–0.115) (–0.122) (0.154) (0.648)	0.0000
$S_0 \rightarrow S_4$	338.70 (3.661)	H–4 → L+1 H–3 → L H–1→ L H→ L+1	(0.108) (0.475) (0.454) (0.214)	0.0574
$S_0 \rightarrow T_7$	320.06 (3.873)	H–5 → L	(0.706)	0.0000
$S_0 \rightarrow S_5$	315.01 (3.936)	H–4 → L H–2 → L H–1 → L+1 H→ L H→ L+4	(0.620) (0.181) (0.125) (–0.169) (–0.125)	0.0066
$S_0 \rightarrow T_8$	306.08 (4.051)	H–4 → L H–4 → L+3 H–3 → L+1 H–3 → L+2 H–2 → L+3 H–1 → L+1 H–1 → L+2 H → L+4	(0.137) (–0.144) (0.215) (0.293) (0.334) (0.354) (–0.222) (–0.120)	0.0000
$S_0 \rightarrow S_6$	303.13 (4.090)	H–5 → L	(0.706)	0.0005
$S_0 \rightarrow T_9$	292.98 (4.314)	H–4 → L+1 H–4 → L+2 H–3 → L+3 H–2 → L+2 H–1 → L+3 H → L+1	(0.157) (0.137) (–0.359) (–0.428) (0.267) (–0.224)	0.0000
$S_0 \rightarrow T_{10}$	287.38 (4.314)	H–3 → L+3 H–2 → L+1 H → L+2	(–0.117) (–0.210) (0.642)	0.0000
$S_0 \rightarrow T_{11}$	287.23 (4.317)	H–3 → L+1 H–1 → L+1 H–1 → L+2 H → L+3	(–0.184) (0.140) (–0.154) (0.638)	0.0000
$S_0 \rightarrow T_{12}$	280.30 (4.423)	H–6 → L H–3 → L+2 H–2 → L+3 H–1 → L+1	(–0.127) (–0.233) (–0.285) (0.541)	0.0000

		H–1 → L+2 (0.173)	
$S_0 \rightarrow S_7$	277.56 (4.467)	H–4 → L+1(–0.119) H–1 → L+3 (0.106) H → L+1 (0.528) H → L+2 (0.391)	0.0331
$S_0 \rightarrow T_{13}$	273.80 (4.528)	H–2 → L+1 (0.655) H → L+2 (0.224)	0.0000
$S_0 \rightarrow S_8$	272.48 (4.550)	H–3 → L+1 (0.208) H–1 → L+1(–0.124) H–1 → L+2 (0.104)	0.0000
$S_0 \rightarrow T_{14}$	271.79 (4.562)	H–6 → L (0.668) H–3 → L+1(–0.159) H–1 → L+1 (0.138)	0.0000
$S_0 \rightarrow S_9$	269.89 (4.594)	H–2 → L+1(–0.319) H → L+1 (0.332) H → L+2 (–0.506)	0.0133
$S_0 \rightarrow T_{15}$	269.01 (4.609)	H–6 → L (0.185) H–3 → L+1 (0.598) H–2 → L+3(–0.121) H–1 → L+2 (0.141) H → L+3 (0.234)	0.0000
$S_0 \rightarrow S_{10}$	267.00 (4.643)	H–6 → L (0.685) H–1 → L+1 (0.112)	0.0420
$S_0 \rightarrow S_{11}$	263.76 (4.701)	H–7 → L (0.703)	0.0012
$S_0 \rightarrow S_{12}$	263.75 (4.701)	H–8 → L (0.702)	0.0012
$S_0 \rightarrow S_{13}$	255.84 (4.846)	H–12 → L (0.101) H–3 → L+1(–0.122) H–3 → L+2 (0.116) H–1 → L+1 (0.577) H–1 → L+2 (0.213) H → L+3 (0.103) H → L+4 (0.191)	0.1622
$S_0 \rightarrow S_{14}$	251.69 (4.926)	H–13 → L (–0.147) H–11 → L (–0.236) H–9 → L (0.110) H–4 → L+1(–0.155) H–3 → L+3(–0.197) H–2 → L+1 (0.478) H–1 → L+3(–0.267) H → L+2 (–0.153)	0.0035
$S_0 \rightarrow S_{15}$	251.48 (4.930)	H–10 → L (0.691) H–3 → L+1(–0.119)	0.0055

Table 1-A12. Electronic Transitions Estimated for Single Molecule of **1fBF$_2$** with Geometry in Crystals (M_0), Simulated Using B97D Method with 6-311G** Basis Sets

	λ_{ET} / nm (eV)	Transition (Coefficient)	*f*
$S_0 \rightarrow T_1$	524.74 (2.362)	H → L (0.702)	0.0000
$S_0 \rightarrow T_2$	426.26 (2.909)	H–1 → L (0.679) H → L+1 (–0.115)	0.0000
$S_0 \rightarrow T_3$	411.04 (3.016)	H–4 → L (0.148) H–2 → L (0.678)	0.0000
$S_0 \rightarrow T_4$	389.80 (3.181)	H–3 → L (0.690) H–1 → L (–0.107)	0.0000
$S_0 \rightarrow S_1$	389.73 (3.181)	H–2 → L (0.108) H → L (0.685)	0.9614
$S_0 \rightarrow T_5$	382.43 (3.242)	H–4 → L (0.676) H–2 → L (–0.162)	0.0000
$S_0 \rightarrow S_2$	363.56 (3.401)	H–4 → L (–0.235) H–2 → L (0.647)	0.0024
$S_0 \rightarrow S_3$	363.25 (3.413)	H–3 → L (–0.456) H–1 → L (0.519)	0.0005
$S_0 \rightarrow S_4$	341.82 (3.627)	H–3 → L (0.511) H–1 → L (0.429) H → L+1 (–0.192)	0.0697
$S_0 \rightarrow T_6$	340.78 (3.638)	H–3 → L (0.119) H–2 → L+1 (0.115) H–1→ L (–0.136) H→ L+1 (0.649)	0.0000
$S_0 \rightarrow S_5$	335.66 (3.694)	H–6 → L (–0.251) H–4 → L (0.614) H–2 → L (0.193)	0.0066
$S_0 \rightarrow T_7$	315.29 (3.932)	H→ L (0.705)	0.0000
$S_0 \rightarrow T_8$	311.13 (3.985)	H–6 → L (0.641) H–4 → L (–0.111) H–3 → L+1 (0.101) H–1 → L+1 (0.161)	0.0000
$S_0 \rightarrow T_9$	303.66 (4.083)	H–6 → L (–0.278) H–4 → L+2 (0.188) H–3 → L+1 (0.207) H–3 → L+3(–0.270) H–2 → L+2(–0.283) H–1 → L+1 (0.312) H–1 → L+3 (0.211) H → L+4 (0.110)	0.0000
$S_0 \rightarrow S_6$	300.38 (4.128)	H–5 → L (0.705)	0.0007
$S_0 \rightarrow T_{10}$	295.60 (4.194)	H–7 → L (0.693)	0.0000

$S_0 \rightarrow S_7$	291.98 (4.246)	H–6 → L (0.637) H–4 → L (0.179) H–1 → L+1(–0.126) H → L (–0.126)	0.0402
$S_0 \rightarrow T_{11}$	290.97 (4.261)	H–4 → L+1 (0.176) H–4 → L+3(–0.198) H–3 → L+2 (0.355) H–2 → L+3 (0.394) H–1 → L+2(–0.257) H → L+1 (–0.223)	0.0000
$S_0 \rightarrow T_{12}$	284.81 (4.353)	H–4 → L+1(–0.119) H–3 → L+2(–0.106) H–2 → L+1 (0.233) H–1 → L+2(–0.113) H → L+2 (–0.128) H → L+3 (0.609)	0.0000
$S_0 \rightarrow T_{13}$	284.77 (4.354)	H–3 → L+1 (0.183) H–1 → L+1(–0.201) H–1 → L+3(–0.154) H → L+2 (0.603) H → L+3 (0.129)	0.0000
$S_0 \rightarrow S_8$	283.31 (4.376)	H–7 → L (0.568) H → L+1 (0.390)	0.0402
$S_0 \rightarrow T_{14}$	279.29 (4.439)	H–4 → L+2(–0.122) H–3 → L+3 (0.219) H–2 → L+2 (0.278) H–1 → L+2 (0.539) H–1 → L+3(–0.189) H → L+2 (0.148)	0.0000
$S_0 \rightarrow T_{15}$	274.18 (4.522)	H–2 → L+1 (0.642) H → L+13 (–0.235)	0.0000
$S_0 \rightarrow S_9$	272.97 (4.542)	H–7 → L (0.347) H–4 → L+1 (0.120) H–1 → L+2 (0.106) H → L+1 (–0.363) H → L+3 (0.448)	0.0015
$S_0 \rightarrow S_{10}$	269.83 (4.595)	H–3 → L+1(–0.215) H–1 → L+1 (0.134) H → L+2 (0.649)	0.0060
$S_0 \rightarrow S_{11}$	267.23 (4.640)	H–8 → L (0.704)	0.0002
$S_0 \rightarrow S_{12}$	267.17 (4.641)	H–9 → L (0.539) H–7 → L (–0.123) H–2 → L+1(–0.241) H → L+1 (0.202) H → L+2 (–0.202) H → L+3 (0.294)	0.0007
$S_0 \rightarrow S_{13}$	266.55 (4.652)	H–9 → L (0.455) H–7 → L (0.170) H–2 → L+1 (0.298) H → L+1 (–0.260) H → L+3 (–0.309)	0.0006
$S_0 \rightarrow S_{14}$	261.37 (4.744)	H–10 → L (0.706)	0.0001
$S_0 \rightarrow S_{15}$	256.14 (4.841)	H–14 → L (–0.142) H–3 → L+3(–0.104) H–1 → L+1 (0.609) H–1 → L+3(–0.159) H → L+2 (–0.115) H → L+4 (–0.171)	0.2108

Table 1-A13. Electronic Transitions Estimated for Stacked Two Molecules of **1fBF$_2$** with Geometries in Crystals (M_0/M_1), Simulated Using B97D Method with 6-311G** Basis Sets

	λ_{ET} / nm (eV)	Transition (Coefficient)	*f*
$S_0 \rightarrow T_1$	536.32 (2.312)	H–1 → L+1(–0.323) H → L (0.626)	0.0000
$S_0 \rightarrow T_2$	531.11 (2.334)	H–1 → L (–0.407) H → L+1 (0.575)	0.0000
$S_0 \rightarrow S_1$	483.56 (2.564)	H–1 → L+1 (0.463) H → L (0.101) H → L+1 (0.518)	0.0019
$S_0 \rightarrow S_2$	483.48 (2.564)	H–1 → L+1 (0.428) H → L (0.547)	0.0473
$S_0 \rightarrow T_3$	483.09 (2.567)	H–1 → L (0.574) H → L+1 (0.410)	0.0000
$S_0 \rightarrow T_4$	480.03 (2.583)	H–1 → L+1 (0.627) H → L (0.325)	0.0000
$S_0 \rightarrow T_5$	439.25 (2.823)	H–5 → L+1 (0.121) H–3 → L+1 (0.290) H–2 → L (0.613)	0.0000
$S_0 \rightarrow T_6$	437.35 (2.835)	H–5 → L (0.616) H–3 → L (0.368) H–2 → L+1 (0.570)	0.0000
$S_0 \rightarrow S_3$	415.33 (2.835)	H–2 → L (0.316) H–1 → L (0.454) H → L+1 (–0.409)	0.0000
$S_0 \rightarrow T_7$	414.03 (2.995)	H–6 → L (0.121) H–5 → L+1(–0.279) H–4 → L (–0.603) H–3 → L+1 (0.104)	0.0000
$S_0 \rightarrow T_8$	412.28 (3.007)	H–7 → L (–0.125) H–3 → L (0.589) H–2 → L+1(–0.353)	0.0000
$S_0 \rightarrow T_9$	411.49 (3.013)	H–7 → L (–0.125) H–6 → L+1(–0.113) H–5 → L (0.380) H–4 → L+1 (0.539) H–2 → L+1(–0.112)	0.0000

$S_0 \rightarrow T_{10}$	410.12 (3.023)	H–7 → L+1(–0.106) H–3 → L+1 (0.625) H–2 → L (–0.289)	0.0000
$S_0 \rightarrow S_4$	409.46 (3.028)	H–4 → L (0.110) H–3 → L+1 (0.390) H–2 → L (–0.504) H–1 → L (0.187) H → L+1 (–0.161)	0.0000
$S_0 \rightarrow S_5$	409.15 (3.030)	H–3 → L(0.510) H–2 → L+1(–0.449) H–1 → L+1 (0.126)	0.0276
$S_0 \rightarrow T_{11}$	396.04 (3.131)	H–7 → L (0.514) H–6 → L+1 (0.354) H–4 → L+1 (0.248) H–2 → L+1(–0.142)	0.0000
$S_0 \rightarrow T_{12}$	395.87 (3.132)	H–7 → L+1 (0.411) H–6 → L (0.511) H–4 → L (0.183) H–2 → L (–0.118)	0.0000
$S_0 \rightarrow S_6$	390.20 (3.177)	H–5 → L (0.376) H–4 → L+1(–0.194) H–3 → L (–0.245) H–2 → L+1(–0.373) H–1 → L+1(–0.248) H → L (0.200)	0.3519
$S_0 \rightarrow T_{13}$	389.07 (3.187)	H–7 → L (0.196) H–5 → L (0.558) H–4 → L+1(–0.345) H–2 → L+1(–0.111)	0.0000
$S_0 \rightarrow S_7$	387.54 (3.199)	H–5 → L+1(–0.262) H–4 → L (0.587) H–3 → L+1(–0.245) H–2 → L (–0.105)	0.0000
$S_0 \rightarrow T_{14}$	387.50 (3.200)	H–9 → L (0.110) H–7 → L+1 (0.192) H–5 → L+1 (0.600) H–4 → L (–0.264) H–2 → L (–0.106)	0.0000
$S_0 \rightarrow S_8$	387.07 (3.203)	H–7 → L (0.186) H–5 → L (0.160) H–3 → L (–0.322) H–2 → L+1(–0.111) H–1 → L+1 (0.440) H → L (–0.331)	1.0695
$S_0 \rightarrow S_9$	383.99 (3.229)	H–5 → L (–0.241) H–4 → L+1 (0.545) H–3 → L (–0.200) H–2 → L+1(–0.252) H–1 → L+1(–0.108) H → L (0.102)	0.1445
$S_0 \rightarrow S_{10}$	383.39 (3.234)	H–7 → L+1(–0.121) H–5 → L+1(–0.362) H–3 → L+1 (0.491) H–2 → L (0.256) H–1 → L (–0.120)	0.0000
$S_0 \rightarrow T_{15}$	376.23 (3.295)	H–9 → L (0.155) H–8 → L+1(–0.149) H–7 → L+1 (0.452) H–6 → L (–0.449) H–5 → L+1(–0.193)	0.0000
$S_0 \rightarrow S_{11}$	373.82 (3.317)	H–7 → L+1(–0.428) H–6 → L (0.531) H–5 → L+1 (0.138)	0.0000
$S_0 \rightarrow S_{12}$	372.97 (3.324)	H–8 → L (–0.123) H–7 → L (–0.452) H–6 → L+1 (0.498) H–5 → L (0.120) H–4 → L+1 (0.124)	0.0026
$S_0 \rightarrow S_{13}$	355.39 (3.489)	H–9 → L+1 (0.420) H–8 → L (0.485) H–7 → L (–0.121) H–5 → L (–0.182) H–2 → L+1(–0.119)	0.0293
$S_0 \rightarrow S_{14}$	354.24 (3.500)	H–9 → L (0.484) H–8 → L+1 (0.458) H–7 → L+1(–0.165)	0.0000
$S_0 \rightarrow S_{15}$	352.76 (3.515)	H–9 → L (–0.154) H–8 → L+1 (0.260) H–7 → L+1 (0.320) H–6 → L (0.400) H–5 → L+1(–0.316) H–4 → L (–0.134)	0.0000

Table 1-A14. Electronic Transitions Estimated for Stacked Three Molecules of **1fBF₂** with Geometries in Crystals ($M_1/M_0/M_1$), Simulated Using B97D Method with 6-311G** Basis Sets

	λ_{ET} / nm (eV)	Transition (Coefficient)	*f*
$S_0 \rightarrow T_1$	545.54 (2.273)	H–2 → L (0.181) H–2 → L+2 (0.220) H+1 → L+1(–0.120) H → L (–0.585) H → L+2 (–0.239)	0.0000
$S_0 \rightarrow T_2$	537.25 (2.308)	H–2 → L+1(–0.243) H–1 → L (–0.326) H–1 → L+2 (0.309) H → L+1 (0.481)	0.0000
$S_0 \rightarrow T_3$	536.23 (2.312)	H–2 → L (0.264) H–1 → L+1 (0.425) H → L (–0.146) H → L+2 (–0.459)	0.0000

$S_0 \rightarrow S_1$	497.10 (2.494)	H–2 → L+2(–0.127) H–1 → L+1 (0.301) H → L (0.517) H → L+2 (–0.352)	0.0468
$S_0 \rightarrow S_2$	496.65 (2.497)	H–1 → L (0.327) H → L+2 (–0.135) H → L+1 (–0.608)	0.0000
$S_0 \rightarrow T_4$	495.56 (2.504)	H–2 → L+1 (0.120) H–1 → L (0.455) H–1 → L+2(–0.187) H → L+1 (0.493)	0.0000
$S_0 \rightarrow T_5$	494.22 (2.502)	H–2 → L+2(–0.152) H–1 → L+1 (0.471) H → L (0.306) H → L+2 (–0.398)	0.0000
$S_0 \rightarrow S_3$	486.87 (2.547)	H–2 → L (–0.395) H–2 → L+2(–0.178) H → L (0.276) H → L+2 (0.485)	0.0176
$S_0 \rightarrow T_6$	485.06 (2.556)	H–2 → L+1(–0.171) H–1 → L (0.417) H–1 → L+2 (0.525) H → L+1 (–0.143)	0.0000
$S_0 \rightarrow S_4$	483.61 (2.564)	H–2 → L+1(–0.120) H–1 → L (0.531) H–1 → L+2 (0.412) H → L+1 (–0.180)	0.0000
$S_0 \rightarrow T_7$	482.52 (2.570)	H–2 → L (0.589) H–2 → L+2 (0.205) H → L (–0.174) H → L+2 (–0.264)	0.0000
$S_0 \rightarrow S_5$	473.51 (2.618)	H–2 → L (–0.324) H–2 → L+2 (0.460) H–1 → L+1 (0.404) H → L (–0.139)	0.0331
$S_0 \rightarrow S_6$	473.01 (2.621)	H–2 → L+1(0.558) H–1 → L (–0.147) H–1 → L+2 (0.396)	0.0000
$S_0 \rightarrow T_8$	472.70 (2.622)	H–2 → L+1 (0.626) H–1 → L (–0.104) H–1 → L+2 (0.303)	0.0000
$S_0 \rightarrow T_9$	471.60 (2.629)	H–2 → L (–0.209) H–2 → L+2 (0.611) H–1 → L+1 (0.265) H → L (–0.103)	0.0000
$S_0 \rightarrow T_{10}$	440.45 (2.815)	H–8 → L+1 (0.122) H–7 → L+2(–0.112) H–5 → L+2 (0.146) H–4 → L (–0.431) H–4 → L+2 (0.218) H–3 → L+1 (0.426)	0.0000
$S_0 \rightarrow T_{11}$	440.30 (2.816)	H–7 → L+1(–0.125) H–5 → L+1 (0.103) H–4 → L+1(0.445) H–3 → L (–0.353) H–3 → L+2 (0.322)	0.0000
$S_0 \rightarrow T_{12}$	438.35 (2.828)	H–7 → L (–0.142) H–5 → L (0.379) H–5 → L+2 (0.204) H–4 → L (–0.279) H–4 → L+2(–0.376) H–3 → L+1(–0.192)	0.0000
$S_0 \rightarrow T_{13}$	424.28 (2.922)	H–12 → L (0.112) H–8 → L (–0.150) H–6 → L (0.231) H–6 → L+2 (0.180) H–4 → L+1 (0.160) H–3 → L (0.486) H–3 → L+2 (0.294)	0.0000
$S_0 \rightarrow S_7$	419.59 (2.955)	H–4 → L+1(–0.163) H–2 → L (0.455) H–2 → L+2 (0.107) H–1 → L+1 (0.285) H → L (0.124) H → L+2 (0.349)	0.0000
$S_0 \rightarrow T_{14}$	416.95 (2.974)	H–8 → L (0.131) H–8 → L+2(–0.199) H–7 → L+1 (0.203) H–6 → L (0.237) H–5 → L+2 (0.381) H–4 → L+1(–0.245) H–3 → L (–0.157) H–3 → L+2 (0.281)	0.0000
$S_0 \rightarrow T_{15}$	416.94 (2.974)	H–8 → L+1(–0.244) H–7 → L (–0.202) H–7 → L+2 (0.111) H–6 → L+1(–0.137) H–5 → L (–0.220) H–5 → L+2 (0.285) H–4 → L (0.136) H–4 → L+2(–0.249) H–3 → L+1 (0.351)	0.0000
$S_0 \rightarrow S_8$	415.67 (2.983)	H–4 → L+1 (0.237) H–3 → L (0.647)	0.0073
$S_0 \rightarrow S_9$	415.02 (2.987)	H–5 → L (0.176) H–4 → L (0.576) H–3 → L+1 (0.316)	0.0001
$S_0 \rightarrow S_{10}$	410.71 (3.019)	H–5 → L+1(–0.423) H–3 → L (–0.119) H–3 → L+2(0.535)	0.0105
$S_0 \rightarrow S_{11}$	410.39 (3.021)	H–5 → L (0.108) H–5 → L+2 (0.162) H–4 → L (0.163) H–4 → L+2 (0.459) H–3 → L+1(–0.423) H–2 → L+1(–0.112)	0.0001

		H–1 → L+2 (0.111)	
$S_0 \rightarrow S_{12}$	407.05 (3.046)	H–5 → L (0.472) H–5 → L+2(–0.113) H–4 → L+2 (0.260) H–3 → L +2(0.137) H–2 → L+2 (0.228) H–1 → L (0.159) H–1 → L+2(–0.220) H → L+1 (–0.161)	0.0289
$S_0 \rightarrow S_{13}$	403.56 (3.072)	H–8 → L (–0.130) H–7 → L+1(–0.151) H–6 → L (–0.101) H–5 → L+1 (0.549) H–4 → L+1(–0.252) H–3 → L+2(–0.198) H–1 → L+1(–0.112)	0.0493
$S_0 \rightarrow S_{14}$	402.41 (3.081)	H–7 → L (0.172) H–7 → L+2(–0.123) H–5 → L (0.155) H–5 → L+2 (0.408)	0.0001
		H–4 → L (0.174) H–3 → L+1(–0.127) H–2 → L+1 (0.251) H–1 → L (–0.183) H–1 → L+2(–0.238) H → L+1 (–0.181)	
$S_0 \rightarrow S_{15}$	394.88 (3.140)	H–8 → L+2 (0.103) H–7 → L+1(–0.179) H–6 → L (0.546) H–6 → L (–0.346)	0.0558

1.7.7. References and Notes

A1. Franek, W. *Monatsh. Chem*. **1996**, *127*, 895–907.

A2. Houlihan, W. J.; Munder, P. G.; Handley, D. A.; Cheon, S. H.; Parrino, V. A. *J. Med. Chem.* **1995**, *38*, 234–240.

A3. Kondolff, I.; Doucet, H.; Santelli, M. *Organometallics* **2006**, *25*, 5219–5222.

A4. Amedio Jr., J. C.; Lee, G. T.; Prasad, K.; Repic, O. *Synth. Commun.* **1995**, *25*, 2599–2612.

A5. Spivey, A. C.; Srikaran, R.; Diaper, C. M.; Turner, D. J. *Org. Biomol. Chem.* **2003**, *1*, 1638–1640.

A6. Yamakawa, T.; Kagechika, H.; Kawachi, E.; Hashimoto, Y.; Shudo, K. *J. Med. Chem.* **1990**, *33*, 1430–1437.

A7. Behal, A.; Auger, V. *Bull. Soc. Chim. Fr.* **1893**, *3*, 699.

A8. Yamada, T.; Nagata, T.; Sugi, K. D.; Yorozu, K.; Ikeno, T.; Ohtsuka, Y.; Miyazaki, D.; Mukaiyama, T. *Chem. Eur. J.* **2003**, *9*, 4485–4509.

A9. Franek, W. *Monatsh. Chem.* **1996**, *127*, 895–907.

A10. Welters, R.; Gehlhaus, J.; Moeschl, G. *Ger. Offen.* **1977**, DE 2544180 A1 19770414.

A11. Mirochnik, A. G.; Fedrenko, E. V.; Kuryavyi, V. G.; Bukvestskii, B. V.; Karasev, V. E. *J. Fluoresc.* **2006**, *16*, 279–286.

A12. Rowland, R. S.; Taylor, R. *J. Phys. Chem.* **1996**, *100*, 7384–7391.

A13. Kollman, P. A.; Allen, L. C. *Chem. Rev.* **1972**, *72*, 283–303.

A14. Yuan, W. Z.; Shen, X. Y.; Zhao, H.; Lam, J. W. Y.; Tang, L.; Lu, P.; Wang, C.; Liu, Y.; Wang, Z.; Zhang, Q.; Sun, J. Z.; Ma, Y.; Tang, B. Z. *J. Phys. Chem. C* **2010**, *114*, 6090–6099.

A15. Bolton, O.; Lee, K.; Kim, H.-J.; Lin, K. Y.; Kim, J. *Nature Chem.* **2011**, *3*, 205–210.

A16. Gong, Y.; Zhao, L.; Peng, Q.; Fan, D.; Yuan, W. Z.; Zhang, Y.; Tang, B. Z. *Chem. Sci.* **2015**, *6*, 4438–4444.

A17. Grimme, S. *J. Comp. Chem.* **2006**, *27*, 1787–1799.

A18. Boys, S. F.; Bernardi, F. *Mol. Phys.* **1970**, *19*, 553–566.

A19. Delley, B. *J. Chem. Phys.* **1990**, *92*, 508–517.

CHAPTER 2

White Light Emission From a Single Component System: Remarkable Concentration Effects on the Fluorescence of Diaroylmethanatoboron Difluoride

2.1. Introduction.

White fluorescent organic materials have attracted great attention in connection with their application to white organic light-emitting diodes (WOLEDs).[1] To obtain white emission, with the Commission Internationale de l'Eclairage (CIE) coordinate (x, y) = (0.33, 0.33), mixing three primary colors (blue, green, and red) or two complementary colors (such as blue and yellow) is necessary. Thus, most of the materials employed for white emission consist of multiple light-emitting components.[2,3] However, some problems exist with systems of this type, such as the need for a complicated fabrication process of the emitting device and a change or degradation of the white color caused by the low stability of fluorescent compounds. Clearly, use of a single-component, white-emitting material would be an ideal solution to this problem.[4–6] However, examples of materials of this type are limited to complexes containing heavy metal atoms or organic compounds with highly π-conjugated skeletons.[6,7]

Dibenzoylmethanatoboron difluoride (**P1BF$_2$**, Scheme 2-1) and its analogues exhibit intense fluorescence (FL) emissions,[8–15] in spite of their small molecular size and lack of heavy metal atoms.[8–13] The parent **P1BF$_2$** was synthesized for the first time by Morgan and Tunstall in 1924.[14] A report on FL property in $CHCl_3$ by Karasev and Korotkikh[15] opened up a field of various emission ability of **P1BF$_2$**, including FL in the crystalline states[16,17] and films,[18] FL induced by two-photon absorption,[19] etc. Motivated by these historical works, the author have prepared a variety of 4,4'-disubstituted derivatives of **P1BF$_2$** and studied their FL properties in KBr and CH_2Cl_2. In the effort described below, the author observed that CH_2Cl_2 solutions of the parent substance, **P1BF$_2$**, and its diisopropyl derivative, bis(4-isopropylbenzoyl)methanatoboron difluoride (**1eBF$_2$**, Scheme 2-1), display remarkable concentration effects on their FL wavelengths. Although no significant difference in FL between **P1BF$_2$** and **1eBF$_2$** exists, the FL colors of these substances undergo dramatic changes from blue at low concentrations to yellow at high concentrations, as a consequence of changes from emitting excited monomers to excimers. Importantly, white emission from these substances can be achieved by adjusting their concentrations to bring about a suitable ratio of blue and yellow FL.

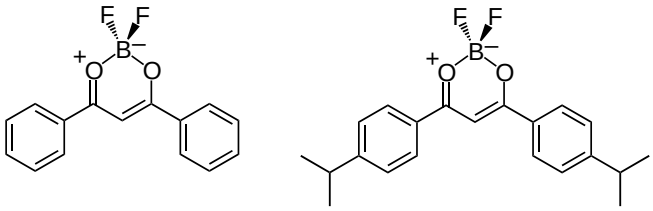

P1BF$_2$ **1eBF$_2$**

Scheme 2-1. Structures of **P1BF$_2$** and **1eBF$_2$**.

2.2. Results and Discussion.

2.2.1. Synthesis of P1BF$_2$ and 1eBF$_2$. The parent substance **P1BF$_2$** and the diisopropyl derivative **1eBF$_2$** were synthesized by treatment of the corresponding diaroylmethanes **P1H** and **1eH** with the boron trifluoride diethyl ether complex.[15–17] Preparation of **1eH** was accomplished by use of a condensation reaction of methyl 4-isopropylbenzoate with 4'-isopropylacetophenone, while **P1H** is commercially available.

2.2.2. Diffuse reflection and FL properties in KBr. The diffuse reflection and FL properties of the parent **P1BF$_2$** and the diisopropyl derivative **1eBF$_2$** in KBr are summarized in Table 2-1.[18] The diffuse reflection maxima of these substances in KBr powders ($\lambda_{DR,P}$) occur at *ca*. 400 nm, indicating that the isopropyl substituents do not alter this property. However, the FL properties of **P1BF$_2$** and **1eBF$_2$** are different. The sharp FL band of **P1BF$_2$** in KBr powder ($\lambda_{FL,P}$) appear at around 542 nm while that of **1eBF$_2$** is evidently broadened with some peaks at 439, 474, and 527 nm (Table 2-1 and Figure 2-1). Moreover, the FL quantum yield ($\Phi_{FL,P}$) of **1eBF$_2$** was found to be 0.13, a value that is much higher than that of **P1BF$_2$** (0.03). Interestingly, the FL color of **1eBF$_2$** in KBr is almost white, with a CIE coordinate (x, y) = (0.29, 0.38), while that of **P1BF$_2$** is yellow with a coordinate (0.35, 0.44) (Figure 2-2). Therefore, the incorporation of isopropyl groups at the 4-position of two phenyl groups in **P1BF$_2$** brings about a change of FL color of the powder from yellow to white and an improvement of $\Phi_{FL,P}$.

Table 2-1. Diffuse Reflection, Absorption, and FL Properties of **P1BF$_2$** and **1eBF$_2$**

	Diffuse Reflection and Absorption				FL	
	KBr		CH_2Cl_2		KBr	CH_2Cl_2
Sub.	$\lambda_{DR,P}$/nm[a]	*K*–*M*	$\lambda_{AB,S}$/nm[b]	log ε	$\lambda_{FL,P}$/nm[a]	$\lambda_{FL,S}$/nm[b]
P1BF$_2$	400	0.05	365	4.37	545	398
			380	4.43		
1eBF$_2$	398	0.16	380	4.84	439	411
					474	
					527	

[a] $\lambda_{DR,P}$ and $\lambda_{FL,P}$ are wavelengths for the diffuse reflection maxima and the FL maxima, respectively, for the mixtures of diaroylmethanatoboron difluoride, **1BF$_2$**, (0.2 μmol) and KBr (500 mg) powdered with ballmill at 50 Hz for 15 min. [b] $\lambda_{AB,S}$ and $\lambda_{FL,S}$ are wavelengths for the absorption maxima and the FL maxima, respectively, for **1BF$_2$** in CH_2Cl_2 when their absorbance values are *ca*. 0.3 at the wavelength indicated (*ca*. 0.5×10^{-5} M).

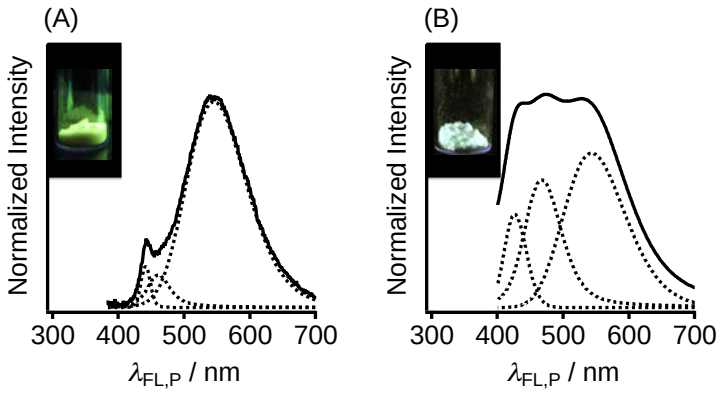

Figure 2-1. Observed FL spectra (solid curves) of **P1BF$_2$** (A) and **1eBF$_2$** (B) in KBr at 294 K with deconvoluted spectra (broken curves) and photographs of measuring samples (insets). λ_{EX} = 365 nm.

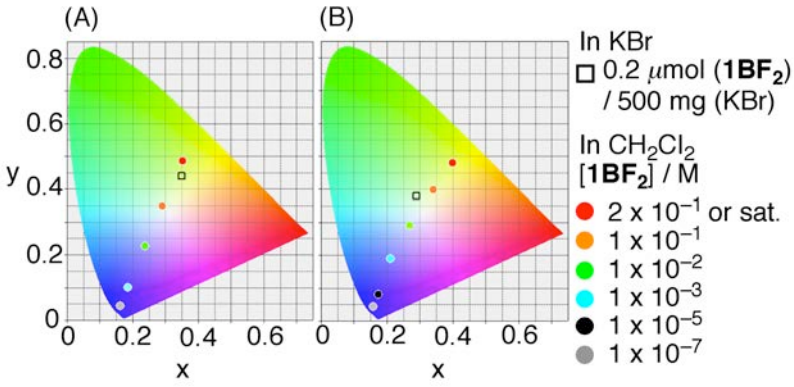

Figure 2-2. The CIE chromaticity diagrams for FL of **P1BF$_2$** (A) and **1eBF$_2$** (B) in KBr (squares) and CH_2Cl_2 (circles) at 294 K. λ_{EX} = 365 nm.

Wave deconvolutions of the FL spectra using a Gaussian function were carried out to determine the origin of differences between the FL properties of **P1BF$_2$** and **1eBF$_2$** in KBr. In both cases, the original FL spectra were deconvoluted to generate three component spectra (Figure 2-1), suggesting that FL of **P1BF$_2$** and **1eBF$_2$** in KBr consists of three components involving multiple FL domains comprised minimally of excited monomers and excimers. It is likely that, the observed differences in the FL of **P1BF$_2$** and **1eBF$_2$**, caused by the presence of isopropyl groups in the latter substance, are a consequence of the difference in the degree of intermolecular interaction existing in the solid state. These diffuse reflection and FL properties, obtained by using powder samples of **P1BF$_2$** or **1eBF$_2$** (0.2 μmol) ground with KBr (500 mg), remain unchanged when different ratios of KBr and the substances are employed.[19]

2.2.3. Absorption and FL properties in CH_2Cl_2. The absorption and FL properties of **P1BF$_2$** and **1eBF$_2$** in CH_2Cl_2 solutions are summarized in Table 2-1.[18] The absorption maxima of both of these substances in CH_2Cl_2 solutions ($\lambda_{AB,S}$) are 380 nm, indicating that no significant effects of the isopropyl substituents exist.

The different FL properties of **P1BF$_2$** and **1eBF$_2$** are also observed in CH_2Cl_2. Specifically, at low concentration (e.g., 1×10^{-7} M), CH_2Cl_2 solutions of both **P1BF$_2$** and **1eBF$_2$** display blue emission at respective FL maxima ($\lambda_{FL,S}$) of 398 and 411 nm (Table 2-1 and Figure 2-3). The 13-nm red shift observed for **1eBF$_2$** vs. **P1BF$_2$** is consistent with the trend seen for FL of members of a series of **1BF$_2$**, in which similar red shift of FL have been observed and rationalized by alterations of the electron-donating ability of diketonate ligands.[13,14] Moreover, the FL quantum yield in CH_2Cl_2 ($\Phi_{FL,S}$) of **1eBF$_2$** is nearly unity (0.99) while that of the parent **P1BF$_2$** is only 0.26 (Table 2–2).

To gain further insight into the observed substituent effects, concentration effects of **P1BF$_2$** and **1eBF$_2$** on FL properties, in the $1 \times 10^{-7} - 2 \times 10^{-1}$ M region, were explored. As is commonly observed for fluorescent organic compounds, self-quenching causes the $\Phi_{FL,S}$ of **1eBF$_2$** to significantly decrease (from 0.99 to 0.32) on increasing concentration (Table 2-2). Surprisingly, however, the parent **P1BF$_2$** at 2×10^{-1} M exhibits a relatively larger $\Phi_{FL,S}$ (0.36) as compared with that at 1×10^{-7} M (0.26). This observation suggests that radiationless relaxation of the excited monomer or related species, such as an excimer, of **P1BF$_2$** is effectively retarded at high concentration.

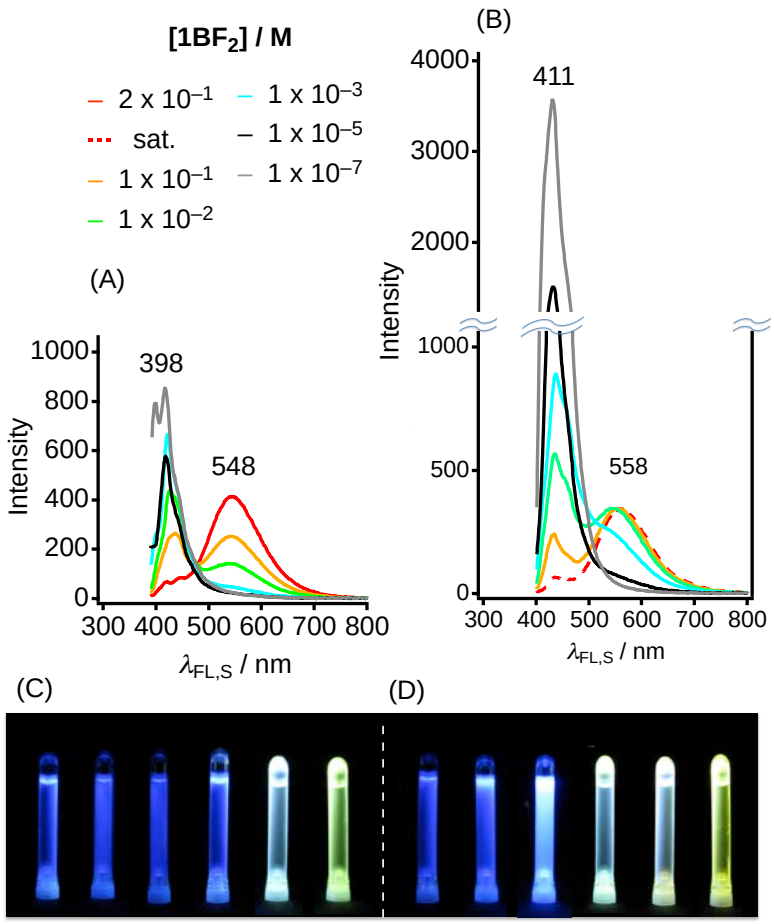

Figure 2-3. Concentration effects on the FL spectral profiles of **P1BF$_2$** (A) and **1eBF$_2$** (B) in CH_2Cl_2 at 294 K. λ_{EX} = 380 nm. Photographs of FL of **P1BF$_2$** (C) and **1eBF$_2$** (D) in CH_2Cl_2 at 294 K. λ_{EX} = 365 nm. The solutions of 1×10^{-7}, 1×10^{-5}, 1×10^{-3}, 1×10^{-2}, 1×10^{-1}, and 2×10^{-1} M for **P1BF$_2$** or the saturated concentration (*ca*. 1.5×10^{-1} M) for **1eBF$_2$** were serially put on from the left to the right.

Importantly, as the concentrations of **P1BF$_2$** and **1eBF$_2$** become higher, an FL band appears at 548 and 558 nm, respectively, in concert with a drastic FL color change from blue to yellow (Figure 2-3). It is significant that at certain concentrations, solutions of **P1BF$_2$** and **1eBF$_2$** emit white FL. The CIE chromaticity diagrams for FL of **P1BF$_2$** and **1eBF$_2$** in CH_2Cl_2 show successive transitions (Figure 2-2).[20] The CIE coordinates for 1×10^{-1} M solutions are (x, y) = (0.29, 0.35) and (0.34, 0.40) for **P1BF$_2$** and **1eBF$_2$**, respectively, values that are close to the coordinate for ideal white emission, (x, y) = (0.33, 0.33).

Table 2-2. FL Quantum Yields and Lifetimes of **P1BF$_2$** and **1eBF$_2$** in CH_2Cl_2

	P1BF$_2$			**1eBF$_2$**		
[**1BF$_2$**]/M [b]	$\Phi_{FL,S}$	τ_{410}/ns [a]	τ_{530}/ns [a]	$\Phi_{FL,S}$	τ_{410}/ns [a]	τ_{530}/ns [a]
	0.36	1.65	50.7	0.32	0.31	48.3
		0.46	6.27		0.91	3.11
			0.47			0.57
1×10^{-1}	0.28	0.41	51.5	0.37	0.80	57.8
		0.74	2.60		1.20	11.5
			0.44			2.03
1×10^{-2}	0.24	0.81	49.3	0.49	1.86	52.0
			1.02			14.2
						3.48
1×10^{-3}	0.22	0.51	39.5	0.53	1.80	23.9
			0.51			1.95
1×10^{-5}	0.26	0.50	32.5	0.68	1.67	16.1
			0.50			1.70
1×10^{-7}	0.26	0.50	0.69	0.99	1.56	13.2
			0.44			1.58

[a] The τ values for the solution at a higher concentration (especially, [**1BF$_2$**] > 1×10^{-2} M) may involve some systematic errors, because a probable intermolecular interaction is not accurately evaluated. [b] 2×10^{-1} M for **P1BF$_2$** and the saturated concentration (*ca*. 1.5×10^{-1} M) for **1eBF$_2$**.

As in the case of KBr powder samples, a study of wave deconvolution analyses is the key to elucidating the effects of substituents on the FL properties of CH_2Cl_2 solutions of **P1BF$_2$** and **1eBF$_2$**. As displayed in Figure 2-4, the original FL spectra at the lowest concentrations were deconvoluted to generate several spectra with $\lambda_{FL,S}$ at *ca*. 400–500 nm (Figure 2-4, blue), which can be reasonably assigned to the excited monomers of diaroylmethanatoboron difluoride (**1BF$_2$**). In contrast, the original FL spectra at higher concentrations were deconvoluted to generate several spectra at *ca*. 400–500 nm and spectra with $\lambda_{FL,S}$ at *ca*. 550–560 nm (red), which are likely associated with the excimers of **1BF$_2$**. Thus, the results of wave deconvolution analyses reveal that the FL of **1BF$_2$** in CH_2Cl_2 consists of two types of the FL domains corresponding to the excited monomers and excimers. These conclusions gain support from the results of FL lifetime (τ) measurements. The τ values at 410 nm for the FL shorter wavelength domains of **P1BF$_2$** and **1eBF$_2$** (< 1×10^{-2} M) are τ_{410} = *ca*. 0.5 and *ca*. 1.7 ns, respectively. In contrast, the τ values at 530 nm for the longer wavelength FL domains of these substances are τ_{530} = *ca*. 50 ns, much longer than the τ_{410} values. The observed τ values are typical for emission from excited monomers and excimers of common organic substances.

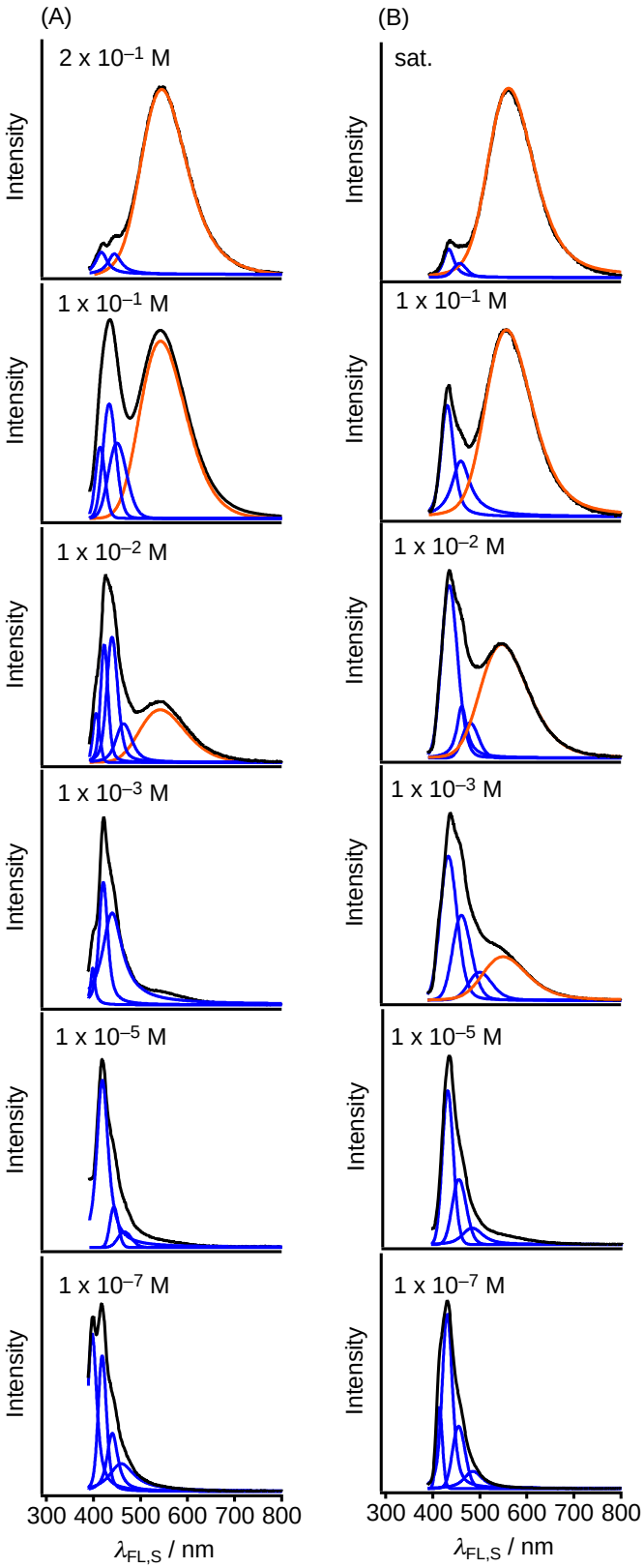

Figure 2-4. Observed FL spectra (black) of **P1BF$_2$** (A) and **1eBF$_2$** (B) with deconvoluted curves (blue: FL domain attributable to the excited monomer, orange: FL domain attributable to the excimer).

The results presented above clearly indicate that increasing concentrations of **1BF$_2$** cause continuous changes of the major FL domain from the excited monomers to excimers that are accompanied by changes of FL colors from blue to yellow. Mixing blue and yellow emissions from the excited monomers and excimers, respectively, in suitable ratios results in white emission.

2.3. Conclusion.

The results of the effort described above show that single component, organoboron complexes **1BF$_2$** exhibit white FL not only in KBr but also in CH_2Cl_2. The white FL consists of blue and yellow FLs (complementary colors), corresponding to the FL domains of excited monomers and excimers, respectively. As compared to conventional systems used for white FL, **1BF$_2$** are single-component, low molecular weight materials that are readily synthesized and do not contain heavy metal atoms.

It is interesting that $\lambda_{FL,P}$ of **1eBF$_2$** in KBr experiences a blue shift, but $\lambda_{FL,S}$ of **1eBF$_2$** in CH_2Cl_2 undergoes a red shift as compared to the parent **P1BF$_2$** (Table 2-1). Although, no clear explanation exists for these phenomena at this stage, the observation may be a consequence of the existence of another FL domain in the KBr powder, which probably depends on the molecular arrangement in the solid state.

2.4. Experimental Section.

2.4.1. General Methods. NMR spectra in $CDCl_3$ were recorded on a Varian Mercury 300 instrument spectrometer, operating at 300 MHz for ^1H NMR, respectively, where chemical shifts were determined with respect to tetramethylsilane (TMS) as an internal standard. Melting points were measured using a Yanako MP-500 and are reported uncorrected. UV-Vis spectra were recorded on a JASCO V-530 spectrophotometer. Diffuse reflection spectra were obtained on a JASCO V-570 spectrophotometer. FL spectra and FL quantum yields were recorded on a HAMAMATSU Photonics C9920-02. Wave deconvolution for FL spectra were carried out using a PeakFit program v4.12.[21]

2.4.2. Materials.

Dibenzoylmethanatoboron difluoride (P1BF$_2$).[15,16] A solution of dibenzoylmethane (**P1H**, 560 mg, 2.5 mmol) and BF_3•OEt_2 (0.47 mL, 3.8 mmol) in dry benzene (10 mL) was stirred under argon atmosphere at room temperature for 16 h. Evaporation to dryness under reduced pressure and recrystallization of resultant residue from benzene gave **P1BF$_2$** as yellow needles (580 mg, 2.1 mmol) in 85% yield. mp 189–191 ºC. ^1H NMR (300 MHz, $CDCl_3$) δ = 7.20 (s, 1H), 7.56 (AA'BB'C, J = 7.5 Hz, 4H), 7.69 (AA'BB'C, J = 7.5 Hz, 2H), 8.15 (AA'BB'C, J = 7.5 Hz, 4H) ppm.

2.5. References and Notes.

1. D'Andrade, B. W.; Forrest, S. R. *Adv. Mater.* **2004**, *16*, 1585–1595.
2. Kido, J.; Kimura, M.; Nagai, K. *Science* **1995**, *267*, 1332–1334.
3. Kido, J.; Shionoya, H.; Nagai, K. *Appl. Phys. Lett.* **1995**, *67*, 2281–2283.
4. Nakaya, T.; Ikeda, A.; Saikawa, T. *Jpn. Kokai Tokkyo Koho* **2005**, JP 2005097537 A 20050414.
5. Shono, H.; Ohkawa, T.; Tomoda, H.; Mutai, T.; Araki, K. *ACS Appl. Mater. Interfaces* **2011**, *3*, 654–657.
6. Kamtekar, K. T.; Monkman, A. P.; Bryce, M. R. *Adv. Mater.* **2010**, *22*, 572–582.
7. Liu, Y.; Nishiura, M.; Wang, Y.; Hou, Z. *J. Am. Chem. Soc.* **2006**, *128*, 5592–5593.
8. Mirochnik, A. G.; Gukhman, E. V.; Karasev, V. E.; Zhikhareva, P. A. *Russ. Chem. Bull.* **2000**, *49*, 1024–1027.
9. Mirochnik, A. G.; Fedorenko, E. V.; Bukvetskii, B. V.; Karasev, V. E. *Russ. Chem. Bull.* **2005**, *54*, 1060–1062.
10. Mirochnik, A. G.; Fedorenko, E. V.; Karpenko, A. A.; Gizzatulina, D. A.; Karasev, V. E. *Luminescence* **2007**, *22*, 195–198.
11. Zhang, G.; Chen, J.; Payne, S. J.; Kooi, S. E.; Demas, J. N.; Fraser, C. L. *J. Am. Chem. Soc.* **2007**, *129*, 8942–8943.
12. Nagai, A.; Kokado, K.; Nagata, Y.; Arita, M.; Chujo, Y. *J. Org. Chem.* **2008**, *73*, 8605–8607.
13. Nagai, A.; Kokado, K.; Nagata, Y.; Chujo, Y. *Macromolecules* **2008**, *41*, 8295–8298.
14. Mirochnik, A. G.; Bukvetskii, B. V.; Fedorenko, E. V.; Karasev, V. E. *Russ. Chem. Bull.* **2004**, *53*, 291–296.
15. Ono, K.; Yoshikawa, K.; Tsuji, Y.; Yamaguchi, H.; Uozumi, R.; Tomura, M.; Taga, K.; Saito, K. *Tetrahedron* **2007**, *63*, 9354–9358.
16. Cogné-Laage, E.; Allemand, J. F.; Ruel, O.; Baudin, J. B.; Croquette, V.; Blanchard-Desce, M.; Jullien, L. *Chem. Eur. J.* **2004**, *10*, 1445–1455.
17. Franek, W. *Monatsh. Chem.* **1996**, *127*, 895–907.
18. For the detail, see Figure 2-A1 in the Appendix Section.
19. The FL properties of **1BF$_2$** in KBr seem to depend on rather the degree of mixing or grinding the sample. A study on this phenomenon is now in progress and results will be published elsewhere.
20. For the detail, see Table 2-A1 in the Appendix Section.
21. PeakFit 4.12, Systat Software, Inc., San Jose CA, http://www.sigmaplot.com/products/peakfit/.

2.6. Appendix Section.

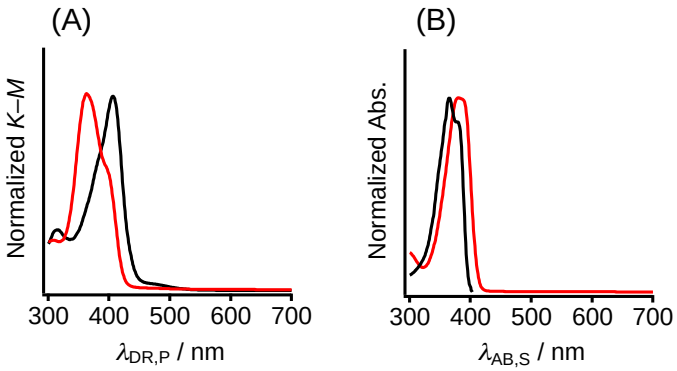

Figure 2-A1. (A) Diffuse reflection spectra of **P1BF$_2$** (black) and **1eBF$_2$** (red) in KBr. (B) UV–vis spectra of **P1BF$_2$** (black) and **1bBF$_2$** (red) in CH_2Cl_2 when their maximal absorbance values are 0.3 (*ca*. 0.5 × 10^{-5} M).

Table 2-A1. CIE Chromaticity Coordinate for FL of **P1BF$_2$** and **1eBF$_2$** in CH_2Cl_2

	P1BF$_2$	**1eBF$_2$**
[**1BF$_2$**]/M [a]	(x, y)	(x, y)
	(0.351, 0.486)	(0.398, 0.481)
1×10^{-1}	(0.290, 0.350)	(0.340, 0.399)
1×10^{-2}	(0.237, 0.227)	(0.268, 0.292)
1×10^{-3}	(0.184, 0.101)	(0.210, 0.190)
1×10^{-5}	(0.161, 0.045)	(0.172, 0.081)
1×10^{-7}	(0.162, 0.045)	(0.158, 0.044)

[a] 2×10^{-1} M for **P1BF$_2$** and the saturated concentration (*ca*. 1.5×10^{-1} M) for **1eBF$_2$**.

CHAPTER 3

Control of Mechanofluorochromism of Diaroylmethanatoboron Difluorides by the Steric Bulk of Substituents

3.1. Introduction.

Mechanofluorochromism (MFC) is a phenomenon in which changes in luminescence wavelength (color) of solid materials are induced by mechanical perturbations such as pulverization, shearing, and application of tension.[1] MFC materials have attracted much attention in connection with their potential applications in sensors,[2] memories,[3] and security inks.[4] Dibenzoylmethanatoboron difluoride is a new and promising framework for MFC materials.[5–10] In 2010, Fraser and coworkers reported that difluoroboron avobenzone in its solid state exhibits an MFC behavior associated with fluorescence (FL) color changes upon pulverization and that can be reversed by heating.[5a] Ito and coworkers also demonstrated that a *t*-Bu derivative of dibenzoylmethanatoboron difluoride (**1fBF$_2$**) in the solid state displays an MFC behavior.[10] In spite of these efforts, the structural features required for these materials to display MFC behavior have not been established. In view of this state of affairs, the author performed a comprehensive investigation focusing on changes in FL color that alkyl and trimetylsilyl *para*-substituted dibenzoylmethanatoboron difluorides **1a–gBF$_2$** [X = *n*-Bu (a), *n*-Pr (b), Et (c), Me (d), *i*-Pr (e), *t*-Bu (f), and Me_3Si (g), Figure 3-1][11,12] undergo in response to pulverization followed by annealing through heating. The results of this effort, described below, show that in their solid states, **1eBF$_2$**, **1fBF$_2$**, and **1gBF$_2$**, which possess bulky secondary or tertiary *para*-phenyl substituents, exhibit reversible MFC.

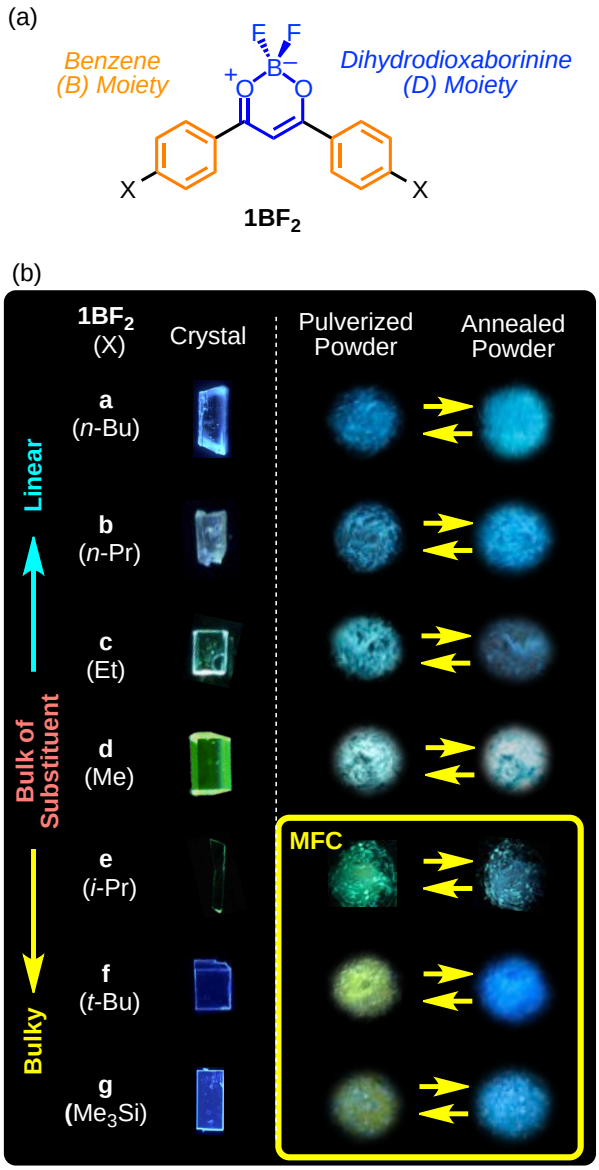

Figure 3-1. (a) Structures of **1a–gBF$_2$**. (b) Photographs of crystals and powders that were made by pulverizing crystals of **1a–gBF$_2$** followed by annealing under 365-nm light.

3.2. Experimental Section.

The synthesis, crystallization, and crystal packing structure determinations of **1a–gBF$_2$** were described in Chapter 1.

Crystals of **1a–gBF$_2$** were pulverized for a few minutes each using a spatula and quartz plate. FL spectra and lifetimes of the pulverized powders were measured. The powders were annealed at 100°C for *ca.* 5 min (**1aBF$_2$**) or at 150°C for *ca.* 5 min (**1b–gBF$_2$**). After cooling to room temperature, the annealed powders were subjected to measurement of FL spectra and lifetimes. The annealed powders were pulverized again to examine repeatability of change in FL spectra and lifetimes.

FL spectra of the solid-state **1a–gBF$_2$** were recorded using an excitation wavelength (λ_{EX}) of 365 nm. Wavelength maxima in FL spectra of the crystalline ($\lambda_{FL,C}$), pulverized powder ($\lambda_{FL,P}$), and annealed powder states ($\lambda_{FL,A}$) were determined. Analyses of time dependent changes of FL intensities were carried out by using first-order and multi-order fittings to give FL lifetimes in the crystalline ($\tau_{FL,C}$), pulverized powder ($\tau_{FL,P}$), and annealed powder states ($\tau_{FL,A}$). The detection wavelengths for determining FL lifetimes (λ_{DET}) were 460, 480, 500, 520, 540, and 560 nm.

3.3. Results and Discussion.

3.3.1. Changes in FL Properties upon Application of Mechanical Stimuli. As mentioned in Chapter 1, $\lambda_{FL,C}$ of **1aBF$_2$**, **1bBF$_2$**, **1cBF$_2$**, **1dBF$_2$**, **1eBF$_2$**, **1fBF$_2$**, and **1gBF$_2$** are observed at 450, 456, 476, 518, 500, 467, and 469 nm, respectively (Table 3-1 and Figure 3-2, left).[12] Powders of **1aBF$_2$** and **1bBF$_2$**, prepared by pulverization of the respective crystals, exhibit FL wavelength maxima at $\lambda_{FL,P}$ of 467 and 461 nm, respectively (Table 3-1 and Figure 3-2, center). Moreover, both $\tau_{FL,C}$ and $\tau_{FL,P}$ are less than 10 ns. Overall, **1aBF$_2$** and **1bBF$_2$** undergo no remarkable changes in their FL properties in that they exhibit excited monomer like blue FL[11,12] both in the crystalline and the pulverized powder state (Figure 3-1).

Table 3-1. FL Wavelength Maxima (λ_{FL}) and Lifetimes (τ_{FL}) of **1a–gBF$_2$** in the Crystalline, Pulverized Powder, and Annealed Powder States at 298 K[11]

	$\lambda_{FL,C}$[a] / nm	$\lambda_{FL,P}$[a] / nm	$\lambda_{FL,A}$[a] / nm	$\tau_{FL,C}$[b,c] / ns	$\tau_{FL,P}$[b,d] / ns	$\tau_{FL,A}$[b,d] / ns
1aBF$_2$	450	467	451	1.8	2–9	2–53
1bBF$_2$	456	461	451 475	1.8	2–17	2–3
1cBF$_2$	476	453 468	470	3.5	1–2	1–3
1dBF$_2$	518	462 522	462 516	3.2	3–13	1–4
1eBF$_2$	500	523	465	1.5	2–43	1–25
1fBF$_2$	467	444 536	441	6.8	3–49	3–19
1gBF$_2$	469	536	448	5.6	1–24	2–4

[a] λ_{EX} = 365 nm. [b] λ_{EX} = 371 nm. [c] For details, see the Chapter 1. [d] The range of values (the component over 40%) detected at $\lambda_{FL,C}$ = 460, 480, 500, 520, 540, and 560 nm. χ^2 values are in the range of 1.0 ± 0.2.

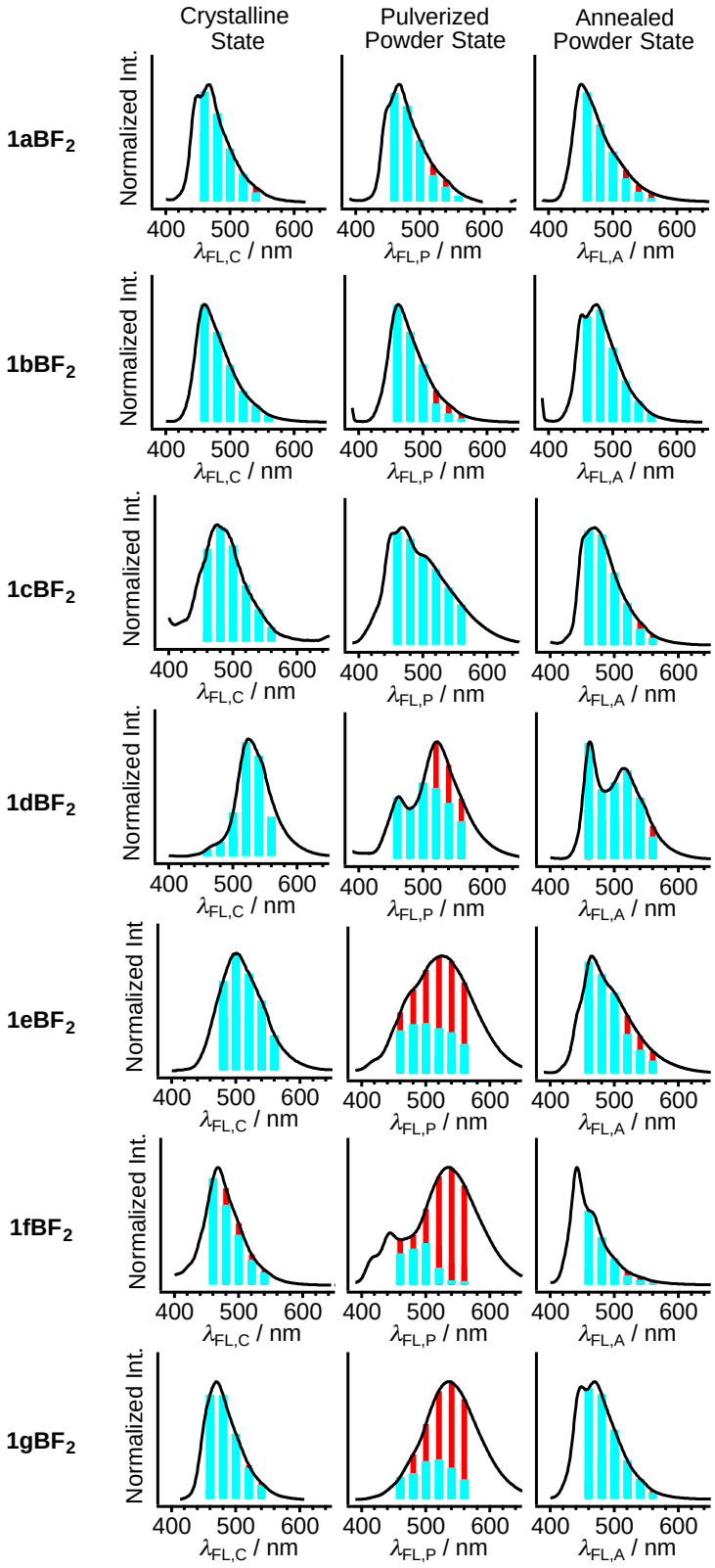

Figure 3-2. FL spectra of **1a–gBF$_2$** in the crystalline (left), pulverized powder (center), and annealed powder states (right) measured using λ_{EX} of 365 nm. The vertical lines drawn in the FL spectra have cyan and red colors that correspond abundance ratios of lifetimes of FL that are less than and more than 10 ns, respectively, at the corresponding wavelengths.[13]

In contrast, the author observed that new bands at $\lambda_{FL,P}$ of 453 and 468 nm, respectively, grew in FL spectra of **1cBF$_2$** and **1dBF$_2$** upon pulverization of the crystals (Table 3-1 and Figure 3-2, center). Judging from their $\lambda_{FL,P}$ and short $\tau_{FL,P}$ values, these short wavelength emission bands are attributable to excited monomer like FL or emission from "excited multimers" with *B-on-D* overlaps (For detail, see the Chapter 1). However, the longer wavelength FL bands of **1cBF$_2$** and **1dBF$_2$** at $\lambda_{FL,P}$ of 470 and 522 nm, respectively, which are also observed in the crystalline state at 468 and 518 nm, respectively, do not change upon pulverization. Importantly, in the retained longer wavelength 522-nm band of **1dBF$_2$**, has a $\tau_{FL,P}$ value of more than 10 ns. This observation indicates that crystalline **1dBF$_2$** undergoes a phase transition to produce a novel solid state species having a metastable packing form that provides long-lived emissive species like that expected for an excimer.[5,6,11,14] Successive annealing of pulverized powders of **1cBF$_2$** and **1dBF$_2$** leads to growth of shorter wavelength FL bands at $\lambda_{FL,A}$ = 470 and 462 nm, respectively, together with decreases in intensities of longer wavelength bands at $\lambda_{FL,P}$ of 470 and 522 nm, respectively (Table 3-1 and Figure 3-2, right). Simultaneously, the FL species with long $\tau_{FL,P}$ in the pulverized powder state of **1dBF$_2$** disappears upon the annealing, suggesting that a phase transition takes place to prevent a formation of excimer.

Furthermore, pulverization of crystals of **1eBF$_2$**, **1fBF$_2$**, and **1gBF$_2$** caused vivid changes in FL spectra. The FL color of crystalline **1eBF$_2$** changes from green to yellow while FL colors of crystalline **1fBF$_2$** and **1gBF$_2$** change to yellow upon pulverization (Figure 3-1). FL bands of **1eBF$_2$**, **1fBF$_2$**, and **1gBF$_2$** in their pulverized powder states have maxima at $\lambda_{FL,P}$ of 523, 536, and 536 nm, respectively, which are all longer than the respective maxima for FL of the corresponding crystalline materials that appear at 500, 467, and 469 nm. Moreover, the FL bands in the pulverized powder states of **1eBF$_2$**, **1fBF$_2$** and **1gBF$_2$** have large $\tau_{FL,P}$ values of more than 10 ns (Table 3-1 and Figure 3-2, center), indicating that novel packing structures, which form excimers upon photoexcitation, are generated.

Upon the successive annealing, pulverized powders of **1eBF$_2$**, **1fBF$_2$**, and **1gBF$_2$** undergo a FL color change from yellow to blue (Figure 3-1). The $\lambda_{FL,A}$ of the resulting annealed powders of **1eBF$_2$**, **1fBF$_2$**, and **1gBF$_2$** are 465, 441, and 448 nm, respectively (Table 3-1 and Figure 3-2, right). Furthermore, the FL bands with $\tau_{FL,P}$ of more than 10 ns disappear almost completely. It should be note that FL properties of **1fBF$_2$** and **1gBF$_2$** in their crystalline states are close to those of the respective annealed powder states.

3.3.2. Reversibility of Changes in FL Properties. To examine the reversibility of changes in FL properties that occur in proceeding from solid state to solid state of **1a–gBF$_2$**, sequential pulverization and annealing was repeated three times. The relative ratios of FL intensities at 540 nm (I_{FL540}) vs. 450 nm (I_{FL450}) of these materials, defined as $R = I_{FL540} / (I_{FL540} + I_{FL450})$, were determined for the crystalline states (R_C) and then for three cycles (n = 1–3) in proceeding from the pulverized powder state (R_{Pn}) to the annealed powder state (R_{An}) and back to the pulverized state (Table 3-2).

Table 3-2. Ratios (R) of FL Intensities at 540 nm vs. 450 nm in the Crystalline (R_C), Pulverized Powder (R_{Pn}), and Annealed Powder States (R_{An}) of **1a–gBF$_2$**

	R_C	R_{P1}	R_{A1}	R_{P2}	R_{A2}	R_{P3}	R_{A3}
1aBF$_2$	0.12	0.37	0.13	0.27	0.13	0.20	0.23
1bBF$_2$	0.15	0.22	0.17	0.23	0.13	0.34	0.16
1cBF$_2$	0.32	0.34	0.18	0.37	0.20	0.38	0.23
1dBF$_2$	0.97	0.67	0.58	0.35	0.30	0.30	0.24
1eBF$_2$	0.77	0.71	0.33	0.70	0.24	0.78	0.27
1fBF$_2$	0.17	0.70	0.08	0.73	0.07	0.62	0.16
1gBF$_2$	0.17	0.89	0.16	0.79	0.22	0.77	0.26

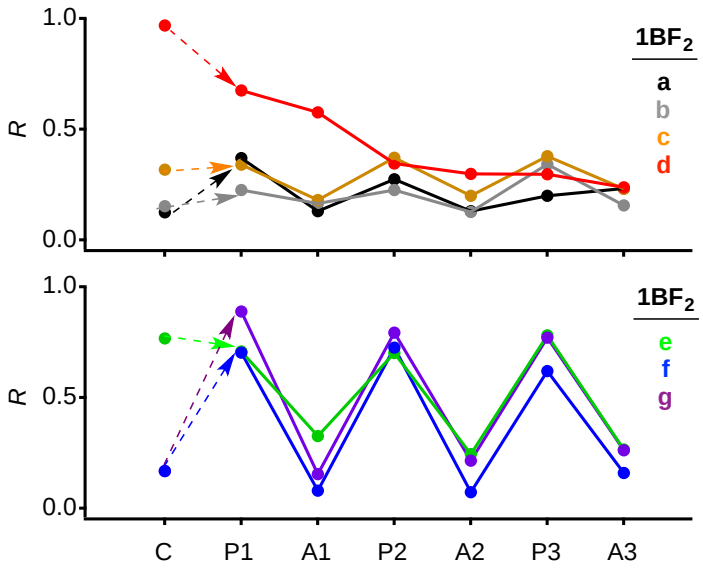

Figure 3-3. Plot of R values for FL in the crystalline (R_C), pulverized powder (R_{Pn}), and annealed powder states (R_{An}) of **1a–gBF$_2$**.

Plots of *R* values for FL of **1a–gBF$_2$** over three sets of pulverization–annealing cycles are displayed in Figure 3-3. As mentioned above, the changes in FL properties, especially λ_{FL}, upon pulverization of solid states of **1aBF$_2$** and **1bBF$_2$** are not drastic. Thus, the *R* values of these materials, which correspond to FL intensities at two different wavelengths, are not altered through the repeating cycles. On the other hand, the *R* values for **1cBF$_2$** display a reversible change of 0.2–0.4 on proceeding from the pulverized to the annealed powder state. However, this change is not large enough to cause a drastic change of FL color of **1cBF$_2$** in going between the pulverized and annealed powder states. This is the reason why the solid-state **1cBF$_2$** does not display typical MFC behavior in that it retains its blue FL color upon pulverization (Figure 3-1). Finally, the *R* value for FL of **1dBF$_2$** simply decreases upon repetitive pulverization and annealing (Table 3-2 and Figure 3-3), indicating that changes in its FL properties are not reversible.

Importantly, *R* values for FL of **1eBF$_2$**, **1fBF$_2$**, and **1gBF$_2$** undergo remarkable and reversible changes. FL in the pulverized powder states of **1eBF$_2$**, **1fBF$_2$**, and **1gBF$_2$** has large R_P values of more than 0.6 because of their FL bands around 520–540 nm. In contrast, the FL in the annealed powder states of these substances has small R_A values of less than 0.3 (except for R_{A1} of **1eBF$_2$**, which is 0.33), which results from their blue FL corresponding to a band around 440–460 nm. The combined observations suggest that **1eBF$_2$**, **1fBF$_2$**, and **1gBF$_2$** show reversible MFC while **1aBF$_2$**, **1bBF$_2$**, **1cBF$_2$**, and **1dBF$_2$** do not.

3.3.3 Key Factors of Mechanofluorochromism. The MFC behaviors of **1eBF$_2$**, **1fBF$_2$**, and **1gBF$_2$** can be attributed to a common, reversible solid–solid phase transition between a metastable state, which is formed upon pulverization, and a stable state, which is reconstituted via recrystallization caused by annealing (Figure 3-4b). It is appropriate, in this regard, that the energy of the transition state separating the former and latter states should be affected by steric bulk of substituents at the *para*-positions of phenyl groups in **1a–gBF$_2$**. The fact that only **1eBF$_2$**, **1fBF$_2$**, and **1gBF$_2$**, which respectively possess sterically bulky *i*-Pr, *t*-Bu, and Me_3Si groups display reversible MFC suggests that the steric bulk of secondary and tertiary substituents is sufficient to cause the degree of elevation of the energy of the transition state that is needed to preserve the metastable state. In these situation, the phase transition is prevented at room temperature while it takes place smoothly upon high temperature annealing. In contrast, the primary *n*-Bu, *n*-Pr, Et, and Me *para*-phenyl substituents present in **1aBF$_2$**, **1bBF$_2$**, **1cBF$_2$**, and **1dBF$_2$**, respectively, are too small to promote a significant elevation of the potential energy of the transition state (Figure 3-4a). This explanation is supported by the observation that the response of FL in the solid-state of **1aBF$_2$** is short lived.

Specifically, upon pulverization, the FL color of the solid state **1aBF$_2$** nearly instantaneously changes from blue to yellow (Figure 3-5), but immediately returns to blue. This finding shows that although the yellow FL emitting metastable state of **1aBF$_2$** is formed upon pulverization, it exists for only a short time at room temperature. Therefore, the bulk of *para*-phenyl substituents plays an important role in determining the MFC behavior of dibenzoylmethanatoboron difluoride derivatives.

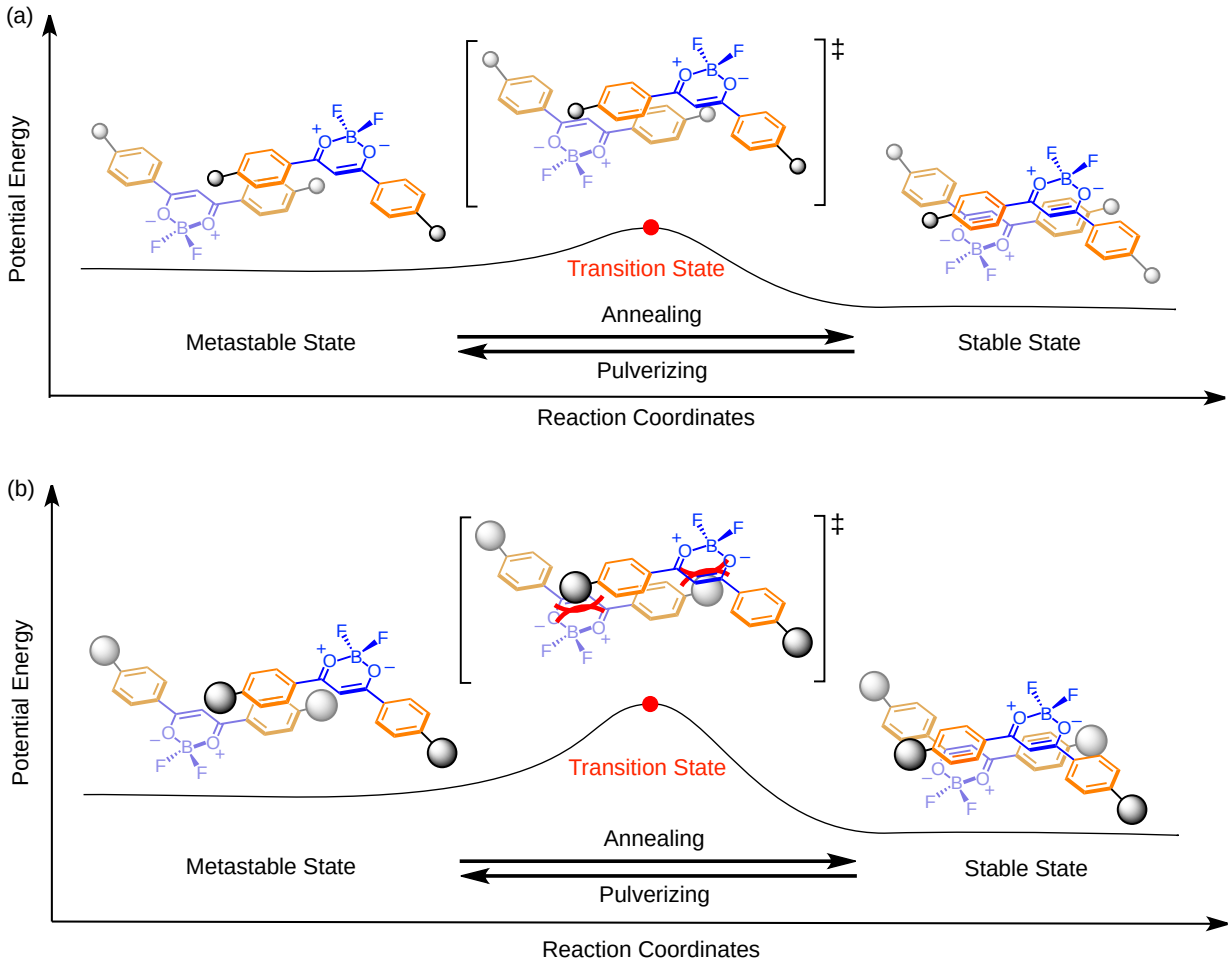

Figure 3-4. Plausible energy diagrams for MFC of **1BF$_2$** possessing (a) small primary *para*-phenyl substituents (**a**: *n*-Bu, **b**: *n*-Pr, **c**: Et, and **d**: Me) and (b) bulky secondary and tertiary *para*-phenyl substituents (**e**: *i*-Pr, **f**: *t*-Bu, and **g**: Me_3Si).

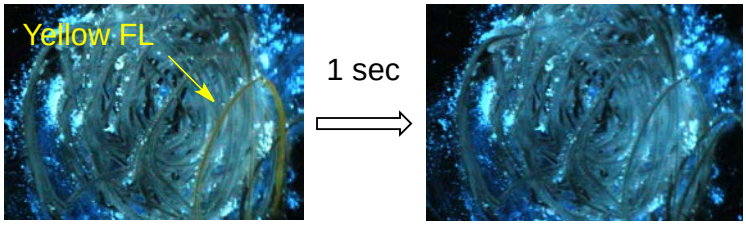

Figure 3-5. Photographs of solid-state **1aBF$_2$** under 365 nm light immediately following (left) and 1 sec after (right) pulverization.

3.4. Conclusion.

In this effort, the author showed that the MFC behavior of alkyl- and silyl-substituted dibenzoylmethanatoboron difluorides **1a–gBF$_2$** depends on the steric bulk of the *para*-substituents. For example, **1eBF$_2$**, **1fBF$_2$**, and **1gBF$_2$** were found to display MFC comprised of a reversible blue to yellow FL color change. However, the other derivatives, **1aBF$_2$**, **1bBF$_2$**, **1cBF$_2$** and **1dBF$_2$**, possessing smaller *n*-Bu, *n*-Pr, Et and Me substituents, do not display MFC. The results suggest that the steric bulk of the substituents are important in determining the stability of the metastable state involved in the MFC process. Importantly, only diaroylmethanatoboron difluoride derivatives that contain secondary and tertiary *para*-phenyl substituents such as *i*-Pr, *t*-Bu, and Me$_3$Si display MFC. This finding should serve as a guide to design of novel MFC materials.

3.5. References and Notes.

1. (a) Chi, Z.; Zhang, X.; Xu, B.; Zhou, X.; Ma, C.; Zhang, Y.; Liu, S.; Xu, J. *Chem. Soc. Rev.* **2012**, *41*, 3878–3896. (b) Xue, P.; Sun, J.; Chen, P.; Gong, P.; Yao, B.; Zhang, Z.; Qiana, C.; Lu, R. *J. Mater. Chem. C* **2015**, *3*, 4086–4092.
2. Pucci, A.; Cuia, F. D.; Signori, F.; Ruggeri, G. *J. Mater. Chem.* **2007**, *17*, 783–790.
3. Hirata, S.; Watanabe, T. *Adv. Mater.* **2006**, *18*, 2725–2729.
4. Kishimura, A.; Yamashita, T.; Yamaguchiand, K.; Aida, T. *Nat. Mater.* **2005**, *4*, 546–549.
5. (a) Zhang, G.; Lu, J.; Sabat, M.; Fraser, C. L. *J. Am. Chem. Soc.* **2010**, *132*, 2160–2162. (b) Nguyen, N. D.; Zhang, G.; Lu, J.; Shermana, A. E.; Fraser, C. L. *J. Mater. Chem.*, **2011**, *21*, 8409–8415. (c) Krishna, G. R.; Kiran, M. S. R. N.; Fraser, C. L.; Ramamurty, U.; Reddy, C. M. *Adv. Funct. Mater.* **2013**, *23*, 1422–1430. (d) Krishna, G. R.; Devarapalli, R.; Prusty, R.; Liu, T.; Fraser, C. L.; Ramamurty, U.; Reddy, C. M. *IUCrJ*, **2015**, *2*, 611–619.
6. (a) Mirochnik, A. G.; Fedorenko, E. V.; Bukvetskii, B. V.; Karasev, V. E. *Russ. Chem. Bull.* **2005**, *54*, 1060–1062. (b) Sun, X.; Zhang, X.; Li, X.; Liu, S.; Zhang, G. *J. Mater. Chem.* **2012**, *22*, 17332–17339.
7. Galer, P.; Korošec, R. C.; Vidmar, M.; Šket, B. *J. Am. Chem. Soc.* **2014**, *136*, 7383−7394.
8. Tanaka, K.; Chujo, Y.; *NPG Asia Mater*. **2015**, *7*, e223.
9. Wang, L.; Wang, K.; Zou, B.; Ye, K.; Zhang, H.; Wang, Y. *Adv. Mater.* **2015**, *27*, 2918–2922.
10. (a) Ito, F.; Sagawa, T.; *RSC Advances* **2013**, *3*, 19785–19788. (b) Ito, F.; Sagawa, T.; *RSC Advances* **2013**, *3*, 19785–19788.
11. For the detail, see Chapters 1 and 2.
12. Tanaka, M. Master thesis, Osaka Prefecture University (**2013**). [Tanaka, M. Ohta, E.; Sakai, A.; Yoshimoto, Y.; Mizuno, K. Ikeda, H. *Tetrahedron Lett.* **2013**, *54*, 4380–4384.]
13. For the detail, see the Appendix Section.
14. Birks, J. B. *Nature* **1967**, *214*, 1187–1190.

3.6. Appendix.

3.6.1. FL Properties.

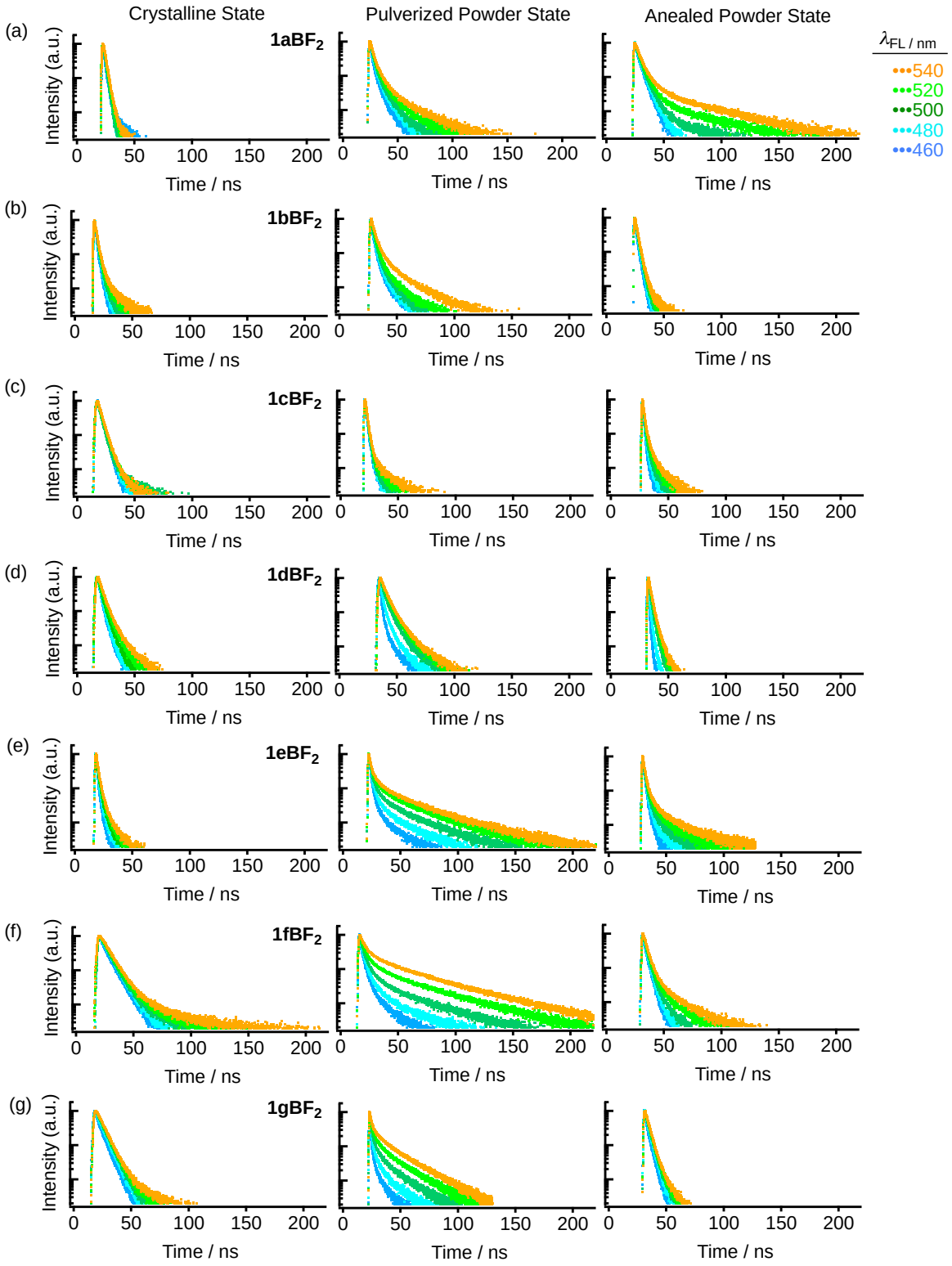

Fig. 3-A1. Time-dependent changes in FL intensities of (a) **1aBF$_2$**, (b) **1bBF$_2$**, (c) **1cBF$_2$**, (d) **1dBF$_2$**, (e) **1eBF$_2$**, (f) **1fBF$_2$**, and (g) **1gBF$_2$** in the crystalline (left), pulverized (center), and annealed powder states at various λ at 298 K. λ_{EX} = 371 nm.

Table 3-A1. The $\tau_{FL,C}$, $\tau_{FL,P}$, and $\tau_{FL,A}$ of **1a–gBF$_2$** at 298 K in the Range of 460–560 nm

	λ_{PL} / nm	$\tau_{FL,C}$ / ns (proportion / %)		$\tau_{FL,P}$ / ns (proportion / %)			$\tau_{FL,A}$ / ns (proportion / %)		
1aBF$_2$	560	N/A		2.9(23)	8.1(39)	30.4(38)	4.0(22)	9.6(21)	52.9(57)
	540	2.1(63)	12.5(37)	2.7(27)	7.3(42)	27.4(31)	3.9(33)	9.1(25)	53.4(41)
	520	2.0(72)	9.7(28)	2.2(25)	5.6(48)	18.9(27)	3.3(32)	6.6(42)	43.1(26)
	500	1.8(75)	7.5(25)	2.7(54)	9.3(46)	/	3.7(68)	9.9(32)	/
	480	1.6(76)	6.1(24)	2.4(50)	7.7(50)	/	2.9(42)	6.1(58)	/
	460	1.3(62)	3.6(38)	1.7(43)	5.7(57)	/	2.4(29)	5.2(71)	/
1bBF$_2$	560	2.0(71)	7.6(29)	3.2(49)	16.8(51)		2.3(83)	9.3(17)	
	540	1.9(73)	6.9(27)	3.3(49)	17.2(51)		2.1(76)	4.7(24)	
	520	1.9(76)	5.3(24)	2.5(59)	11.1(41)		1.9(59)	3.4(41)	
	500	1.6(73)	4.2(27)	2.4(65)	8.9(35)		1.9(67)	3.4(33)	
	480	1.4(55)	2.8(45)	2.2(64)	7.9(36)		1.5(40)	2.7(60)	
	460	1.0(36)	2.2(64)	1.9(60)	6.7(40)		0.8(13)	2.2(87)	
1cBF$_2$	560	3.6(82)	9.0(18)	0.8(71)	6.9(29)		0.9(17)	2.5(52)	10.6(31)
	540	3.5(86)	8.4(14)	1.6(74)	9.5(26)		0.9(19)	2.5(52)	10.9(29)
	520	3.3(80)	7.6(20)	1.5(81)	6.6(19)		0.7(22)	2.0(52)	7.3(26)
	500	3.1(64)	4.7(36)	1.4(84)	6.2(16)		0.7(27)	1.8(51)	6.3(22)
	480	2.0(17)	3.9(83)	1.3(79)	3.7(21)		0.5(12)	1.2(64)	4.3(25)
	460	1.6(11)	3.6(89)	1.3(78)	3.6(22)		0.7(61)	2.1(39)	/
1dBF$_2$	560	4.1(69)	11.2(31)	4.9(63)	14.2(37)	/	2.2(69)	5.2(31)	
	540	3.8(68)	9.5(32)	4.7(60)	12.8(40)	/	2.0(66)	4.5(34)	
	520	3.4(70)	8.7(30)	4.4(61)	11.9(39)	/	1.8(54)	3.6(46)	
	500	2.6(56)	4.6(44)	3.4(50)	9.1(50)	/	1.1(27)	2.6(73)	
	480	2.3(58)	4.6(41)	1.0(15)	3.0(51)	8.8(33)	0.6(37)	1.8(63)	
	460	1.8(43)	4.0(57)	0.6(28)	2.1(40)	7.8(31)	0.5(49)	1.1(51)	
1eBF$_2$	560	1.9(63)	6.4(37)	2.1(9)	10.6(24)	42.5(67)	1.6(26)	4.8(33)	25.1(41)
	540	1.7(63)	5.8(37)	2.0(12)	9.6(25)	39.9(64)	1.5(31)	4.4(33)	22.6(36)
	520	1.5(61)	4.8(39)	1.9(14)	8.5(25)	36.1(61)	1.4(35)	3.8(33)	17.6(32)
	500	1.3(60)	4.1(40)	1.4(21)	5.6(28)	29.2(51)	1.6(65)	8.6(35)	/
	480	1.6(60)	4.8(40)	1.2(26)	3.8(33)	20.0(41)	1.3(66)	4.9(34)	/
	460	N/A		0.6(15)	2.0(55)	10.9(30)	1.2(68)	3.3(32)	/
1fBF$_2$	560	N/A		3.3(4)	14.2(15)	48.9(81)	3.6(59)	19.1(41)	
	540	7.2(83)	27.6(17)	3.5(4)	14.5(15)	49.0(81)	3.4(64)	16.4(36)	
	520	6.7(83)	21.7(17)	3.1(16)	10.9(21)	45.4(63)	3.1(71)	12.9(29)	
	500	6.(82)	15.9(19)	2.5(26)	7.9(29)	38.6(45)	2.9(77)	9.5(23)	
	480	6.5(83)	12.6(17)	2.3(38)	6.5(35)	28.3(26)	2.7(72)	5.3(27)	
	460	4.0(19)	7.6(81)	1.2(12)	3.1(58)	11.8(12)	1.6(20)	3.4(80)	
1gBF$_2$	560	N/A		1.7(4)	7.5(16)	23.8(80)	3.3(80)	10.2(20)	
	540	5.9(89)	23.8(11)	1.6(7)	6.8(20)	23.2(73)	3.2(80)	9.5(20)	
	520	5.8(92)	11.8(8)	1.3(12)	5.4(25)	21.4(63)	3.0(80)	7.6(20)	
	500	5.6(89)	8.6(11)	1.2(20)	4.5(31)	18.7(49)	2.9(71)	5.7(29)	
	480	5.1(70)	7.3(30)	0.7(20)	2.3(38)	11.0(42)	2.3(40)	3.9(60)	
	460	1.9(9)	5.5(91)	0.3(16)	1.3(50)	6.5(35)	1.2(17)	3.2(83)	

3.6.2. Thermal Properties. The Differential Scanning Calorimetry (DSC) analyses were used RIGAKU DSC8230. The respective sample quantities and Alumina (AlO_3) as standard material sample were 3 mg. Scan rates are 5 °C/min (**1a,b,c,e,gBF$_2$**) or 10 °C/min (**1d,fBF$_2$**). (Figure 3-A2).

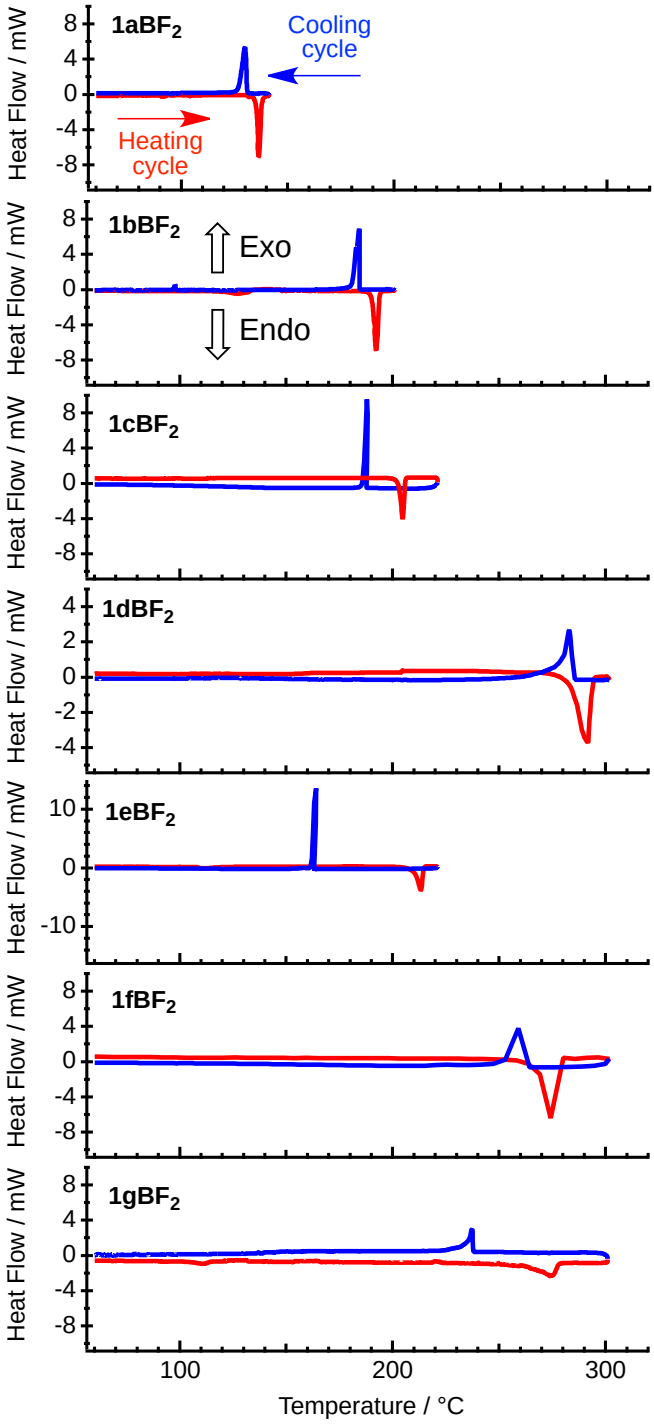

Figure 3-A2. DSC curves of **1a–gBF$_2$** in the crystalline state.

Table 3-A2. Thermodynamic Parameters for Crystallization of **1a–gBF$_2$**

1BF$_2$	T_{mp} / K	T_C / K	ΔH_C / kJ•mol^{-1}	ΔS_C / J•K^{-1}	$\Delta G_{C,\ 293K}$ / kJ•mol^{-1}
a	409	403	18.4	45.7	5.0
b	466	457	19.7	43.1	7.1
c	477	461	11.6	25.2	4.2
d	564	556	12.3	22.1	5.7
e	486	437	13.6	31.2	4.5
f	545	532	23.2	43.6	10.4
g	548	510	17.8	34.9	7.6

The enthalpy (ΔH_C), entropy (ΔS_C), and Gibbs energy (ΔG_C) of crystallization, and temperature of melting point (T_{mp}) and crystallization (T_C). The ΔH_C and ΔS_C based on the peak area of the DSC curves and by using the equation: $\Delta H_C = T_C \Delta S_C$.[10b]

3.6.3. X-ray diffraction patterns. The X-ray diffraction (XRD) patterns of **1aBF$_2$**, **1dBF$_2$**, and **1fBF$_2$** in the crystalline state and in the pulverized powder state were investigated (Figure 3-A3). In the crystalline state, the XRD peaks of **1aBF$_2$** were observed at 10°, and 23°. Those of **1dBF$_2$** were observed at 11°, and 25°. The XRD peak of **1fBF$_2$** was observed only at 6°. After pulverizing the crystalline **1a,d,fBF$_2$**, those peaks were almost lost.

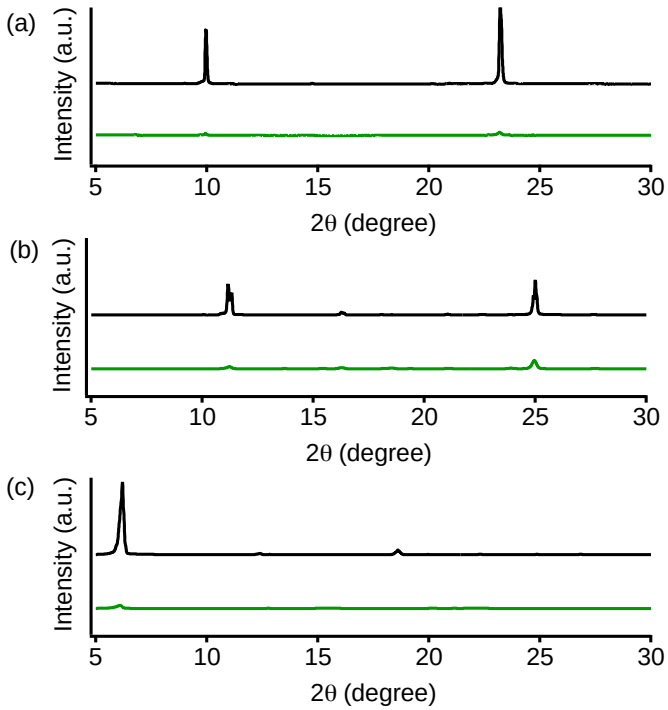

Figure 3-A3. The XRD patterns of (a) **1aBF$_2$**, (b) **1dBF$_2$**, and (c) **1fBF$_2$** in the crystalline (black) and pulverized powder states (green).

CHAPTER 4

Room-Temperature Phosphorescent Crystal of Bis(4-iodobenzoyl)methanato-boron Difluoride: Enhanced Intersystem Crossing and Suppressed Thermal Deactivation of Excited States Derived by Packing Structure

4.1. Introduction.

Metal-free polymers,[1] organic crystals[2] and amorphous solids[3] that display room-temperature phosphorescence (RTP) emission are interesting substances. However, these materials are not common because of the requirement for enhanced intersystem crossing (ISC) and/or suppressed thermal deactivation of their excited states.[2–5] A large effort has been given to elucidate photoluminescence (PL) properties of metal-free organoboron complexes.[1,6,7] In one study, Fraser and co-workers found that a derivative of dibenzoylmethanatoboron difluoride, possessing a poly(lactic acid) side chain, displays not only blue fluorescence (FL) but also long lived green RTP in the thin film state.[1] Although incorporation of a polymer side chain on the backbone of dibenzoylmethanatoboron difluoride is one approach to suppress thermal deactivation of excited states, general principles guiding strategies to design efficient RTP materials that exhibit enhanced ISC have not been established.

In the study described below, we observed that bis(4-iodobenzoyl)methanatoboron difluoride (**1hBF$_2$**) (Figure 4-1a)[8], which contains heavy iodine atoms that enhance ISC through a spin–orbit coupling effect, emits not only FL but also green RTP in the crystalline state (Figure 4-1b). This phenomenon contrasts with the finding that **1hBF$_2$** exhibits only blue FL in a degassed *n*-BuCl. In this investigation, we explored the PL properties and packing structure of **1hBF$_2$** in the crystalline state. Moreover, results of theoretical and crystallographic investigations have led to the proposal that RTP emission is a consequence of the effect of intermolecular interactions in the crystalline structure of **1hBF$_2$** on electronic transitions.

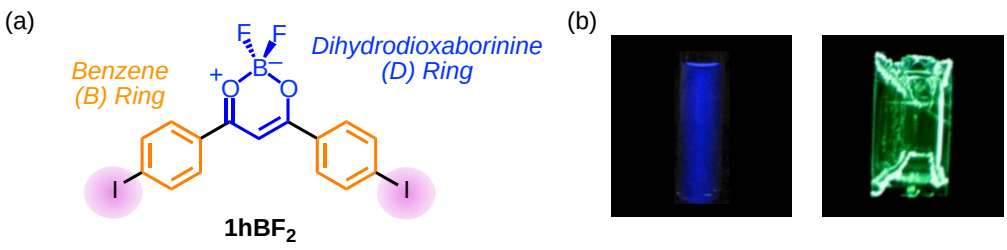

Figure 4-1. (a) Structure of **1hBF$_2$**. (b) Photographs of degassed *n*-BuCl solution (left) and a crystal (right) of **1hBF$_2$** under 365-nm light.

4.2. Results and Discussion.

The PL spectrum of **1hBF$_2$**[9,10] in *n*-BuCl at room temperature (298 K) contains a single emission band centered at wavelength (λ) of 421 nm (Table 4-1 and Figure 4-2, black). This PL is assigned to FL on the basis of the fact that it has a short lifetime (τ) of 0.5 ns. At 77 K, a glassy *n*-BuCl matrix containing **1hBF$_2$** displays PL bands at 421, 441, 468, 512, and 545 nm (Figure 4-2, blue), the first three of which are assigned to FL judging from the τ value that falls in the ns range and the λ values that are similar to that of room temperature FL. In contrast, the 512 and 545 nm bands are attributed to phosphorescence (PH) because the τ value is 3.6 ms (510-nm monitoring). Furthermore, crystals of **1hBF$_2$** at room temperature emit two PL peaks at 460 and 527 nm (Figure 4-2, green solid). Although the former band maximum is 40 nm longer than the maximum of FL in *n*-BuCl, it is attributed to FL because it has the τ of ns range. On the other hand, the latter band has a long τ of 1.3 ms, which is similar to that of the 538-nm peak seen in the delayed PL spectrum measured using an integration time of 2–5 ms (Figure 4-2, green dotted). These observations clearly show that the latter 527-nm band is RTP of crystalline **1hBF$_2$**. The enhancement of PL of **1hBF$_2$** induced by crystallization was confirmed by the finding that the quantum yield of PL in the crystalline state is 0.25 while that in degassed *n*-BuCl is 0.05.

Table 4-1. PL Properties of **1hBF$_2$** in Degassed *n*-BuCl and in the Crystalline State Under Air

In *n*-BuCl				In the Crystalline State			
$\lambda_{FL,S}$[a,b]	$\lambda_{PH,S}$[a,c]	$\tau_{FL,S}$[b,d,e]	$\tau_{PL,S}$[c,d,f]	$\lambda_{FL,C}$[a,b]	$\lambda_{PH,C}$[a,b]	$\tau_{FL,C}$[b,d,g]	$\tau_{PL,C}$[c,d,h]
nm	nm	ns (%)	ms	nm	nm	ns (%)	ms
421	512 545	0.5 (100)	3.6	460	527	0.5 (40) 4.0 (60)	1.3

[a] λ_{EX} = 365 ± 2.5 nm. [b] At room temperature. [c] At 77 K. [d] λ_{EX} = 371 ± 10 nm. [e] λ_{DET} = 450 nm. [f] λ_{DET} = 510 ± 2.5 nm. [g] λ_{DET} = 460 nm. [h] λ_{DET} = 520 ± 2.5 nm.

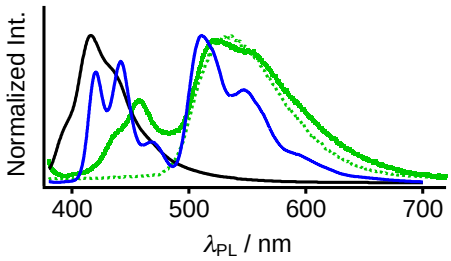

Figure 4-2. PL spectra of **1hBF$_2$** in degassed *n*-BuCl at room temperature (*ca*. 298 K, black) and 77 K (blue), and in the crystalline state at room temperature under air (green). Delayed PL spectrum (green dotted) of **1hBF$_2$** in the crystalline state at room temperature (integration time: 2–5 ms after the excitation light is turned off). λ_{EX} = 365 nm, under air.

X-ray crystallographic analysis was carried out on a single crystal of **1hBF$_2$**. The results show that an arbitrarily-chosen molecule of this substance, M_0, has a planar geometry and possesses 14 neighbors, *i.e.*, two sets of seven kinds of the pair, M_0/M_1, M_0/M_2, M_0/M_3, M_0/M_4, M_0/M_5, M_0/M_6, and M_0/M_7. Molecules in the M_0/M_1 pair appear to be π-stacked between a benzene ring on one (B, Figure 4-1) and the 1,2-dihydro-2,6-dioxaborinine (*D*) ring of the other (*B-on-D* overlap)[7b,c] on the basis of the existence of a short face-to-face distance of 3.74 Å (Figure 4-3b). In addition, a short distance of 2.57 Å exists between an H atom in the 4-iodophenyl group of M_0 and the F atom in M_2. The fact that this distance is shorter than the sum of van der Waals radii of H (1.20 Å) and F (1.47 Å)[11] clearly shows the presence of H•••F hydrogen bonding[2a,12] in the M_0/M_2 pair. Furthermore, that the M_0/M_6 pair contains an I•••F halogen bonding is strongly suggested by the 3.24 Å distance between the I atom in M_0 and F atom in M_6,[2b,13,14] which is shorter than the sum of van der Waals radii of I (1.98 Å) and F.[11]

To gain further insight into the presence and consequences of intermolecular interactions that take place in the crystal structure of **1hBF$_2$**, density functional theory (DFT) calculations[15] were performed using the B97D method[16] with basis set superposition error (BSSE) correction by employing the counterpoise method.[17] The DGDZVP[18] and 6-311G** basis sets were used for the respective iodine and other elements. Geometries of molecules in the crystal packing structure were optimized[19] at the PW91/DNP level[20,21] utilizing periodic boundary conditions with fixed cell parameters. Intermolecular interaction energies, $E_{0/1}$, $E_{0/2}$, $E_{0/3}$, $E_{0/4}$, $E_{0/5}$, $E_{0/6}$, and $E_{0/7}$, for the respective M_0/M_1, M_0/M_2, M_0/M_3, M_0/M_4, M_0/M_5, M_0/M_6, and M_0/M_7 pairs were determined to be –17.1, –9.85, –6.13, –4.39, –3.99, –3.99, and –2.20 kcal mol^{-1}, respectively. The M_0/M_5 and M_0/M_6 pairs are equivalent to each other although the F and I atoms of M_0 behave as interaction site in the M_0/M_5 and M_0/M_6 pair, respectively. The observation that the absolute value of $E_{0/1}$ is larger than

the others, suggests that π-stacking interactions that occur in a continuous manner along the columns of stacked **1hBF$_2$** molecules (••••M_1/M_0/M_1••••) are dominant. The calculated absolute $E_{0/2}$ and $E_{0/6}$, which are substantially smaller than $E_{0/1}$, show that the H•••F and I•••F bonding interactions add to stabilization of the crystal packing structure. The combination of these intermolecular interactions promotes the formation of a rigid crystal packing structure that suppresses thermal deactivation of the S_1 and T_1 excited states of **1hBF$_2$**.[2]

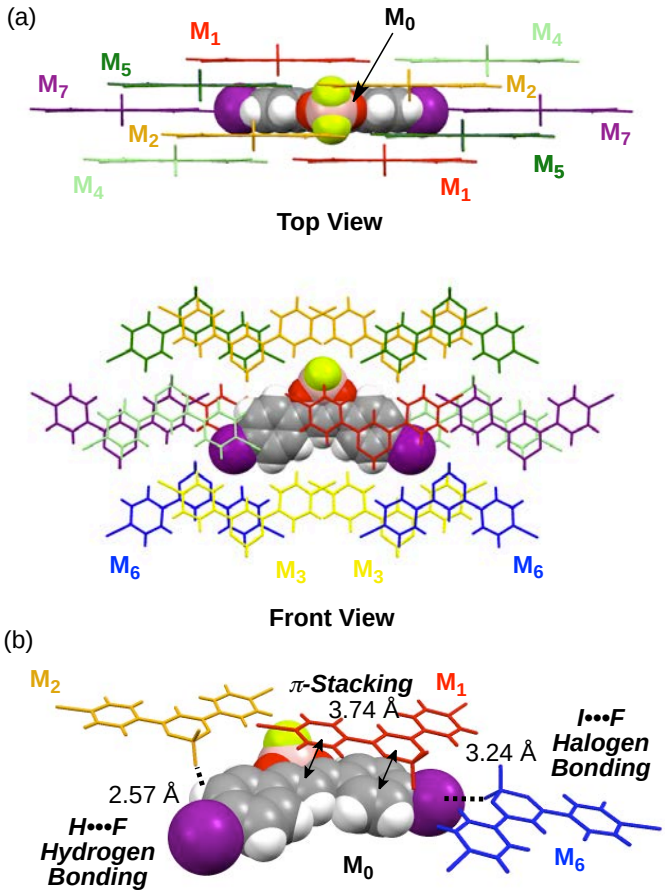

Figure 4-3. (a) Crystal packing structure of **1hBF$_2$** in which a couple of molecules $M_{1–6}$ are adjacent to M_0. In top view, M_3 and M_6 molecules are hidden behind M_2 and M_5 molecules, respectively. (b) The M_0/M_1, M_0/M_2, and M_0/M_6 pairs in the crystal packing structure that form π-stacking, H•••F hydrogen bonding, and I•••F halogen bonding, respectively.

The HOMO and LUMO are delocalized over two stacked molecules in the M_0/M_1 pair (Figure 4-4), suggesting that π-stacking strongly affects the electronic properties of **1hBF$_2$**. The wavelength associated with the $S_0 \rightarrow S_1$ electronic transition ($\lambda_{ET,S0\rightarrow S1}$) of a single molecule of **1hBF$_2$** was calculated to be 447 nm (2.77 eV) with an oscillator strength ($f_{S0\rightarrow S1}$) of 0.6617 by utilizing

time-dependent (TD)-DFT with the B97D method and DGDZVP and 6-311G** basis sets for iodine and other elements, respectively (Figure 4-5a). In contrast, the calculated $\lambda_{ET,S0\rightarrow S1}$ for the M_0/M_1 pair was found to be 557 nm (2.22 eV) with a small $f_{S0\rightarrow S1}$ (< 0.0000) and that of $\lambda_{ET,S0\rightarrow S6}$ was found to be 465 nm (2.67 eV) with a large $f_{S0\rightarrow S6}$ of 0.9772 (Figure 4-5b). These results strongly suggest that deactivation of the S_1 excited state of **1hBF$_2$** via an $S_1\rightarrow S_0$ electronic transition is substantially blocked in the crystalline state.

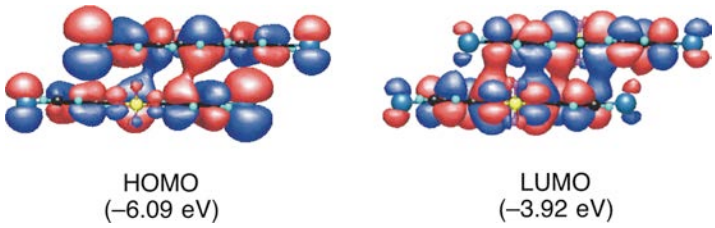

Figure 4-4. The HOMO and LUMO of the M_0/M_1 pair of **1hBF$_2$** simulated by using DFT calculations using the B97D method with DGDZVP and 6-311G** basis sets for iodine and other elements, respectively. Isovalue = 0.01.

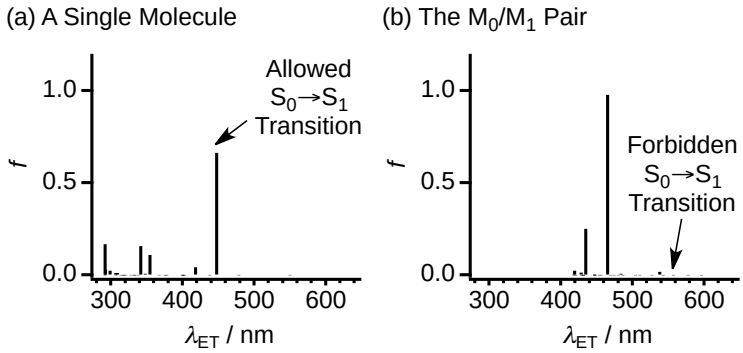

Figure 4-5. Electronic transitions of a single molecule (a) and the M_0/M_1 pair (b) of **1hBF$_2$** estimated by using TD-DFT calculations using the B97D method with DGDZVP and 6-311G** basis sets for iodine and other elements, respectively.

In Chapter 1, the author demonstrated that a relationship exists between the π-stacking interactions in crystalline diaroylmethanatoboron difluorides and the $S_1\rightarrow S_0$ electronic transitions.[7c] When π-stacking in the crystalline structures of these substances takes place through continuous *B-on-D* overlap,[22] the $S_1\rightarrow S_0$ electronic transition is forbidden and an "excited multimer" is generated by photoexcitation. Based on this finding, it is expected that the $S_1\rightarrow S_0$ electronic transition would be forbidden in **1hBF$_2$** and an "excited multimer" is formed upon photoexcitation.

Importantly, because the S_1 state of **1hBF$_2$** in the crystalline state is not deactivated via the $S_1 \rightarrow S_0$ electronic transition, it is able to undergo efficient ISC. Furthermore, the S_1–T_1 and S_1–T_2 (ΔE_{S1-T1} and ΔE_{S1-T2}, respectively) energy gaps in the M_0/M_1 pair of **1hBF$_2$** in the crystal packing structure are computed to be 0.14 and 0.08 eV, respectively (Figure 4-6b). Both of these values are smaller than the ΔE_{S1-T3} energy gap (0.18 eV) in a single molecule of **1hBF$_2$** (Figure 4-6a). Therefore, ISC from the S_1 to T_2 or T_1 states should be enhanced in the crystalline state of **1hBF$_2$** as a result of not only the heavy atom effect of iodine but also the existence of small ΔE_{S1-T1} and ΔE_{S1-T2} values.[4] Finally, the results of calculations show that the $S_1 \rightarrow S_0$ electronic transition is forbidden and ΔE_{S1-T1} and ΔE_{S1-T2} are small even in the stacked three molecules of **1hBF$_2$** ($M_1/M_0/M_1$).[10] These observations suggest that the conclusions summarized above are applicable to packed crystals consisting of many molecules.

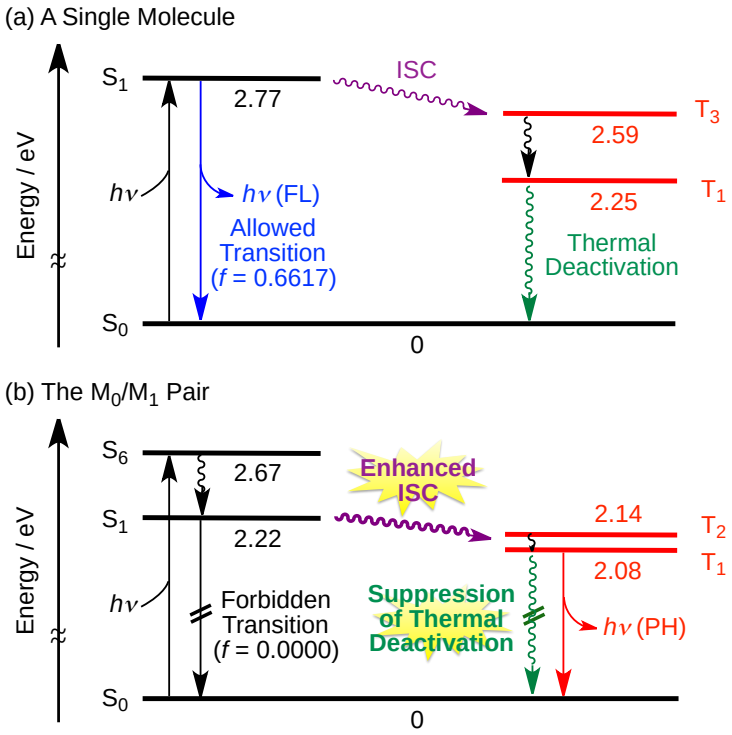

Figure 4-6. Energy diagrams for PL emission of the optimized single molecule (a) and the M_0/M_1 pair (b) of **1hBF$_2$**. Energies were estimated by using DFT calculations using the B97D method with DGDZVP and 6-311G** basis sets for iodine and other elements, respectively.

4.3. Conclusion.

Metal-free **1hBF$_2$** was found to display not only FL but also remarkable RTP in the crystalline state. Two key factors contribute to RTP emission of **1hBF$_2$** in the crystalline state. The first is the suppression of thermal deactivation of the S_1 and T_1 excited states. This event is caused by the rigid crystal packing structure of **1hBF$_2$** that contains many intermolecular interactions, including in particular π-stacking with *B-on-D* overlap. The second factor is enhancement of ISC that enables the T_1 excited state to be efficiently produced (Figure 4-6b). Importantly, the crystal packing structure of **1hBF$_2$** also plays a crucial role in enhancing ISC by causing the formation of an "excited multimer" having a forbidden $S_1 \rightarrow S_0$ electronic transition and small ΔE_{S1-T1} and ΔE_{S1-T2}. Note that the RTP of **1hBF$_2$** is not only caused by a heavy atom effect. As a result, the crystal packing structure based design of this material differs from those conventionally used to generate metal-free RTP materials. Consequently, the results of this study should provide valuable insight into a new mechanistic approach to enhance ISC.

4.4. Experimental Section.

4.4.1. General Methods. ^{1}H NMR spectra in $CDCl_3$ were recorded on a Varian Mercury 300 spectrometer, operating at 300 MHz, where chemical shifts were determined with respect to tetramethylsilane (TMS) as an internal standard. Melting points were measured using a Yanako MP-500 and are reported uncorrected. FAB-mass spectra were recorded on a JEOL JMS-700 spectrometer. Elemental analyses were performed at Research Institute for Instrumental Analysis, Advanced Science Research Center, Kanazawa University. UV-Vis spectra were recorded on a JASCO V-530 spectrophotometer. Diffuse reflection spectra were obtained on a JASCO V-570 spectrophotometer. FL and PH spectra, and PH lifetimes were recorded on a JASCO FP-8500 spectrofluorometer. FL quantum yields were recorded on a HAMAMATSU Photonics C9920-02 apparatus.

4.4.2. Materials. X-Ray crystallographic analyses were performed on a single crystal of **1hBF$_2$**, obtained by recrystallization from $CHCl_3$–benzene. Crystal data for $C_{15}H_{11}O_2BF_2I_2$ (**1hBF$_2$**): Colorless plates, 0.1 × 0.1 × 0.1 mm^3, monoclinic, *C*2/*c*, *a* = 11.851(2), *b* = 13.595(2), *c* = 10.999(2) Å, β = 114.906(4)°, *V* = 1607.4(5) Å^3, *Z* = 4, ρ_{calcd} = 2.165 g cm^{-3}, μ = 3.935 mm^{-1}, Mo*K*α radiation, λ = 0.71075 Å, *T* = 296(2) K, $2\theta_{max}$ = 55.0°, 7536 reflections measured, 1831 unique reflections, R_{int} = 0.147, 101 parameters, R_1 = 0.062 ($I > 2\sigma I$), wR_2 = 0.138 (all data), CCDC-1443558. These data can be obtained free of charge from The Cambridge Crystallographic Data Centre via www.ccdc.cam.ac.uk/ data_request/cif.

4.5. References and Notes.

1. (a) Zhang, G.; Chen, J.; Payne, S. J.; Kooi, S. E.; Demas, J. N.; Fraser, C. L. *J. Am. Chem. Soc.* **2007**, *129*, 8942–8943. (b) Zhang, G.; Kooi, S. E.; Demas, J. N.; Fraser, C. L. *Adv. Mater.* **2008**, *20*, 2099–2104. (c) Zhang, G.; Palmer, G. M.; Dewhirest, M. W.; Fraser, C. L. *Nature Mater.* **2009**, *8*, 747–751. (d) Samonina-Kosicka, J.; DeRosa, C. A.; Morris, W. A.; Fan, Z.; Fraser, C. L. *Macromolecules* **2014**, *47*, 3736–3746. (e) Sun, X.; Wang, X.; Li, X.; Ge, J. Zhang, Q.; Jiang, J.; Zhang. G. *Macromol. Rapid Commun.* **2015**, *36*, 298−303.
2. (a) Yuan, W. Z.; Shen, X. Y.; Zhao, H.; Lam, J. W. Y.; Tang, L.; Lu, P.; Wang, C.; Liu, Y.; Wang, Z.; Zhang, Q.; Sun, J. Z.; Ma, Y.; Tang, B. Z. *J. Phys. Chem. C* **2010**, *114*, 6090–6099. (b) Bolton, O.; Lee, K.; Kim, H.-J.; Lin, K. Y.; Kim, J. *Nature Chem.* **2011**, *3*, 205–210. (c) Gong, Y.; Zhao, L.; Peng, Q.; Fan, D.; Yuan, W. Z.; Zhang, Y.; Tang, B. Z. *Chem. Sci.* **2015**, *6*, 4438–4444.
3. (a) Hirata, S.; Totani, K.; Zhang, J.; Yamashita, T.; Kaji, H.; Marder, S. R.; Watanabe, T.; Adachi, C. *Adv. Funct. Mater.* **2013**, *23*, 3386–3397. (b) Lee, D.; Bolton, O.; Kim, H.-J.; Youk, J. H.; Takayama, S.; Kim, J. *J. Am. Chem. Soc.* **2013**, *135*, 6325–6329.
4. Turro, N. J.; Ramamurthy, V.; Scaiano, J. C. *Principles of Molecular Photochemistry: An Introduction **2009***, University Science Books: Herndon, VA.
5. Kearns, D. R.; Case, W. A. *J. Am. Chem. Soc.* **1966**, *88*, 5087–5097.
6. (a) Mirochnik, A. G.; Gukhman, E. V.; Karasev, V. E.; Zhikhareva, P. A. *Russ. Chem. Bull.* **2000**, *49*, 1024–1027. (b) Cogné-Laage, E.; Allemand, J.-F.; Ruel, O.; Baudin, J.-B.; Croquette, V.; Blanchard Desce, M.; Jullien, L. *Chem. Eur. J.* **2004**, *10*, 1445–1455. (c) Ono, K.; Yoshikawa, K.; Tsuji, Y.; Yamaguchi, H.; Uozumi, R.; Tomura, M.; Taga, K.; Saito, K.; *Tetrahedron* **2007**, *63*, 9354–9358. (d) Safonov, A. A.; Bagaturyants, A. A.; Sazhnikov, V. A. *J. Phys. Chem. A* **2015**, *119*, 8182–8187. (e) Tanaka, K.; Chujo, Y. *NPG Asia Mater.* **2015**, *7*, e223.
7. The details have been described in (a) Chapter 2 and (b) Tanaka, M. Master thesis, Osaka Pref. Univ. (**2014**). [Tanaka, M. Ohta, E.; Sakai, A.; Yoshimoto, Y.; Mizuno, K. Ikeda, H. *Tetrahedron Lett.* **2013**, *54*, 4380–4384.], and, (c) Chapter 1.
8. Yoshii, R.; Nagai, A.; Tanaka, K.; Chujo, Y.; *Macromol. Rapid Commun.* **2014**, *35*, 1315–1319.
9. **1hBF$_2$** was synthesized utilizing the method described in ref. 8. Slow recrystallization of **1hBF$_2$** from $CHCl_3$–benzene gives yellow needles (mp 245–248 °C) together with a small amount of colorless plates (250–252 °C). The colorless crystals were collected and used in this effort.
10. For details, see the Appendix Section.

11. Rowland, R. S.; Taylor, R. *J. Phys. Chem.* **1996**, *100*, 7384–7391.
12. Kollman, P. A.; Allen, L. C. *Chem. Rev.* **1972**, *72*, 283–303.
13. (a) Hassel, O.; *Nobel Lecture*, June 9 1970. (b) Auffinger, P.; Hays, F. A.; Westhof, E.; Ho, P. S. *Proc. Natl. Acad. Sci.* **2004**, *48*, 16789–16794. (c) Priimagi, A.; Cavallo, G.; Metrangro, P.; Resnati, G. *Acc. Chem. Res.* **2013**, *46*, 2686–2695.
14. Tsuzuki, S.; Wakisaka, A.; Ono, T.; Sonoda, T. *Chem. Eur. J.* **2012**, *18*, 951–960.
15. Frisch, M. J.; Trucks, G. W.; Schlegel, H. B.; Scuseria, G. E.; Robb, M. A.; Cheeseman, J. R.; Scalmani, G.; Barone, V.; Mennucci, B.; Petersson, G. A.; Nakatsuji, H.; Caricato, M.; Li, X.; Hratchian, H. P.; Izmaylov, A. F.; Bloino, J.; Zheng, G.; Sonnenberg, J. L.; Hada, M.; Ehara, M.; Toyota, K.; Fukuda, R.; Hasegawa, J.; Ishida, M.; Nakajima, T.; Honda, Y.; Kitao, O.; Nakai, H.; Vreven, T.; Montgomery, J. A., Jr.; Peralta, J. E.; Ogliaro, F.; Bearpark, M.; Heyd, J. J.; Brothers, E.; Kudin, K. N.; Staroverov, V. N.; Kobayashi, R.; Normand, J.; Raghavachari, K.; Rendell, A.; Burant, J. C.; Iyengar, S. S.; Tomasi, J.; Cossi, M.; Rega, N.; Millam, J. M.; Klene, M.; Knox, J. E.; Cross, J. B.; Bakken, V.; Adamo, C.; Jaramillo, J.; Gomperts, R.; Stratmann, R. E.; Yazyev, O.; Austin, A. J.; Cammi, R.; Pomelli, C.; Ochterski, J. W.; Martin, R. L.; Morokuma, K.; Zakrzewski, V. G.; Voth, G. A.; Salvador, P.; Dannenberg, J. J.; Dapprich, S.; Daniels, A. D.; Farkas, Ö.; Foresman, J. B.; Ortiz, J. V.; Cioslowski, J.; Fox, D. J. *Gaussian 09, (Revision A.02 and C.01)*, Gaussian, Inc., Wallingford CT, 2009.
16. Grimme, S.; *J. Comp. Chem.* **2006**, *27*, 1787–1799.
17. Boys, S. F.; Bernardi, F. *Mol. Phys.* **1970**, *19*, 553–566.
18. Godbout, N.; Salahub, D. R.; Andzelm, J.; Wimmer, E. *Can. J. Chem.* **1992**, *70*, 560–571.
19. Delley, B. *J. Chem. Phys.* **1990**, *92*, 508–517.
20. Delley, B.; *J. Chem. Phys.* **2000**, *113*, 7756–7764.
21. Perdew, J. P.; Chevary, J. A.; Vosko, S. H.; Jackson, K. A.; Pederson, M. R.; Singh, D. J.; Fiolhais, C. *Phys. Rev. B*, **1992**, *46*, 6671–6687.
22. If the *B* ring of the molecule is stacked on the *B* ring of a neighbouring molecule in the crystal packing structure (*B-on-B* overlap), the $S_1 \rightarrow S_0$ electronic transition associated with “excited multimer” is allowed.

4.6. Appendix Section.

4.6.1. Synthesis of Bis(4-iodobenzoyl)methanatoboron difluoride (1hBF$_2$).[8] A benzene solution (12 mL) containing 1,3-bis(4-iodophenyl)propane-1,3-dione (0.952 g, 2.0 mmol) and BF_3•OEt_2 (0.30 mL, 2.4 mmol) was stirred for 24 h under argon atomosphere at room temperature. The resultant mixture was concentrated under reduced pressure, then subjected to a slow recrystallization from $CHCl_3$–benzene to give **1hBF$_2$**, (0.685 g, 1.3 mmol) in 65% yield as a mixture mainly consisting of yellow needles together with a small amount of colorless plates. Note that only colorless plates were used for the investigation on optical properties. Data for yellow needles: mp 245–248 °C; IR (KBr) ν 1680, 1582 cm^{-1}. Data for colorless plates: mp 250–252 °C; IR (KBr) ν 1681, 1584 cm^{-1}. Data for **1hBF$_2$**: ^{1}H NMR (300 MHz, $CDCl_3$) δ 7.12 (s, 1H), 7.85 (AA'BB', J = 8.1 Hz, 4H), 7.95 (AA'BB', J = 8.1 Hz, 4H) ppm; FAB-mass m/z 524 [M$^+$]; Anal. Calcd. for $C_{15}H_9BF_2O_2I_2$: C, 34.40; H, 1.73, Found: C, 34.14; H, 2.01.

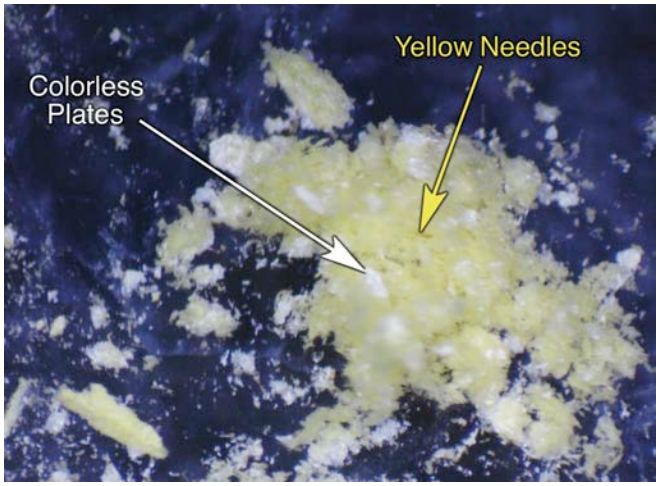

Figure 4-A1. Photograph of a mixture, which is obtained after recrystallization of **1hBF$_2$** from $CHCl_3$–benzene, mainly consisting of yellow needles together with a small amount of colorless plates.

4.6.2. X-Ray Crystallographic Analysis. X-Ray reflection data of crystals were corrected on a Rigaku RAXIS RAPID apparatus, and then analyzed using SHELX-97[A1] and Yadokari-XG programs.[A2]

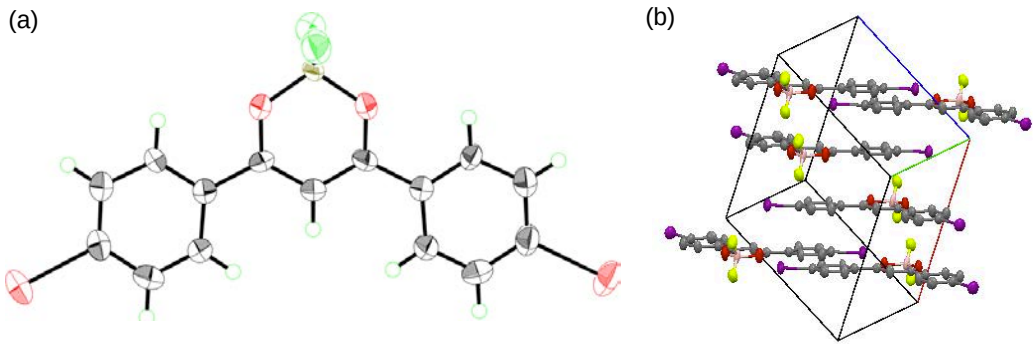

Figure 4-A2. Molecular geometry (a) and packing diagram (b) of **1hBF$_2$** in crystals represented by the ORTEP drawing.

4.6.3. Optical Properties.

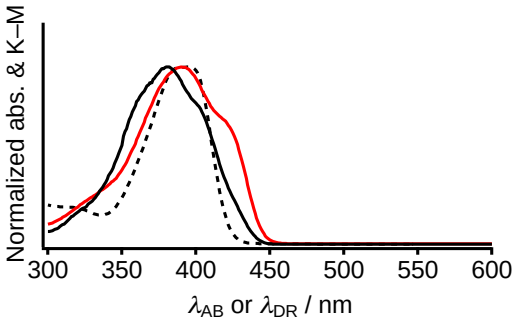

Figure 4-A3. UV–vis absorption spectrum in *n*-BuCl (dotted curve, the maximal absorbance value is 1×10^{-5} M) and diffuse reflection spectrum in KBr powder (solid curves, yellow needles: red; colorless plates: black, substance: 0.2 μmol, KBr: 500 mg, powdered with ball mill at 50 Hz for 15 min) of **1hBF$_2$**.

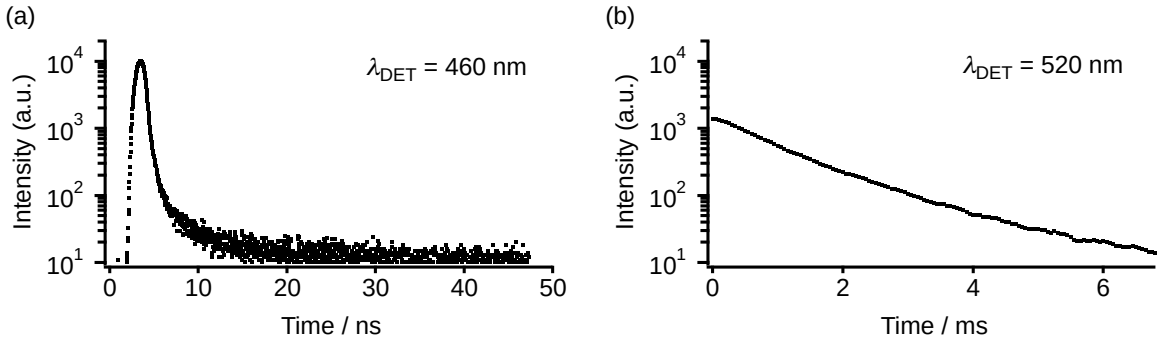

Figure 4-A4. Time-dependent changes of PL intensity of **1hBF$_2$** in the crystalline state at 298 K under air at (a) λ_{DET} = 460 nm and (b) λ_{DET} = 520 nm.

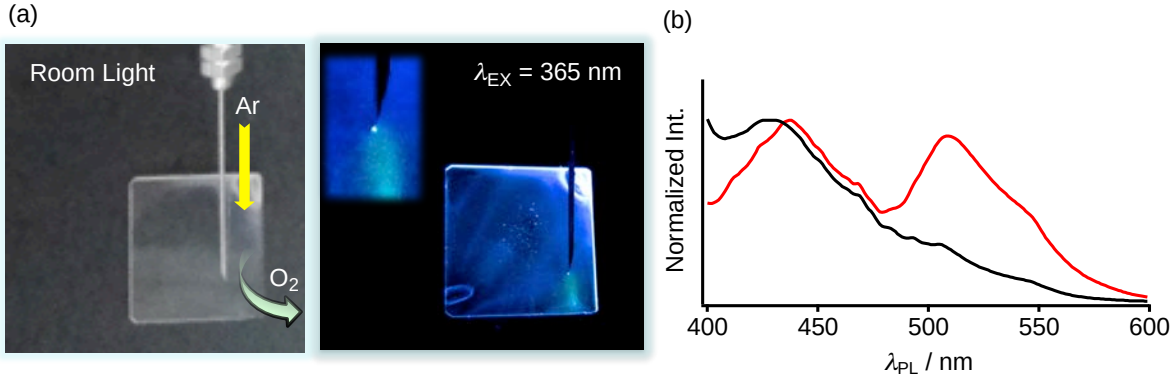

Figure 4-A5. (a) Photographs of emission of **1BF$_2$** in polymethyl methacrylate, PMMA, (**1BF$_2$**/PMMA = 0.01 wt%) with blown argon under the room light (left) and under the 365-nm light (right). (b) The PL spectra of **1BF$_2$** in PMMA (**1BF$_2$**/PMMA = 0.01 wt%) at 298 K under air (black) and under vacuum (red).

4.6.4. DFT Calculations. Optimizations for molecular geometry in vacuum and estimations of the molecular orbital, electronic transitions, and intermolecular interaction energies were performed on a Gaussian Inc. Gaussian (R) 09W Revision A.02 and C.01 programs.[15] Optimizations for molecular geometry in crystals were performed using an Accelrys Dmol3 program. [19]

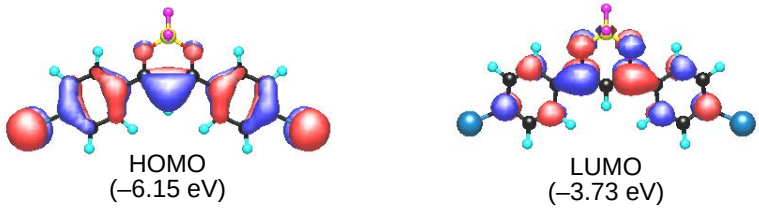

Figure 4-A6. Optimized geometry of **1hBF$_2$** with the HOMO and LUMO simulated using B97D method with DGDZVP and 6-311G** basis sets for iodine and for other atoms, respectively. Isovalue = 0.03.

Table 4-A2. Cartesian Coordinates of Optimized Geometry of **1hBF$_2$**

Atom	Coordinates		
	X / Å	Y / Å	Z / Å
C	–2.529340	0.668183	0.054244
C	–1.214797	1.346162	0.079823
C	–3.676663	1.396994	–0.326089
C	–2.678961	–0.688552	0.410137
C	–3.929875	–1.305879	0.380074
C	–4.931796	0.788990	–0.367861
C	–5.051889	–0.563126	–0.015666
H	–1.823802	–1.273739	0.738952
H	–4.029685	–2.349707	0.665147
H	–3.573608	2.445190	–0.593148
H	–5.804584	1.361764	–0.669954
I	–6.970791	–1.507390	–0.076579
O	–1.247634	2.639241	–0.048968
C	–0.000004	0.649348	0.185711
C	1.214801	1.346163	0.079945
B	–0.000015	3.525766	0.101721
O	1.247648	2.639253	–0.048702
H	–0.000014	–0.429807	0.231265
C	2.529342	0.668178	0.054338
F	0.000087	4.445490	–0.912710
C	2.678933	–0.688633	0.409953
C	3.676699	1.397061	–0.325762
C	4.931833	0.789062	–0.367563
C	3.929848	–1.305958	0.379855
C	5.051895	–0.563127	–0.015642
H	3.573670	2.445312	–0.592612
H	5.804647	1.361896	–0.669470
H	1.823753	–1.273897	0.738572
H	4.029632	–2.349848	0.664712
I	6.970797	–1.507389	–0.076613
F	–0.000148	4.041194	1.377764

HOMO
(–6.20 eV)

LUMO
(–3.85 eV)

Figure 4-A7. Representation of the HOMO and LUMO of single molecule of **1hBF$_2$** with geometry in crystals (M_0) simulated by single-point calculations using B97D method with DGDZVP and 6-311G** basis sets for iodine and for other atoms, respectively. The geometry was optimized at PW91/DNP based on results of X-ray crystallographic analyses of **1hBF$_2$**. Isovalue = 0.01.

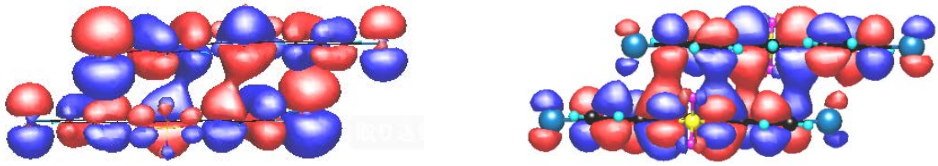

HOMO
(–6.09 eV)

LUMO
(–3.92 eV)

Figure 4-A8. Representation of the HOMO and LUMO of stacked two molecules of **1hBF$_2$** with geometries in crystals (M_0/M_1) simulated by single-point calculation using B97D method with DGDZVP and 6-311G** basis sets for iodine and for other atoms, respectively. The geometry was optimized at PW91/DNP based on results of X-ray crystallographic analyses of **1hBF$_2$**. Isovalue = 0.01.

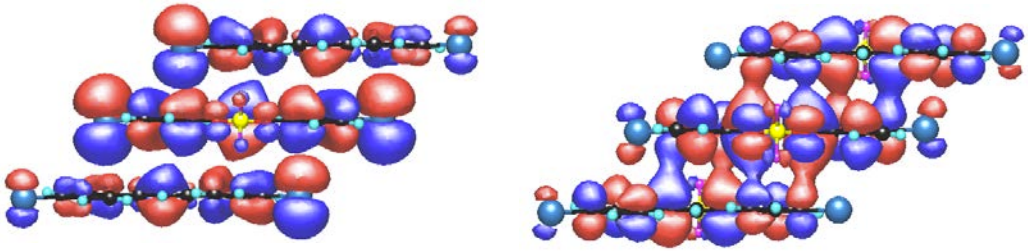

HOMO
(–6.06 eV)

LUMO
(–3.95 eV)

Figure 4-A9. Representation of the HOMO and LUMO of stacked three molecules of **1hBF$_2$** with geometries in crystals (M_1/M_0/M_1) simulated by single-point calculation using B97D method with DGDZVP and 6-311G** basis sets for iodine and for other atoms, respectively. The geometry was optimized at PW91/DNP based on results of X-ray crystallographic analyses of **1hBF$_2$**. Isovalue = 0.01.

Table 4-A3. Electronic Transitions Estimated for **1hBF$_2$** with Optimized Geometry

	λ_{ET} / nm (eV)	Transition (Coefficient)		f
$S_0 \rightarrow T_1$	549.95 (2.255)	H–2 → L H → L	(–0.108) (0.697)	0.0000
$S_0 \rightarrow T_2$	478.76 (2.590)	H–1 → L	(0.698)	0.0000
$S_0 \rightarrow S_1$	447.72 (2.769)	H–2 → L H → L	(0.227) (0.665)	0.6617
$S_0 \rightarrow T_3$	437.99 (2.831)	H–2 → L H–2 → L	(0.693) (0.102)	0.0000
$S_0 \rightarrow S_2$	418.03 (2.966)	H–1 → L H → L+1	(0.680) (–0.139)	0.0421
$S_0 \rightarrow T_4$	402.10 (3.083)	H–3 → L	(0.700)	0.0000
$S_0 \rightarrow T_5$	402.09 (3.084)	H–4 → L	(0.700)	0.0000
$S_0 \rightarrow S_3$	399.70 (3.102)	H–4 → L	(0.704)	0.0003
$S_0 \rightarrow S_4$	399.67 (3.102)	H–3 → L	(0.704)	0.0001
$S_0 \rightarrow T_6$	378.22 (3.278)	H–5 → L	(0.700)	0.0000
$S_0 \rightarrow T_7$	375.70 (3.300)	H–6 → L	(0.701)	0.0000
$S_0 \rightarrow T_8$	367.46 (3.374)	H–8 → L H–7 → L+1 H → L+1	(–0.158) (–0.119) (0.646)	0.0000
$S_0 \rightarrow S_5$	354.20 (3.500)	H–6 → L H–2 → L H → L	(0.386) (0.538) (0.178)	0.1087
$S_0 \rightarrow S_6$	347.76 (3.565)	H–5 → L H → L+5	(0.686) (0.107)	0.0059
$S_0 \rightarrow S_7$	341.34 (3.632)	H–6 → L H–2 → L H → L+4	(–0.566) (0.341) (–0.153)	0.0157
$S_0 \rightarrow T_9$	337.85 (3.670)	H–9 → L H–6 → L+4 H–5 → L+5 H–1 → L+4	(–0.444) (0.132) (0.130) (0.468)	0.0000
$S_0 \rightarrow T_{10}$	333.25 (3.721)	H–1 → L+3 H → L+2	(–0.228) (0.662)	0.0000
$S_0 \rightarrow T_{11}$	332.69 (3.727)	H–1 → L+2 H → L+3	(–0.251) (0.654)	0.0000
$S_0 \rightarrow T_{12}$	328.02 (3.780)	H–8 → L H–7 → L H → L+1	(0.139) (0.664) (0.174)	0.0000
$S_0 \rightarrow T_{13}$	320.56 (3.868)	H–7 → L H → L+1	(–0.192) (0.150)	0.0000
$S_0 \rightarrow S_8$	317.92 (3.900)	H–1 → L+3 H → L+1 H → L+2	(0.167) (0.141) (0.670)	0.0002
$S_0 \rightarrow S_9$	317.15 (3.909)	H–1 → L+2 H → L+3	(0.175) (0.683)	0.0000
$S_0 \rightarrow T_{14}$	313.72 (3.952)	H–9 → L H–1 → L+1	(0.505) (0.489)	0.0000
$S_0 \rightarrow S_{10}$	309.12 (4.011)	H–7 → L H → L+1 H → L+2 H → L+5	(0.486) (0.461) (–0.114) (0.101)	0.0106
$S_0 \rightarrow S_{11}$	306.80 (4.041)	H–8 → L H–7 → L H → L+1	(0.390) (–0.417) (0.372)	0.0097
$S_0 \rightarrow T_{15}$	306.75 (4.042)	H–1 → L+2 H → L+3	(0.650) (0.257)	0.0000
$S_0 \rightarrow S_{12}$	298.92 (0.023)	H–9 → L H–1 → L H → L+4	(0.338) (0.570) (0.185)	0.0227
$S_0 \rightarrow S_{13}$	292.38 (4.241)	H–10 → L H–9 → L H–2 → L+3 H–1 → L+1 H–1 → L+2 H → L+3	(0.104) (–0.277) (0.201) (0.137) (0.573) (–0.136)	0.0283
$S_0 \rightarrow S_{14}$	291.79 (4.249)	H–2 → L+2 H–1 → L+3 H → L+2	(0.235) (0.649) (–0.142)	0.0003

Table 4-S4. Electronic Transitions Estimated for Single Molecule of **1hBF$_2$** with Geometry in Crystals (M_0)

	λ_{ET} / nm (eV)	Transition (Coefficient)		f
$S_0 \rightarrow T_1$	568.19 (2.182)	H → L	(0.697)	0.0000
$S_0 \rightarrow T_2$	490.31 (2.529)	H–1 → L	(0.701)	0.0000
$S_0 \rightarrow S_1$	456.28 (2.717)	H–2 → L H → L	(0.216) (0.667)	0.7058
$S_0 \rightarrow T_3$	450.29 (2.753)	H–1 → L	(0.696)	0.0000
$S_0 \rightarrow S_2$	425.05 (2.917)	H–1 → L H → L+1	(0.680) (0.142)	0.0433
$S_0 \rightarrow T_4$	412.01 (3.084)	H–4 → L H–3 → L	(–0.106) (0.699)	0.0000
$S_0 \rightarrow T_5$	411.99 (3.009)	H–4 → L H–3 → L	(0.699) (0.106)	0.0000

$S_0 \rightarrow S_3$	409.16 (3.030)	H–4 → L (–0.171) H–3 → L (0.686)	0.0000
$S_0 \rightarrow S_4$	409.15 (3.030)	H–4 → L (0.685) H–3 → L (0.171)	0.0000
$S_0 \rightarrow T_6$	381.82 (3.247)	H–5 → L (0.701)	0.0000
$S_0 \rightarrow T_7$	379.17 (3.270)	H–6 → L (0.701)	0.0000
$S_0 \rightarrow T_8$	369.43 (3.356)	H–8 → L (–0.195) H → L+1 (0.656)	0.0000
$S_0 \rightarrow S_5$	367.92 (3.370)	H–10 → L (0.154) H–7 → L (–0.180) H–6 → L (0.133) H–2 → L (0.613) H → L (–0.191)	0.0970
$S_0 \rightarrow S_6$	349.54 (3.547)	H–6 → L+1(–0.102) H–5 → L (0.686) H → L+5 (–0.104)	0.0048
$S_0 \rightarrow S_7$	346.86 (3.575)	H–7 → L (0.134) H–6 → L (0.667) H → L+4 (0.100)	0.0185
$S_0 \rightarrow T_9$	346.30 (3.580)	H–10 → L (0.197) H–7 → L (–0.597) H–1 → L+1 (0.261)	0.0000
$S_0 \rightarrow T_{10}$	335.85 (3.692)	H–8 → L (0.228) H → L+1 (0.527)	0.0000
$S_0 \rightarrow T_{11}$	329.81 (3.759)	H–10 → L (0.228) H–7 → L (–0.359) H–1 → L+1 (0.527)	0.0000
$S_0 \rightarrow T_{12}$	325.05 (3.814)	H–1 → L+3(–0.216) H → L+2 (0.663)	0.0000
$S_0 \rightarrow T_{13}$	324.32 (3.823)	H–1 → L+2(–0.231) H → L+3 (0.664)	0.0000
$S_0 \rightarrow S_8$	323.18 (3.836)	H–7 → L (0.657) H–2 → L (0.158) H → L (–0.129)	0.2415
$S_0 \rightarrow T_{14}$	322.30 (3.847)	H–9 → L (0.706)	0.0000
$S_0 \rightarrow S_9$	311.32 (3.983)	H–8 → L (–0.315) H–2 → L+1(–0.102) H → L+1 (–0.516) H → L+3 (0.282) H → L+5 (0.104)	0.0061
$S_0 \rightarrow S_{10}$	310.48 (3.993)	H–1 → L+3 (0.168) H → L+2 (0.683)	0.0014
$S_0 \rightarrow S_{11}$	309.24 (4.009)	H–8 → L (0.193) H–1 → L+2 (0.158) H → L+1 (0.203) H → L+3 (0.619)	0.0004
$S_0 \rightarrow T_{15}$	307.66 (4.030)	H–10 → L (0.596) H–1 → L+1(–0.351)	0.0000
$S_0 \rightarrow S_{12}$	307.45 (4.033)	H–9 → L (0.707)	0.0004
$S_0 \rightarrow S_{13}$	303.78 (4.081)	H–11 → L (0.246) H–8 → L (0.551) H → L+1 (–0.290) H → L+5 (0.119)	0.0723
$S_0 \rightarrow S_{14}$	299.82 (4.135)	H–10 → L (–0.185) H–1 → L+1 (0.643) H → L+4 (0.139) H → L+6 (0.116)	0.0846
$S_0 \rightarrow S_{15}$	287.79 (4.308)	H–5 → L+1 (0.176) H–1 → L+1(–0.124) H–1 → L+5(–0.193) H–1 → L+2 (0.461) H → L+4 (0.628)	0.0035

Table 4-A5. Electronic Transitions Estimated for Stacked Two Molecules of **1hBF$_2$** with Geometries in Crystals (M_0/M_1)

	λ_{ET} / nm (eV)	Transition (Coefficient)	*f*
$S_0 \rightarrow T_1$	596.57 (2.079)	H–1 → L+1(–0.185) H → L (0.677)	0.0000
$S_0 \rightarrow T_2$	577.61 (2.147)	H–1 → L (0.461) H → L+1 (0.524)	0.0000
$S_0 \rightarrow S_1$	557.46 (2.224)	H–1 → L+1 (0.247) H → L (0.660)	0.0000
$S_0 \rightarrow T_3$	542.96 (2.284)	H–1 → L (0.525) H → L+1 (0.471)	0.0000
$S_0 \rightarrow S_2$	538.19 (2.304)	H–1 → L (0.499) H → L+1 (0.500)	0.0169
$S_0 \rightarrow T_4$	527.63 (2.350)	H–3 → L+1(–0.102) H–1 → L (0.664) H → L (0.196)	0.0000
$S_0 \rightarrow T_5$	510.16 (2.431)	H–3 → L+1 (0.201) H–2 → L (0.671)	0.0000
$S_0 \rightarrow T_6$	504.17 (2.459)	H–3 → L (0.616) H–2 → L+1 (0.319) H–1 → L+1 (0.125)	0.0000
$S_0 \rightarrow S_3$	486.61 (2.548)	H–3 → L (0.487) H–2 → L+1(–0.288) H–1 → L+1 (0.394) H → L (–0.117)	0.0000
$S_0 \rightarrow S_4$	483.94 (2.562)	H–3 → L+1(–0.358) H–2 → L (0.608)	0.0055
$S_0 \rightarrow T_7$	480.37 (2.581)	H–3 → L (0.328) H–2 → L+1 (0.623)	0.0000
$S_0 \rightarrow T_8$	474.57 (2.613)	H–3 → L+1 (0.674) H–2 → L (–0.209)	0.0000

$S_0 \rightarrow S_5$	469.42 (2.642)	H–3 → L (0.260) H–2 → L+1 (0.361) H–1 → L+1 (0.494) H → L (0.189)	0.0000
$S_0 \rightarrow S_6$	465.16 (2.666)	H–6 → L (–0.223) H–1 → L (–0.453) H → L+1 (0.458)	0.9772
$S_0 \rightarrow T_9$	456.24 (2.718)	H–7 → L+1(–0.257) H–6 → L (0.556) H–4 → L (–0.332)	0.0000
$S_0 \rightarrow T_{10}$	453.28 (2.736)	H–7 → L (–0.525) H–6 → L+1 (0.327) H–5 → L (0.299) H–4 → L+1(–0.105)	0.0000
$S_0 \rightarrow T_{11}$	447.73 (2.770)	H–7 → L (0.246) H–6 → L+1(–0.146) H–5 → L (0.640)	0.0000
$S_0 \rightarrow T_{12}$	447.38 (2.772)	H–7 → L+1(–0.107) H–6 → L (0.312) H–4 → L (0.622)	0.0000
$S_0 \rightarrow S_7$	447.00 (2.774)	H–4 → L (0.694)	0.0045
$S_0 \rightarrow S_8$	446.96 (2.774)	H–5 → L (0.697)	0.0001
$S_0 \rightarrow S_9$	434.71 (2.852)	H–7 → L+1(–0.144) H–5 → L+1 (0.137) H–3 → L+1(–0.564) H–2 → L (–0.314) H–1 → L (0.100)	0.2491
$S_0 \rightarrow T_{13}$	431.44 (2.874)	H–5 → L+1 (0.700)	0.0000
$S_0 \rightarrow T_{14}$	431.39 (2.874)	H–7 → L (–0.124) H–4 → L+1 (0.691)	0.0000
$S_0 \rightarrow S_{10}$	431.03 (2.877)	H–7 → L (–0.378) H–6 → L+1(–0.204) H–4 → L+1 (0.141) H–3 → L (–0.321) H–2 → L+1(–0.405)	0.0000
$S_0 \rightarrow S_{11}$	428.72 (2.892)	H–4 → L+1 (0.687) H–2 → L+1 (0.107)	0.0000
$S_0 \rightarrow S_{12}$	428.28 (2.895)	H–5 → L+1 (0.692) H–3 → L+1 (0.109)	0.0124
$S_0 \rightarrow T_{15}$	420.63 (2.948)	H–8 → L (–0.156) H–7 → L (0.359) H–6 → L+1 (0.577)	0.0000
$S_0 \rightarrow S_{13}$	419.13 (2.959)	H–9 → L (–0.192) H–8 → L (0.127) H–7 → L+1(–0.415) H–6 → L (–0.487) H–3 → L+1 (0.111)	0.0228
$S_0 \rightarrow S_{14}$	418.41 (2.964)	H–9 → L (0.344) H–8 → L (0.616)	0.0000
$S_0 \rightarrow S_{15}$	418.31 (2.964)	H–9 → L (–0.586) H–8 → L (0.320) H–7 → L+1 (0.154) H–6 → L (0.157)	0.0032

Table 4-A6. Electronic Transitions Estimated for Stacked Three Molecules of **1hBF$_2$** with Geometries in Crystals ($M_1/M_0/M_1$)

	λ_{ET} / nm (eV)	Transition (Coefficient)	*f*
$S_0 \rightarrow T_1$	609.53 (2.034)	H–2 → L+2 (0.108) H → L (0.677) H → L+2 (0.133)	0.0000
$S_0 \rightarrow T_2$	589.29 (2.104)	H–2 → L+1 (0.199) H–1 → L (0.501) H–1 → L+2(–0.177) H → L+1 (–0.411)	0.0000
$S_0 \rightarrow T_3$	580.60 (2.135)	H–2 → L (0.366) H–1 → L+1 (0.449) H → L+2 (0.383)	0.0000
$S_0 \rightarrow S_1$	575.76 (2.153)	H–2 → L+2(–0.108) H–1 → L+1 (0.128) H → L (0.661) H → L+2 (–0.165)	0.0008
$S_0 \rightarrow T_4$	567.23 (2.186)	H–1 → L (0.450) H → L+1 (0.543)	0.0000
$S_0 \rightarrow S_2$	563.91 (2.199)	H–1 → L (0.440) H → L+1 (0.550)	0.0023
$S_0 \rightarrow S_3$	554.80 (2.235)	H–2 → L+1(–0.211) H–1 → L (0.509) H–1 → L+2 (0.193) H → L+1 (–0.396)	0.0000
$S_0 \rightarrow T_5$	553.73 (2.239)	H–2 → L+2(–0.121) H–1 → L+1 (0.470) H → L (0.192) H → L+2 (–0.463)	0.0000
$S_0 \rightarrow T_6$	544.75 (2.276)	H–2 → L (0.588) H–1 → L+1(–0.198) H → L+2 (–0.337)	0.0000
$S_0 \rightarrow S_4$	541.92 (2.288)	H–2 → L (0.562) H–1 → L+1(–0.116) H → L+2 (–0.412)	0.0321
$S_0 \rightarrow T_7$	540.44 (2.294)	H–3 → L (0.101) H–2 → L+1(–0.405) H–1 → L (0.198) H–1 → L+2 (0.492) H → L+1 (–0.187)	0.0000
$S_0 \rightarrow S_5$	535.79 (2.314)	H–2 → L (0.127) H–2 → L+2 (0.260) H–1 → L+1 (0.501)	0.0009

		H → L (–0.149)	
		H → L+2 (–0.311)	
$S_0 \rightarrow T_8$	527.18 (2.352)	H–3 → L (0.206) H–2 → L+1 (0.522) H–1 → L+2 (0.419)	0.0000
$S_0 \rightarrow S_6$	523.38 (2.369)	H–2 → L+1 (0.461) H–1 → L+2 (0.530)	0.0032
$S_0 \rightarrow T_9$	521.68 (2.377)	H–3 → L (0.650) H–3 → L+2 (0.130) H–2 → L+1(–0.104) H–1 → L+2 (0.216)	0.0000
$S_0 \rightarrow T_{10}$	515.64 (2.405)	H–4 → L (–0.133) H–2 → L+2 (0.657) H–1 → L+1 (0.155)	0.0000
$S_0 \rightarrow T_{11}$	508.18 (2.440)	H–5 → L+1 (0.295) H–4 → L (0.591) H–4 → L+2(–0.127) H–3 → L+1 (0.124) H–2 → L+2 (0.166)	0.0000
$S_0 \rightarrow T_{12}$	507.03 (2.445)	H–5 → L (0.578) H–5 → L+2(–0.124) H–4 → L+2 (0.360)	0.0000
$S_0 \rightarrow S_7$	499.58 (2.482)	H–5 → L (–0.102) H–3 → L (0.545) H–3 → L+2(–0.320) H–2 → L+1 (0.219) H–1 → L+2(–0.158)	0.0000
$S_0 \rightarrow S_8$	495.19 (2.504)	H–4 → L (–0.417) H–3 → L+1 (0.473) H–2 → L+2(–0.290)	0.0014
$S_0 \rightarrow T_{13}$	494.24 (2.509)	H–4 → L (–0.168) H–3 → L+1 (0.681)	0.0000
$S_0 \rightarrow S_9$	492.48 (2.518)	H–5 → L (0.614) H–4 → L+1(–0.280) H–3 → L (0.139)	0.0003
$S_0 \rightarrow S_{10}$	491.14 (2.524)	H–5 → L+1(–0.286) H–4 → L (0.469) H → L+2 (0.422)	0.0126
$S_0 \rightarrow T_{14}$	488.73 (2.537)	H–5 → L (–0.396) H–5 → L+2(–0.102)	0.0000
		H–4 → L+1 (0.564)	
		H–3 → L+2(–0.110)	
$S_0 \rightarrow T_{15}$	487.53 (2.543)	H–5 → L+1 (0.596) H–4 → L (–0.316) H–4 → L+2 (0.151) H–3 → L+1 (0.136)	0.0000
$S_0 \rightarrow S_{11}$	478.38 (2.586)	H–5 → L+1 (0.270) H–4 → L+2 (0.223) H–3 → L+1 (0.250) H–2 → L (0.115) H–2 → L+2 (0.471) H → L (0.140) H → L+2 (0.183)	0.0289
$S_0 \rightarrow S_{12}$	472.29 (2.625)	H–5 → L+2 (0.458) H–4 → L+1 (0.434) H–3 → L (0.134) H–2 → L+1(–0.186) H–1 → L+2 (0.158)	0.0005
$S_0 \rightarrow S_{13}$	468.33 (2.647)	H–10 → L (0.126) H–5 → L+1 (0.307) H–4 → L (0.131) H–4 → L+2 (0.480) H–2 → L (–0.170) H–2 → L+2(–0.199) H → L+2 (–0.215)	0.2235
$S_0 \rightarrow S_{14}$	467.49 (2.652)	H–12 → L (0.105) H–5 → L (0.147) H–5 → L+2 (0.285) H–3 → L+2 (0.292) H–2 → L+1 (0.347) H–1 → L (0.153) H–1 → L+2(–0.298) H → L+1 (–0.142)	0.0000
$S_0 \rightarrow S_{15}$	462.87 (2.679)	H–10 → L (–0.214) H–6 → L (0.307) H–4 → L+2 (0.205) H–3 → L+1(–0.151) H–2 → L (0.258) H–2 → L+2(–0.204) H–1 → L+1 (0.317) H → L+2 (0.257)	0.9381

4.6.5. References.

A1. Sheldrick, G. *SHELX-97* **1997**.

A2. Wakita, K. *Yadokari-XG* **2001**.

CONCLUSIONS

In present doctoral thesis, the author showed that the photoluminescence (PL) properties of diaroylmethanatoboron difluorides (**1BF$_2$**) are influenced by the arrangement of molecules with complicated intermolecular interactions.

In chapter 1, the author reported results of a thorough investigation packing structure and fluorescence (FL) properties of seven derivatives, **1a–gBF$_2$**, in their crystalline state. The crystal-packing structures of **1a–gBF$_2$** fall into three types I–III, differing in the degree and manner of intermolecular interactions between the π-conjugated orbitals in the individual molecules. Specifically, they are characterized by *no* overlap of the π-conjugated main units of two adjacent molecules (type I), overlap of the π-orbitals of the benzene rings of two adjacent molecules (type II), and overlap of the π-orbitals of the benzene ring and the dihydrodioxaborinine ring of adjacent molecules (type III). Moreover, the crystal-packing structures of **1a–gBF$_2$** govern their FL properties in the crystalline state. The nature of the fluorophore domain present in type I crystals leads to FL properties that are similar to those observed in CH_2Cl_2 solution. In the case of the type II crystals, the presence of intermolecular overlap of benzene rings' π-orbitals generates new fluorophore domains, referred to as "excited multimers", which possess the allowed $S_1 \rightarrow S_0$ electronic transitions that result in FL at longer wavelengths compared to that with the type I crystals. Finally, the intermolecular overlap of π-orbitals belonging to the benzene and dihydrodioxaborinine rings for type III crystals leads to "excited multimer" domains with forbidden $S_1 \rightarrow S_0$ electronic transitions. Probably due to the participation of $S_n \rightarrow S_0$ ($n \geq 2$) electronic transitions, type III crystals emit FL at similar wavelengths with longer lifetime as that emitted by type I crystals. Overall, the investigations carried out with these substances have provided a greater understanding of the relationship between FL properties and intermolecular interactions in crystal-packing structures.

In chapter 2, the author demonstrated that white FL emission can be achieved by using a single component, either dibenzoylmethanatoboron difluoride (**P1BF$_2$**) or its diisopropyl derivative **1eBF$_2$**, not only in KBr but also in CH_2Cl_2 at a specific concentrations. A FL peak of **1bBF$_2$** in KBr appeared at λ_{FL} = 523 nm. Interestingly, the FL color of **1bBF$_2$** was almost white. The author then investigated the FL property of **1bBF$_2$** in CH_2Cl_2 at various concentrations. At low concentration, the solution showed blue FL with a band at λ_{FL} = 411 nm. In contrast, at high concentrations of **1bBF$_2$**, an intense yellow FL band at λ_{FL} = *ca.* 550 nm was observed. Moreover, at the moderate concentrations, the solution of **1bBF$_2$** emitted white FL. The deconvolution results for the FL spectrum of **1bBF$_2$** suggest that increasing the solution concentration causes a continuous change in the major FL domain, from excited monomer to excimer. Therefore, controlling the solution

concentration to achieve an adequate ratio of blue and yellow FL results in the white emission from a single component, **1bBF$_2$**. Compared to the traditional white fluorescent organic materials, **1BF$_2$** has some clear advantages, *e.g.*, ease of synthesis, low molecular weight, and absence of heavy metals.

In chapter 3, the author revealed that the mechanofluorochromism (MFC) behavior of alkyl- and silyl-substituted **1a–gBF$_2$** depends on the bulkiness of the substituents. The **1e,f,gBF$_2$** showed that MFC comprised of a reversible FL color change of FL between blue and yellow. However, other derivatives did not show MFC, suggesting that *n*-Bu, *n*-Pr, Et, and Me substituents in **1aBF$_2$**, **1bBF$_2$**, **1cBF$_2$**, and **1dBF$_2$**, respectively, are not large enough in preserving the metastable state. The observations made in this chapter strongly suggest that the bulkiness of secondary and tertiary substituents such as *i*-Pr, *t*-Bu, and Me_3Si in **1eBF$_2$**, **1fBF$_2$**, and **1gBF$_2$**, respectively, is required for the manifestation of MFC. This finding should provide a useful guide in designing novel MFC materials.

In chapter 4, the author performed a thorough investigation on the packing structure and room temperature phosphorescence (RTP) properties of bis(4-iodobenzoyl)methanatoboron difluoride (**1hBF$_2$**) crystals. In degassed *n*-BuCl at 298 K, **1hBF$_2$** emits only FL, while it exhibiting FL together with phosphorescence (PH) at 77 K. In contrast, the crystals of **1hBF$_2$** emit PL, comprising of FL and PH, even at room temperature. Using X-ray crystallographic analysis, the crystal packing structure of **1hBF$_2$** was found to exhibit continuous π-stacking, H•••F hydrogen bonding, and I•••F halogen bonding. These intermolecular interactions should provide a rigid crystal packing structure in which a thermal deactivation of the photo-excited S_1 or T_1 state of **1hBF$_2$** is suppressed. Density functional theory calculations revealed that the π-stacking strongly affects the electronic properties of **1hBF$_2$**. The stacked two **1hBF$_2$** molecules with geometry in crystals exhibited a small energy gap between the S_1 and T_1 states and a forbidden $S_1 \rightarrow S_0$ electronic transition. Therefore, it is strongly suggested that the intersystem crossing (ISC) of photo-excited **1hBF$_2$** via the S_1 to T_1 state in the crystalline state is enhanced. It is noteworthy that the RTP of **1hBF$_2$** is caused by not only the heavy atom effect, but also the specific crystal packing structure. As a result, the design of this material differs from those conventionally used to generate metal-free RTP materials. Consequently, the results of this study should provide insights into a new mechanistic approach to realize RTP.

LIST OF PUBLICATIONS

1. “White Light Emission from a Single Component System: Remarkable Concentration Effects on the Fluorescence of 1,3-Diaroylmethanatoboron Difluoride”, Sakai, A.; Tanaka, M.; Ohta, E.; Yoshimoto, Y.; Mizuno, K.; Ikeda H. *Tetrahedron Lett.* **2012**, *53*, 4138–4141.

2. “Remarkable Difference in Fluorescence Lifetimes of the Crystalline States of Dibenzoylmethanatoboron Difluoride and Its Diisopropyl Derivative”, Tanaka, M.; Sakai, A.; Ohta, E.; Yoshimoto, Y.; Mizuno, K.; Ikeda H. *Tetrahedron Lett.* **2013**, *54*, 4380–4384.

3. “White-Light Photoluminescence Observed for Diaroylmethanatoboron Difluoride”, Sakai, A.; Tanaka, M; Ohta, E.; Ikeda, H. *Kagaku Kogyo* **2014**, *65*, 27–31.

4. “Preparation of a Cyclic Polyphenylene Array for a Zigzag-Type Carbon Nanotube Segment”, Sekiguchi, R.; Takahashi, K.; Kawakami, J.; Sakai, A.; Ikeda, H.; Ishikawa, A.; Ohta, K.; Ito, S. *J. Org. Chem.*, **2015**, *80*, 5092–5110.

5. “Fluorescence Behavior Associated with a Possible Intercolumnar Charge-transfer Interaction Formed in the Crystalline State of Dyad Consisting of Mesitylene (Donor) and 1,4-Dicyano-2-methylnaphthalene (Acceptor) Units”, Ohta, E.; Kobayashi, H.; Sakai, A.; Matsui, Y.; Sato, H.; Ikeda, H. *Rapid Commun. Photosci.* **2015**, *4*, 31–33.

6. “Novel Fluorescence Domain "Excited Multimer" Formed upon Photoexcitation of Continuously Stacked Diaroylmethanatoboron Difluoride Molecules with Fused π-Orbital in Crystals”, Sakai, A.; Ohta, E.; Yoshimoto, Y.; Tanaka, M.; Matsui, Y.; Mizuno, K.; Ikeda H. *Chem. Eur. J.* **2015**, *21*, 18128–18137.

7. “Substituent-Dependent Backward Reaction in Mechanofluorochromism of Dibenzoylmethanato Difluoroboron Derivative”, Sagawa, T.; Ito, F.; Sakai, A.; Ogata, Y.; Tanaka, K.; Ikeda, H. *Photochem. Photobiol. Sci.* **2016**, *15*, 420–430.

8. “Preparation of a Cyclic Polyphenylene Array for a Chiral-Type Carbon Nanotube Segment”, Sekiguchi, R.; Kudo, S.; Kawakami, J.; Sakai, A.; Ikeda, H.; Nakamura, H.; Ohta, K.; Ito, S. *J. Org. Chem. Submitted*.

9. “Room-Temperature Phosphorescent Crystal of Organoboron Complex: Enhanced Intersystem Crossing and Suppressed Thermal Deactivation of Excited States Derived by Packing Structure”, Sakai, A.; Tsuzuki, S.; Ohta, E.; Matsui, Y.; Ikeda, H. *Submitted*.

ACKNOWLEDGEMENTS

The author would like to express his deepest gratitude to Prof. Hiroshi Ikeda at Osaka Prefecture University for his continuous and valuable guidance as well as encouragement throughout this study. In addition, the author appreciates the kind comments and suggestions from Prof. Akikazu Matsumoto and Prof. Akiya Ogawa at Osaka Prefecture University.

The author gratefully acknowledges to Prof. Kazuhiko Mizuno at the Nara Institute of Science and Technology, Assistant Prof. Eisuke Ohta, and Assistant Prof. Yasunori Matsui for their encouragement and useful comments. The author also acknowledges Prof. Shunji Ito at Hirosaki University, Prof. Fuyuki Ito at Shinshu University, Prof. Yoshiro Yamashita at Tokyo Institute of Technology, Prof. Hajime Maeda at Kanazawa University, and Chief Senior Researcher, Dr. Seiji Tsuzuki at the National Institute of Advanced Industrial Science and Technology (AIST) for their useful advice for researches. The author thanks all the members of the Ikeda-Mizuno research groups at Osaka Prefecture University, especially Yuichi Yoshimoto, Mirai Tanaka, and Shota Nishida for the advice given, and Takuya Ogaki, Atsushi Yamamoto, and Yutaro Kuramoto for their help in lab. The author also gratefully acknowledges the financial support given by the Research Fellowships for Young Scientists Program of the Japan Society for the Promotion of Science.

Finally, the author thanks his family, Shingo Sakai, Shigeko Sakai, Miyo Sakai, Shinya Sakai, and Mariko Sakai, and his fiancée, Kana Takeda, for all the support given.

Department of Applied Chemistry, Graduate School of Engineering, Osaka Prefecture University

Material Creation Chemistry Research Group

Atsushi Sakai